Université de Montréal

Étude numérique de la diffusion des défauts ponctuels dans les alliages de nickel

par

Sami Mahmoud

Département de physique

Faculté des arts et des sciences

Thèse présentée à la Faculté des études supérieures

en vue de l'obtention du grade de

Philosophiæ Doctor (Ph.D.)

en physique

Décembre 2018

Université de Montréal

Faculté des études supérieures

Cette thèse intitulée

Étude numérique de la diffusion des défauts ponctuels dans les alliages de nickel

présentée par

Sami Mahmoud

a été évaluée par un jury composé des personnes suivantes :

Michel Côté

(président-rapporteur)

Normand Mousseau

(directeur de recherche)

Sjoerd Roorda

(membre du jury)

Pierre Bénard

(examinateur externe)

(représentant du doyen de la FAS)

Thèse acceptée le

RÉSUMÉ

Grâce à sa grande polyvalence , le nickel est très utilisé en industrie sous forme pure ou plus fréquemment en alliages. Ces métaux possèdent plusieurs bonnes caractéristiques physiques telles que la grande solidité mécanique, la faible expansion à haute température ainsi que la résistance à la corrosion impliquant une utilisation intensive dans plusieurs domaines industriels tels que l'aérospatial, la construction des voitures, les tubes conducteurs dans les centrales nucléaires et même pour des composants électroniques. L'étude de la diffusion des défauts ponctuels dans les alliages à base de nickel est en pleine effervescence, et ce puisque ça affecte directement leurs propriétés bénéfiques. Dans cette thèse, nous décrivons en détail la cinétique de ces défauts dans le nickel et ses alliages en utilisant la méthode ART cinétique qui est une méthode Monte Carlo cinétique hors réseau avec construction du catalogue à la volée. Nous décrivons en détail la surface d'énergie potentielle pour ces défauts dans le nickel pur. Nos résultats montrent des mécanismes de diffusion complexes même pour des défauts aussi simples que des petits amas lacunaires ou d'interstitiels. Nous avons aussi étudié des alliages ordonnés de nickel avec une lacune et interstitiel ce qui nous a permis de comprendre que ses défauts peuvent entrainer une évolution structurelle de tels alliages les poussant ainsi vers une phase désordonnée. Nous avons également examiné la diffusion des lacunes dans l'alliage NiFe ce qui nous a permis d'explorer le comportement diffusif exact de ce défaut dépendamment de la composition chimique de son entourage immédiat de ses premiers voisins.

Mots clés : Défauts ponctuels, diffusion, Monte-Carlo cinétique, nickel, alliages

SUMMARY

Thanks to its great versatility, nickel is widely used in industry in pure form or more frequently in alloys. These metals have several good physical characteristics such as high mechanical strength, low expansion at high temperature and corrosion resistance involving intensive use in several industrial fields such as aerospacial, car construction, conductive tubes in nuclear power plants and even for electronic components. The study of point defects diffusion in nickel-based alloys is in increase and this since it directly affects their beneficial properties. In this thesis, we describe in detail the kinetics of these defects in nickel and its alloys using the kinetic ART method which is an off-lattice kinetic Monte Carlo method with on-the-fly catalog building. We describe in detail the energy landscape for these defects in pure nickel. Our results show complex diffusion mechanisms even for defects as simple as vacancy aggregates or interstitials. We also studied nickel alloys with a vacancy and interstitial defects, which allows us to find that these defects can cause a structural evolution of such alloys thus pushing them to a disordered phase. We also examine the diffusion of the vacancy in the NiFe alloy which allows us to explore the exact diffusive behavior of this defect depending on the chemical composition of its immediate surroundings of its first neighbors.

Keywords: Point defects, diffusion, Kinetic Monte Carlo, nickel, alloys

Table des matières

Liste des tableaux

Table des figures

LISTE DES SIGLES ET DES ABRÉVIATIONS

ARTc	La Technique de l'Activation-Relaxation cinétique
ARTn	La Technique de l'Activation-Relaxation nouveau
KMC	La méthode de Monte-Carlo cinétique
TST	Théorie de l'état de transition (de l'anglais Transition State Theory)
eV	Unité d'énergie, l'électron volt
K	Unité de température, le Kelvin
Å	Unité de distance, l'Angström
NAUTY	No AUTomorphisms, Yes ?
LAMMPS	Large-scale Atomic/Molecular Massively Parallel Simulator

NOTATIONS

ΔF	Différence d'énergie libre
ΔE	Une variation d'énergie interne
ΔS	Une variation d'entropie
k_B	La constante de Boltzmann
T	La température
$\tilde{r}$	Une fréquence effective
E	Une énergie interne
F	Une énergie libre
S	Une entropie
r^*	La fréquence d'essai

REMERCIEMENTS

Je tiens à remercier toutes les personnes qui ont contribué au succès de mon doctorat et qui m'ont aidée moralement de la rédaction de ce mémoire.

Je voudrais remercier vivement mon directeur de thèse Normand Mousseau pour sa patience, sa disponibilité et surtout ses judicieux conseils, qui ont contribué à m'encourager et à alimenter ma réflexion.

Je remercie également tous mes collègues avec qui j'ai vécu de belles cinq années ; Mickaël Trochet, Kokou Gawonou N'Tsouaglo, Oscar Restrepo, Vincent Binette, Sébastien Côté, Md Mijanur Rahman, Simon Gelin, Roger Gaudreault et tous les anciens et les nouveaux membres que j'ai connu dans notre équipe.

J'exprime ma gratitude à messieurs Michel Côté (professeur à l'Université de Montréal), Pierre Bénard (professeur à l'Université du Québec à Trois-Rivières) et Sjoerd Roorda (professeur à l'Université de Montréal) pour l'honneur qu'ils m'ont fais d'être dans mon jury de thèse.

Il m'est impossible d'oublier ma mère pour son encouragement et soutien. Elle a toujours fait tout son possible pour m'aider. Mes remerciements ne pourront jamais égaler son grand coeur qui m'a apporté du soutien au moment où j'avais besoin d'aide.

Merci à mon père, Ibrahim Mahmoud, décédé le 29 novembre 2016. Je sais que tu aimerais lire ma thèse, je sais que tu serais content et fier de moi, j'aurais tellement aimé fêter cet accomplissement avec toi ...

Mes derniers remerciements vont à ma femme Hana, à tous mes amis (Hassen, Ezzeddine, Daniel, Catherine, et tous les autres) et aux membres de ma famille (Thouraya, Karem, Ilhem

et tous les autres) qui ont tout fait pour m'aider, qui m'ont soutenu et surtout supporté durant ma thèse.

INTRODUCTION GÉNÉRALE

L'optimisation des performances physiques des matériaux constitue toujours un enjeu majeur en recherche. Des matériaux qui possèdent une grande solidité mécanique, une dureté mécanique élevée, une haute plasticité, une bonne résistance à la corrosion sont souvent demandés dans plusieurs domaines en industrie. Il est évident que, pour pouvoir améliorer ces qualités, il faut déterminer les facteurs affectant les différentes caractéristiques. Pour les métaux, il a été montré que la configuration et la concentration de divers défauts jouent un rôle important dans de nombreux phénomènes, tels que le glissement de dislocations et la diffusion d'impuretés modifiant ainsi certaines de leurs propriétés physico-mécaniques[1]. Plusieurs travaux de recherche ont essayé de décrire les propriétés thermodynamiques des métaux en présence de défauts tels que l'équilibre chimique caractérisé par la minimisation de l'énergie libre de Gibbs (dans le cas où la température et la pression restent constantes), l'enthalpie et l'entropie de formation des défauts ponctuels dans les cristaux par la façon standard de l'utilisation de l'équation d'Arrhenius. Cependant, beaucoup de détails quant à la cinétique exacte de ces défauts ainsi que leur agrégation restent incompris à cause des limitations des méthodes numériques et expérimentales.

Malgré le développement considérable des méthodes numériques permettant de simuler la trajectoire de la diffusion à l'échelle atomique dans les cristaux, plusieurs d'entre elles restent incapables de briser les limitations temporelles des méthodes standard. La description exacte de la cinétique des défauts ponctuels est importante pour pouvoir comprendre et expliquer d'autres phénomènes tels que l'activité et la diffusion des dislocations affectant directement les propriétés mécaniques des matériaux [2], les caractéristiques électriques de

certains matériaux [3] ainsi que les effets sur la magnétisation [4]. L'utilisation d'une approche multi-échelle est la façon idéale pour traiter les différentes propriétés des défauts. Les méthodes ab-initio, qui consistent à résoudre l'équation quantique de Schrödinger, donnent les meilleurs résultats en ce qui concerne la structure électronique. Cependant, pour modéliser et donc comprendre le mouvement des défauts à l'échelle atomique il faut utiliser d'autres approches telles que dynamique moléculaire et Monte Carlo cinétique. Ces dernières feront le lien entre les méthodes ab-initio et expérimentales pour donner une image complète de l'évolution de la matière à différentes dimensions spatiales.

Le plan de la thèse est le suivant : les deux premiers chapitres sont des chapitres bibliographiques consacrés à la description de la problématique étudiée (les défauts ponctuels dans les matériaux) ainsi que les méthodes numériques permettant de l'étudier. Les chapitres suivants (3, 4 et 5) , sous forme d'articles, présentent nos résultats obtenus. Dans le premier chapitre, on décrira les différents types de défauts ponctuels qu'on peut avoir dans les matériaux. La fin du chapitre est dédiée à la cinétique de ces défauts. Ensuite, dans le deuxième chapitre, on détaillera les méthodes numériques permettant d'étudier la cinétique des défauts qui sont la dynamique moléculaire et Monte Carlo cinétique, mais on se concentrera plus sur la méthode utilisée dans nos études qui est la méthode ARTc. Dans le troisième chapitre, qui constitue les résultats du premier article, on a étudié la diffusion des défauts ponctuels (allant de un à cinq lacunes et interstitiels) dans le nickel pur. Cet article est composé de deux grandes parties : Une première partie dans laquelle on a essayé de choisir le meilleur potentiel parmi quatre testés (EAM, MEAM1NN, MEAM2NN et ReaxFF) en comparant nos résultats obtenus avec des résultats trouvés par des calculs DFT et expérimentaux. Une fois que le potentiel le plus adéquat est choisi, on le considère pour traiter le reste des défauts. Au quatrième chapitre, qui constitue les résultats du deuxième article, on a étudié la diffusion des monodéfauts ponctuels dans des structures hautement ordonnées d'alliages à base de nickel. Les résultats obtenus montrent que la cinétique des lacunes et interstitielle joue un rôle important dans la stabilité des structures ordonnées. Finalement, dans le dernier chapitre, on présentera nos résultats préliminaires issus de l'investigation de la mobilité des

lacunes dans une structure complètement désordonnée de l'alliage NiFe. La thèse est clôturée par une conclusion résumant toutes les nouveautés ainsi que des perspectives de nos travaux de recherche.

Chapitre 1

DÉFAUTS PONCTUELS DANS LES MATÉRIAUX

1.1. Introduction

Les cristaux en réalité ne sont jamais parfaits et contiennent toujours des défauts. Ces derniers, dépendamment de leurs dimensionnalités, peuvent être classé en quatre types : les défauts zéro-dimensionnels appelés également défauts ponctuels, les défauts uni-dimensionnels ou dislocations, les défauts bi-dimensionnels ou joints de grains et les défauts tri-dimensionnels ou agrégats de lacunes ou d'interstitiels. Dans ce chapitre en particulier, et la thèse en général, on se concentre uniquement sur l'étude des défauts zéro-dimensionnels.

Dans cette thèse, on se concentre uniquement sur l'étude des défauts ponctuels dans les métaux de nickel non-ioniques. Ces défauts jouent un rôle très important dans le contrôle des propriétés macroscopiques des matériaux surtout quand ils sont soumis à des irradiations qui multiplient la présence des lacunes et interstitiels. Dans la littérature, on peut classer les défauts ponctuels selon leur nature atomique c'est-à-dire une distinction entre les défauts intrinsèques ou extrinsèques, ou bien selon leur configuration dans laquelle il y a un manque d'atomes ou un atome de plus ou même un atome d'un autre type remplaçant un autre du réseau. Nous, on va adopter le deuxième critère de classification dans lequel on distingue trois types de défauts : les lacunes, les atomes interstitiels et les atomes en substitution. Ces défauts seront détaillés dans ce chapitre ainsi que leur cinétique.

1.2. Défauts ponctuels et leurs propriétés

1.2.1. Les différents types de défauts ponctuels

1.2.1.1. *La lacune*

La lacune, comme indiqué dans la figure 1.1 a) , c'est tout simplement un site cristallin non occupé. À température nulle (absolue), les atomes formant le cristal dans un métal sont tous placés dans leurs sites cristallins.

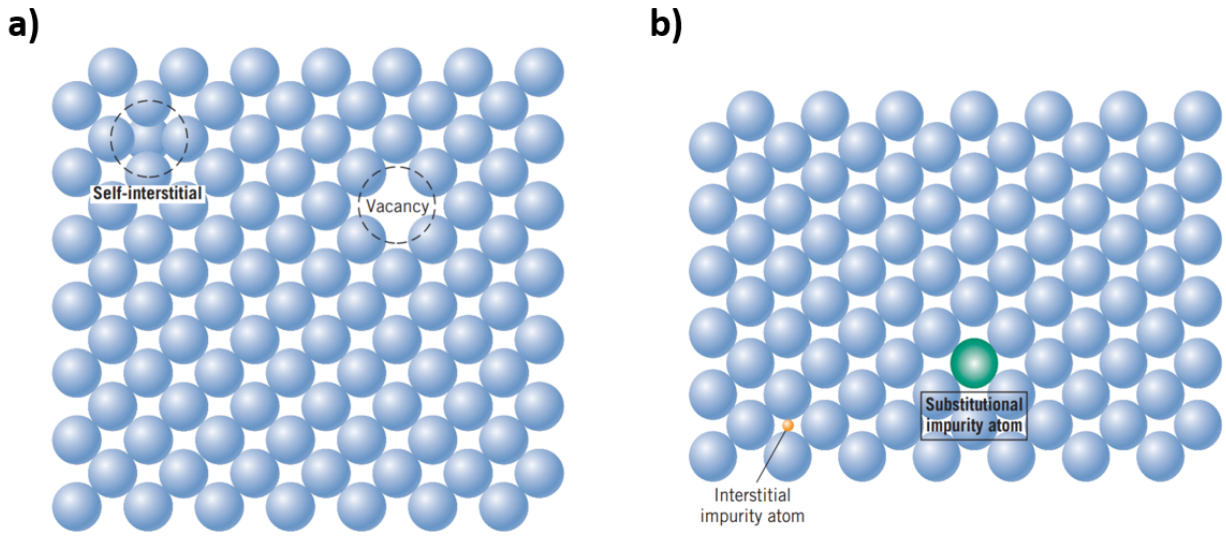

Figure 1.1. Illustration schématique des défauts ponctuels[5] a) intrinsèques et b) extrinsèques. Les défauts intrinsèques sont la lacune et l'auto-interstitiel qui sont un site cristallin non occupé et un atome de plus dans réseau du même type que le ceux du cristal, respectivement. Les défauts ponctuels extrinsèques sont les atomes subtitutionnels (en vert dans la figure b)) et les atomes interstitiels (en orangé dans la figure b)), tous les deux de nature différentes que ceux du cristal.

La présence d'une lacune dans un matériau n'entraine pas beaucoup de distorsion dans le cristal puisque les atomes entourant cette lacune préféreront rester à leurs positions cristalline plutôt que d'aller la combler ou même s'y approcher. Ceci peut expliquer le fait que le saut d'une lacune (donc le saut de l'atome qui va le combler) nécessite généralement une grande barrière énergétique. Thermodynamiquement, la présence des lacunes influe sur le cristal en augmentant son entropie et leur nombre est fonction de la température comme suit :

$$N_v = Nexp(-\frac{E_f}{k_B T}), \tag{1.1}$$

où N est le nombre d'atomes dans le cristal, E_f est l'énergie de formation d'une lacune, T est la température du cristal et k_B est la constante de Boltzmann. L'effet de la présence de la lacune va être discuté dans la section 1.3.

1.2.1.2. *L'interstitiel*

L'interstitiel est un atome se trouvant dans une position qui n'est pas régulière du cristal, appelé également interstice d'où le nom du défaut. Pour les métaux en général, et pour ceux les plus compacts en particulier, les atomes sont plus grands que les espaces interstices ce qui implique que la présence des interstitiels est peu probable comparée à celle des lacune. En effet, pour que l'interstitiel puisse s'incorporer dans le réseau, il faut créer de grandes distorsions.

Deux cas peuvent se présenter pour l'interstitiel dépendemment de son type ; un auto-interstitiel (figure 1.1 a)) dans le cas où l'atome est du même nature que les atomes formant le cristal (un métal pur ou alliage simple), ou une impureté (figure 1.1 b)) quand l'atome interstitiel est d'un autre type que les atomes du cristal. Logiquement, les atomes qui demeurent en interstitiel sont ceux qui possèdent une taille plus petite (tels que l'hydrogène, l'oxygène, ou le carbone) que celle des atomes formant le réseau métallique.

1.2.1.3. *Les atomes en substitution*

Les atomes en substitution, comme leur nom l'indique, sont les impuretés qui viennent substituer un atome du réseau initial. Contrairement aux interstitiels, les atomes en substitution sont en général des atomes de même ou de plus grande taille que les atomes du réseau. Dans les alliages ordonnés, la substitution implique l'apparition d'antisites qui sont des atomes de nature différente à celle attendue et imposée par l'ordre de la structure. La figure 1.1 b) illustre le défaut substitutionnel.

1.2.2. Détermination des propriétés des défauts ponctuels

Les grandeurs les plus importantes à déterminer pour décrire la stabilité et la diffusion des lacunes dans les matériaux sont les énergies de formation et migration, respectivement. L'énergie de formation est l'énergie requise pour produire le défaut (lacune ou interstitiel) dans la structure cristalline parfaite. L'énergie de migration est la différence en énergie entre l'état d'équilibre initial et le point de selle dans le cadre de la Théorie de l'État de Transition (TST) (voir section 2.4). La somme de l'énergie de formation est de migration est appelée énergie d'activation.

1.2.2.1. *Méthodes expérimentales*

On peut classer les méthodes expérimentales en deux catégories : la première classe est celle correspondante à des méthodes sensibles uniquement à la présence des défauts telle que l'annihilation des positrons ou les expériences de mesures de résistivité, tandis que la deuxième s'intéresse à la présence et à la mobilité de ces défauts comme dans les expériences de diffusion[6] ou d'anisotropie magnétique induite[7].

En spectroscopie d'annihilation de positron, la durée de vie du positron injecté dans le matériau est déterminée, et ce par la détection des particules Gamma issues de l'annihilation électron-positron. En effet, le positron, une fois injecté dans le matériau, ralentit jusqu'à l'énergie thermique dans un intervalle de temps de quelques picosecondes par ionisation et excitation du matériau[8]. Une durée de vie plus longue d'un positron est signe de la présence d'un défaut (lacune ou dislocation) car le positron y sera piégé à cause que la densité électronique est plus faible et donc il y a moins de probabilité d'annihiler un électron. La figure 1.3 montre la différence entre les densités des positrons présents dans un cristal parfait et un cristal avec lacune dans le tungstène.

Pour les mesures de diffusion on distingue entre les expériences directes faites au moyen de traceurs radioactifs[9] et celles indirectes comme l'anisotropie magnétique induite. L'énergie d'activation peut être extraite en calculant la pente dans la courbe d'Arrhenius[10] (la diffusion en fonction de l'inverse de la température) ce qui impose des mesures à différentes

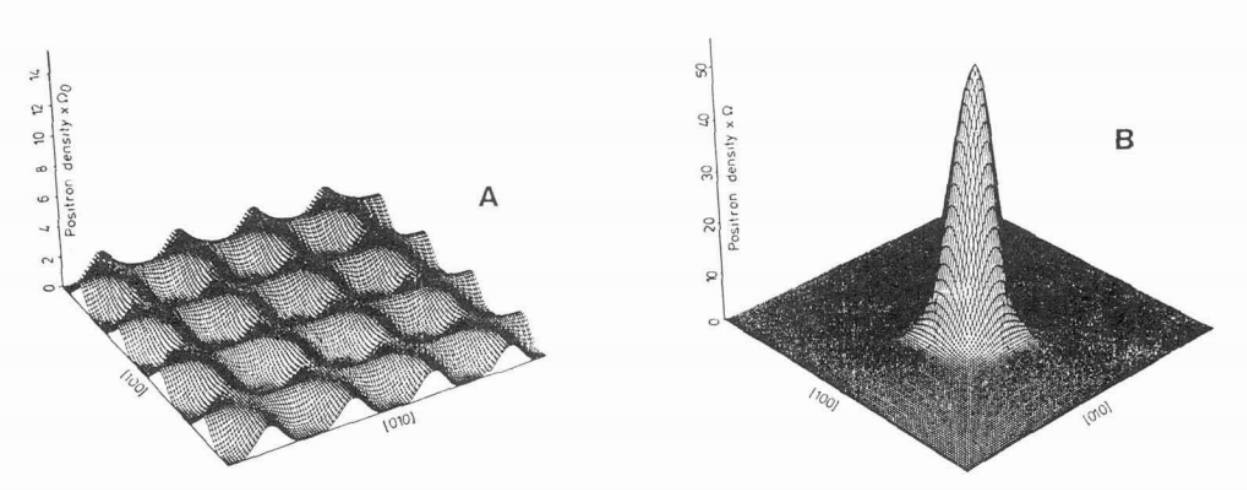

FIGURE 1.2. Densité de positrons pour le tungstène dans A) une structure cristalline parfaite B) et dans une structure cristalline en présence d'une lacune[8].

températures. La figure illustre des exemples de courbes d'Arrhenius pour des interstitiels dans certains métaux. Le coefficient de diffusion, dans le cadre d'un graphe d'Arrhenius, est la mesure de la mobilité d'une espèce diffusante et s'écrit sous la forme :

$$D = D_0 exp(-\frac{E_a}{k_B T}) \tag{1.2}$$

où D_0 est un facteur préexponentiel indépendant de la température T et E_a est l'énergie d'activation. Les mesures expérimentales à différentes températures permettent donc de trouver E_a.

Malgré le développement considérable dans ces méthodes de spectroscopie, ces méthodes restent restreintes dans les défauts simples ne pouvant pas dépasser la mono-, la bilacune et la monointerstitiel.[11]

1.2.2.2. *Méthodes numériques*

Numériquement l'énergie de formation est calculée comme suit :

$$E_f = E_{conf} - \frac{n}{N} E_{par} \tag{1.3}$$

où E_{conf} est l'énergie du système en présence de(s) défaut(s), E_{par} est l'énergie du cristal parfait, N est le nombre d'atomes dans le cristal parfait et n est le nombre d'atomes en

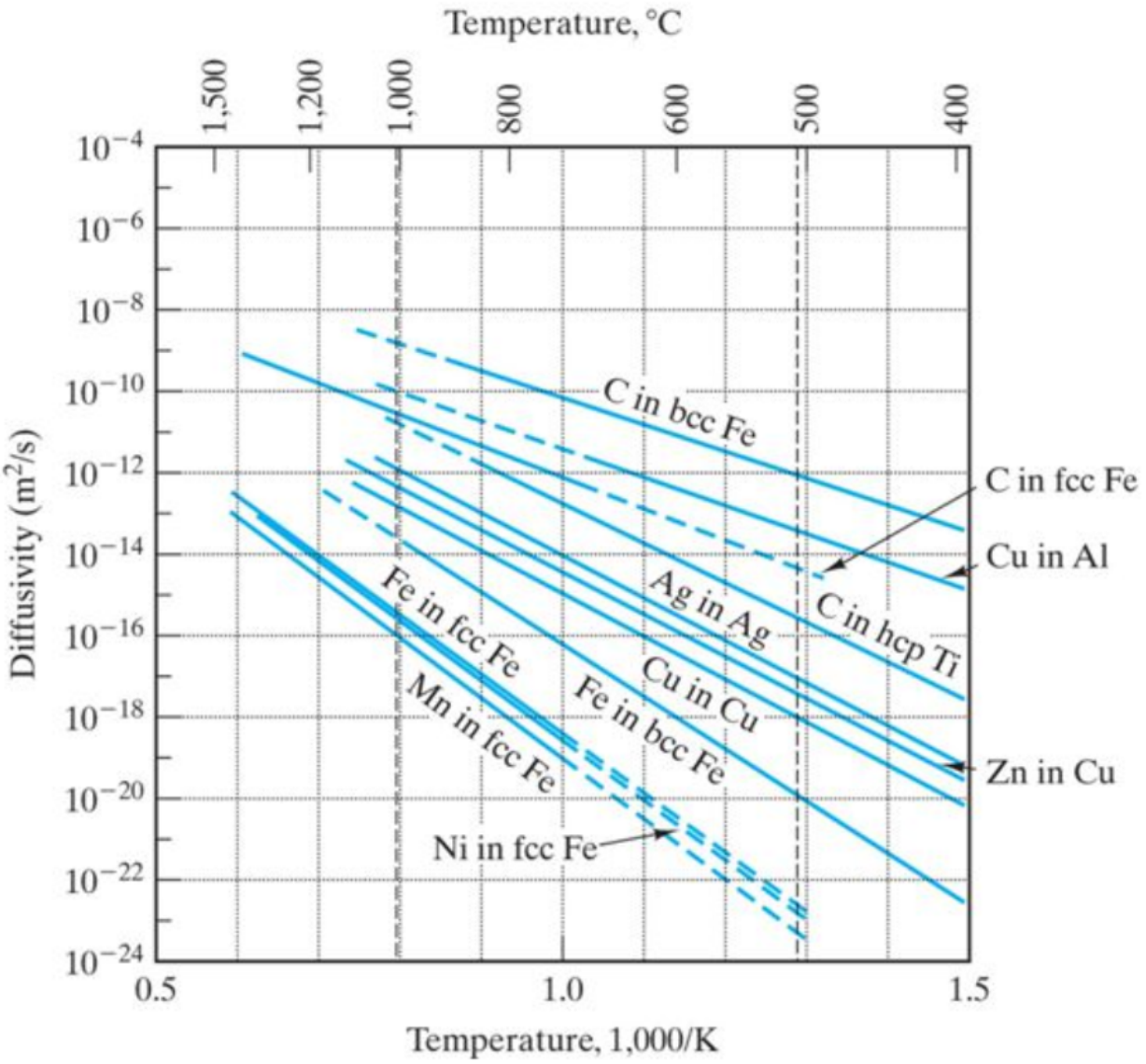

Figure 1.3. Courbes d'Arrhenius montrant la diffusivité de certains interstitiels dans certains métaux en fonctions de l'inverse de la température. [6].

tenant compte de(s) défaut(s) (n=N-1 dans les cas d'une lacune par exemple). Les énergies du cristal avec et sans défauts peuvent être trouvées par des méthodes *ab-initio* ou par de la dynamique moléculaire qui fera l'objet de la section 2.3.

L'énergie de migration peut être calculée par différentes méthodes. Le défi dans le calcul de l'énergie de migration est de trouver le point de selle. Généralement, des calculs DFT couplés à la méthode NEB (Nudged-elastic band)[13] sont utilisés pour la détermination de l'énergie de migration et d'activation. La méthode NEB permet de trouver le point de selle

Tableau 1. I. Énergies de formation E_f et migration E_m de la monolacune dans certains matériaux calculées en DFT[12].

	Al	Cu	Au	Ni	Pd	Pt	Pu
E_f	0.580[i]	1.04[d]	0.782[i]	1.37,[e] 1.43,[r] 1.65[r]	1.70[j]	1.18[j]	1.31, 1.36, 1.08[t]
E_m	0.57[m]	0.72[d]	–	1.285,[e] 1.08[r]	–	1.51[j]	–
	V	**Nb**	**Ta**	**Cr**	**Mo**	**W**	**Fe**
E_f	2.51[l]	2.99[l]	3.14[l]	2.64[l]	2.96,[j] 2.96[l]	3.56[l]	2.02,[b] 2.07,[k] 2.15[l]
E_m	0.62[l]	0.91[l]	1.48[l]	0.91[l]	1.28[l]	1.78[l]	0.65,[b] 0.67,[k] 0.64[l]
	C	**Si**	**Ge**	**Be**	**Ti**	**Zr**	**Hf**
E_f	8.2[f]	3.17,[c] 3.29[g]	2.3[h]	0.81,[n] 1.09[o]	1.97,[p] 2.13[q]	2.17,[q] 1.86[s]	2.22[q]
E_m	1.7[f]	0.4[g]	–	0.72B, 0.89NB[o]	0.47B, 0.61NB[p]	0.51B, 0.67NB[q]	0.79B, 0.91NB[q]

et ce à travers l'optimisation d'un certain nombre d'images intermédiaires le long du chemin de réaction dans le cadre de la Théorie de l'état de transition (TST) que nous allons décrire en détails dans la section 2.4. La méthode NEB peut être aussi couplée à des méthodes Monte Carlo cinétique [14]. Une autre méthode de calcul du point de selle (et donc du calcul de l'énergie de migration) est la méthode du dimère [15] qui est plus adoptée dans le cas où on ne connait pas l'état final. De plus, une autre méthode qui prend de plus en plus de place récemment (utilisée justement dans tous nos travaux dans cette thèse) c'est la méthode ARTnouveau (ARTn) qui permet de trouver les points de selle et qui fera l'objet de la section 2.6.2). L'énergie de migration peut être aussi extraite numériquement en calculant la pente dans la courbe d'Arrhenius (comme pour les méthodes expérimentales vues dans la section 1.2.2.1) dans le cadre de la dynamique moléculaire.

Comme pour le cas des lacunes, les grandeurs à déterminer pour décrire les propriétés thermodynamique et cinétique des interstitiels sont les énergies de formation et migration.

1.3. Effet de la diffusion des défauts ponctuels

La diffusion est la migration progressive des atomes d'un site à un autre. Pour les lacunes, comme indiqué dans la figure 1.4 a), un atome saute d'un site cristallin occupé à un autre adjacent ce qui est équivalent à la migration d'une lacune dans le sens opposé. Ceci exige

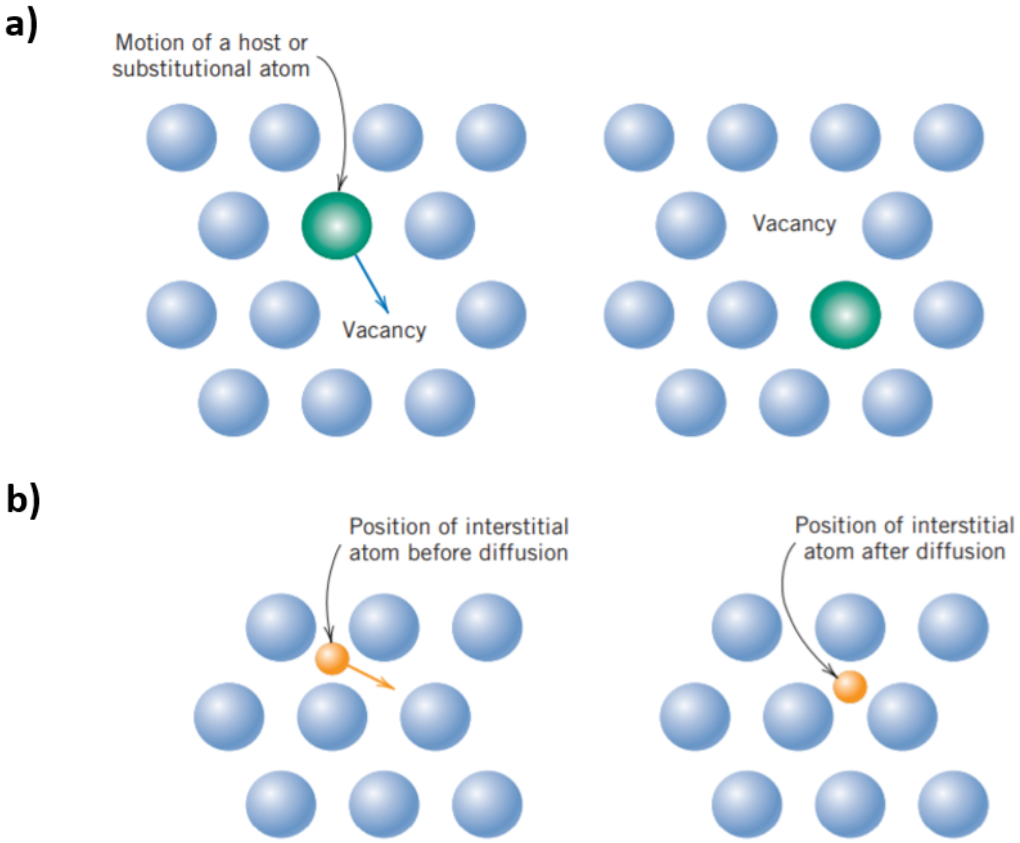

FIGURE 1.4. Illustration schématique de la diffusion de a) la lacune, et de b) l'interstitiel[5]. Pour la lacune, un atome voisin (en vert) saute pour la combler et ainsi la lacune a diffusé dans le site initial de cet atome. Pour l'interstitiel (en orangé). il saute d'un site interstice à un autre voisin.

de l'atome diffusant d'avoir suffisamment d'énergie pour pouvoir rompre ses liaisons avec les voisins et créer les distorsions lui permettant de migrer.

Pour les métaux, vu qu'ils sont très compacts en général, la diffusion d'un interstitiel implique beaucoup de distorsions dans le réseau. La haute compacité des métaux (entre 68 et 74%) implique aussi qu'il n'y a pas assez d'espace pour que l'atome de plus se mette à l'interstice, c'est pour ça que la diffusion des interstitiels dans les métaux correspond souvent à des mouvements en dumbbells c'est-à-dire des mouvements impliquant un couple d'atomes se partageant le même site cristallin. De plus, dans la majorité des métaux, la diffusion des interstitiels est en général beaucoup plus rapide que celle des lacunes et ce car il y a plus de sites interstitiels que ceux des positions cristallines. La figure 1.4 b) illustre la diffusion d'un interstitiel. La structure en dumbbells est présente également parfois en équilibre[16].

La présence et la diffusion des lacunes et interstitiels peuvent directement affecter des propriétés macroscopiques des matériaux. Les lacunes, par exemple, activent la montée des dislocations (de type coin seulement)[17]. Le mouvement collectif de ces dernières induit des déformations plastiques brutes dans les métaux [18]. Contrairement aux lacunes, la présence d'interstitiels peut augmenter la dureté d'un matériau car ils gênent la mobilité des dislocations et par conséquent réduisent sa déformation plastique [19, 20]. Une autre propriété mécanique des matériaux, le fluage sous contrainte appliquée, est décrit par le mouvement collectif des lacunes individuelles ou sous forme d'amas[18, 21]. La diffusion des défauts ponctuels affectent non seulement les propriétés mécaniques, mais aussi celles électriques. Dans ce cadre, il a été montré que les matériaux incluant des lacunes et des interstitiels extrinsèques possèdent une résistivité électrique différente que celle sans défauts[3, 22] à cause de la déformation dans la surface de Fermi crée par ces défauts. Le mouvement des lacunes et des interstitiels peut également expliquer la transition de l'ordre au désordre dans des structures initialement symétriques.[23, 24].

Malgré que l'effet de la diffusion des lacunes sur les propriétés physiques des matériaux a été postulé il y a longtemps et observé pour la première fois en 1956 [25] par microscopie électronique, beaucoup de détails quant à leur cinétique exacte reste incomprises comme l'agrégation et le comportement collectif de ces défauts. Ceci réside dans les limitations des techniques expérimentales et théoriques.

1.4. Conclusion

Nous avons décrit les différents types de défauts ponctuels dans les matériaux ainsi que leur diffusion et effet sur les propriétés macroscopiques des matériaux. Nous avons vu l'impact important de ces défauts malgré leur taille réduite. Il est donc très important d'étudier leur mouvement sur des échelles de temps expérimentales. Le problème c'est que l'expérience est incapable de fournir plusieurs informations à l'échelle atomique. Les méthodes numériques standards, à cause de certaines limitations fondamentales et computationnelles, sont incapables de décrire en détail le paysage énergétique de ces défauts. Le but du deuxième chapitre

est de mettre en lumière ces limitations ainsi que la méthode utilisée dans nos travaux (ART cinétique) pour résoudre cette problématique.

Chapitre 2

MÉTHODES NUMÉRIQUES DE SIMULATION DE LA CINÉTIQUE DES DÉFAUTS PONCTUELS

2.1. Introduction

Le but des simulations à l'échelle atomique est de modéliser explicitement le mouvement individuel des atomes dépendamment des conditions (pression, température ...) auxquelles ils sont soumis. Malheureusement, les méthodes de simulations possèdent des limitations spatio-temporelles fondamentales ou/et techniques. Pour avoir une description détaillée des défauts quant à leurs propriétés thermodynamiques et cinétiques, une modélisation multiéchelle est nécessaire pour bien les décrire. Les méthodes *ab initio*, en résolvant l'équation de Schrödinger, permettent de calculer et de caractériser la structure électronique des matériaux. Pour étudier l'évolution en fonction du temps des défauts dans les matériaux, cependant, il faut utiliser des méthodes de dynamique moléculaire ou Monte Carlo cinétique. Les caractéristiques fondamentales à l'échelle atomique imposent des limitations à la dynamique moléculaire et donc on a recours à une autre méthode qui est la Monte Carlo cinétique.

Dans ce chapitre nous présenterons des méthodes de simulation de la diffusion des défauts dans les matériaux, la dynamique moléculaire ainsi que Monte Carlo cinétique. Nous nous concentrerons plus sur la Technique d'Activation et de Relaxation cinétique (ARTc) qui est la méthode de base de nos travaux de recherche, mais nous discuterons brièvement de la dynamique moléculaire pour mettre en lumière les avantages d'utiliser ARTc, et aussi car la dynamique moléculaire est utilisée un peu dans nos travaux et précisément pour le traitement

des défauts de SFT, de l'anglais Stacking Fault Tetrahedra, les défauts d'empilement en tétraèdre.

Nous donnerons au début une description de différents potentiels permettant de calculer les forces d'interaction puis de la méthode de dynamique moléculaire. Ensuite, nous parlerons des méthodes de Monte Carlo cinétique en général ainsi que l'approche de base la Théorie de l'État de Transition (TST). Enfin, nous décrirons en détail ARTc et ce après avoir illustré les approches de base ; la classification topologique ainsi que ARTnouveau (ARTn).

2.2. Calculs de forces à l'échelle atomique dans les simulations des défauts

Le développement de potentiels empiriques permettant de décrire les interactions atomiques dans les métaux était et est toujours un sujet de recherche actif et stimulant. Daw et Baskes [26] ont proposé, il y a plusieurs décennies une approche semi-empirique EAM (Embedded Atom Method) basée sur la loi universelle d'échelle de Rose [27] tentant de reproduire, au niveau classique, certaines caractéristiques de la densité électronique. Au cours des années suivantes, plusieurs extensions du potentiel EAM ont été proposées afin de pouvoir traiter convenablement d'autres matériaux. Dans ce cadre, le potentiel MEAM (Modified Embedded Atom Method) [28] ou MEAM1NN a été proposé pour mieux décrire des métaux non-cfc. Le potentiel original MEAM a permis de mieux calculer les forces dans les structures non-cfc, mais une modification nommée MEAM2NN [29] a été apportée à ce potentiel afin d'améliorer les résultats obtenus par le MEAM original. Plus récemment, une autre approche ReaxFF (Reax Force Field) a été proposée [30] pour modéliser les réactions chimiques en tenant compte des charges. Dans cette partie, on va expliquer les principes de base de ces potentiels empiriques utilisés dans les simulations pour le cas des métaux.

2.2.1. Potentiel EAM

EAM (Embedded Atom Method), proposé par Foiles et Baskes [31], est une approximation de l'énergie sous forme de somme de fonctions de séparation entre un atome et ses

voisins. Ces dernières sont calculées à partir des densités électroniques dans le cadre du modèle de liaisons fortes [32]. L'énergie potentielle dans le cadre du modèle EAM est calculée comme suit :

$$E_i = F_\alpha \left(\sum_{i \neq j} \rho_\beta(r_{ij}) \right) + \frac{1}{2} \sum_{i \neq j} \phi_{\alpha\beta}(r_{ij}), \tag{2.1}$$

où ρ_β est la contribution à la densité de charge de l'atome j de type β pour la position de l'atome i, r_{ij} est la distance entre les atomes i et j, F_α représente la fonction d'incorporation signifiant l'énergie nécessaire pour placer l'atome i de type α dans le champ électronique, $\phi_{\alpha\beta}$.

2.2.2. Potentiel MEAM1NN

Baskes [28] voulait étendre l'approche EAM pour l'étude de plusieurs matériaux, et ce en incluant des termes angulaires à la densité électronique. En effet, dans les cristaux ayant une structure diamant, il faut tenir compte des forces de flexion ce qui nécessite une modification de la densité électronique. Par conséquent, l'énergie dans le cadre de EAM modifié (MEAM) s'écrit de la forme :

$$E_i = F_\alpha \left(\sum_{i \neq j} \overline{\rho_\beta}(r_{ij}) \right) + \frac{1}{2} \sum_{i \neq j} \phi_{\alpha\beta}(r_{ij}), \tag{2.2}$$

où $\overline{\rho_\beta}(r_{ij})$ est la densité électronique modifiée comparé à celle du EAM, et s'écrit sous la forme :

$$\overline{\rho_\beta}(r_{ij}) = \rho_\beta(r_{ij}) + \sum_{k \neq i} \chi(\theta_{jik}), \tag{2.3}$$

$\chi(\theta_{jik})$ est une fonction de l'angle theta entre les atomes i,j et k avec i étant l'atome central.

2.2.3. Potentiel MEAM2NN

Le formalisme original du potentiel MEAM (MEAM1NN) a été développé pour tenir compte uniquement des premiers voisins. Ceci peut être une bonne approximation pour des structures cfc par exemple dans lesquelles les seconds premiers voisins sont plus loin d'un facteur de près de 30% par rapport aux premiers voisins. Néanmoins, pour le cas des

métaux ayant une structure cc, ce rapport descend à moins de 15% et par conséquent l'effet des deuxièmes voisins sur la densité électronique ne peut pas être négligé. C'est pour cette raison que le formalisme en second voisin du potentiel MEAM (MEAM2NN) a été développé [29]. L'énergie dans le cadre MEAM2NN s'écrit de la même façon que celle du MEAM1NN (équation (2.2)) avec une densité plus développée qui tient compte des seconds voisins.

2.2.4. Potentiel ReaxFF

Le potentiel interatomique ReaxFF [30], contrairement aux autres potentiels empiriques, inclut des termes quantiques dans sa formulation dans le but de calculer les forces plus adéquatement. L'énergie du système dans le cadre du potentiel ReaxFF s'écrit sous la forme :

$$E_{systeme} = E_{bond} + E_{over} + E_{val} + E_{tors} + E_{vdWaals} + E_{Coulomb} \ ,$$

avec :

- E_{bond} : énergie de liaison qui est un terme attractive
- E_{over} : énergie de surcoordination qui représente une pénalité dans le cas de surcoordination d'atomes
- E_{val} : énergie relative à la déformation angulaire
- E_{tors} : énergie de torsion
- $E_{vdWaals}$: énergie de Van der Waals calculée entre tous les atomes
- $E_{Coulomb}$: énergie d'interaction coulombienne, ce terme est relatif aux charges polarisables donc il est mis à jour après chaque itération.

Dépendamment du type et de la composition du matériau, il peut y avoir des simplifications dans les termes de l'énergie de ReaxFF. Les termes E_{val} et E_{tors} sont dépendants de l'ordre des liaisons et par conséquent ils disparaissent dès qu'il y ait dissociation des liaisons. De plus, pour les métaux purs, le terme d'interaction colombienne $E_{Coulomb}$ est sans intérêt.

Les potentiels interatomiques sont très utilisés dans les méthodes de Monte Carlo cinétique et dynamique moléculaire. Cette dernière sera l'objet de la prochaine section.

2.3. Dynamique moléculaire

2.3.1. Principe

La dynamique moléculaire est une méthode de simulation permettant d'étudier le mouvement des atomes ou des molécules en fonction du temps, et ce en résolvant l'équation classique du mouvement, la deuxième loi de Newton :

$$\vec{F}_i = m_i \vec{a}_i \tag{2.4}$$

où $\vec{F}$ est le vecteur force et $\vec{a}$ est le vecteur accélération

Les forces en dynamique moléculaire sont déterminées par les interactions entre les atomes décrites par des potentiels ou des champs de forces. Une fois que les forces sont calculées, on obtient les positions et les vitesses par des intégrations de l'accélération. Les relations suivantes récapitulent les liens avec l'équation de Newton :

$$m\vec{a} = m\frac{d^2\vec{x}}{dt^2} = \vec{F}_i = -\vec{\nabla}V, \tag{2.5}$$

où $\vec{x}$ est le vecteur position et V est le potentiel.

Il existe plusieurs intégrateurs permettant de trouver les vitesses ou/et les positions à partir de l'équation 2.4. Verlet[33] est un algorithme fréquemment utilisé pour faire ces intégrations. Ce dernier permet de trouver la position d'une particule au pas suivant $t + \Delta t$ connaissant sa position à pas courant t ainsi que le pas d'avant $t - \Delta t$. Les équations permettant de trouver la position pas postérieure sont :

$$\vec{x}(t + \Delta t) = \vec{x} + \vec{v}\Delta t + \frac{\vec{a}(t)\Delta t^2}{2} + \frac{\vec{b}(t)\Delta t^3}{6} + O(\Delta t^4), \tag{2.6}$$

$$\vec{x}(t - \Delta t) = \vec{x} - \vec{v}\Delta t + \frac{\vec{a}(t)\Delta t^2}{2} - \frac{\vec{b}(t)\Delta t^3}{6} + O(\Delta t^4), \tag{2.7}$$

où $\vec{x}$ représente la position de la particule, $\vec{v}$ est sa vitesse, $\vec{a}$ est le vecteur accélération et $\vec{b}$ est la dérivée du vecteur accélération appelé également jerk. En sommant les équations (2.6) et (2.7) on obtient :

$$\vec{x}(t+\Delta t) = 2\vec{x}(t) - \vec{x}(t-\Delta t) + \vec{a}(t)\Delta t^2 + O(\Delta t^4). \tag{2.8}$$

Le problème principal de la dynamique moléculaire est d'avoir un bon potentiel d'interaction permettant de calculer adéquatement les forces. Néanmoins, d'autres problèmes et limitations se posent pour la dynamique moléculaire que l'on va énumérer dans la prochaine section.

2.3.2. Limitations

Malgré son principe simple et son efficacité dans la détermination exacte de la trajectoire atomique, la dynamique moléculaire souffre de certaines limitations. C'est évident que, à cause du manque de description explicite des corrélations électroniques dans son formalisme classique, la dynamique moléculaire donne parfois des résultats qui ne sont pas trop proches de ceux obtenus en *ab initio* ou dans l'expérience. C'est pour cette raison que le développement des potentiels de plus en plus adéquat est toujours un sujet actif de recherche. Au point de vue computationnel, et pour assurer une stabilité numérique, les simulations en dynamique moléculaire nécessitent des pas d'intégration temporelle courts de l'ordre d'une à deux femtosecondes ($\sim 1,2 \times 10^{-15} s$). Pour pouvoir atteindre des temps simulés à l'échelle des millisecondes, il faut exécuter une séquence en billion (10^{12}) de pas ce qui très couteux computationnellement et très difficile à réaliser même avec des superordinateurs possédant un très grand nombre de processeurs. La limitation temporelle pose problème dans la description des effets de la diffusion des défauts ponctuels dans les matériaux, car plusieurs de propriétés directement affectées par le mouvement de ces défauts sont observables à plus grande échelle que la microseconde. Compte tenu de ces limitations, il est indispensable d'utiliser une autre approche pour étudier la problématique de la diffusion des défauts ponctuels sur des échelles temporelles expérimentales. En effet, on aura recours aux méthodes Monte Carlo cinétique. Mais avant ça, nous devons décrire la théorie de l'état de transition qui est un concept de base pour la méthode Monte Carlo cinétique.

2.4. Théorie de l'État de Transition

La Théorie de l'État de Transition (TST) a été développée en 1935 par Henry Eyring [34] dans le but de comprendre et décrire les processus activés en calculant les taux associés aux transitions sur une surface d'énergie potentielle. Cette dernière, dans le cadre de la TST, est constituée de deux régions voisines caractérisées chacune par un minimum local et sont reliées par au moins un point de selle. Dans le cas où celui-ci est du premier ordre, ce qui est le cas d'un état de transition, la séparation dans la surface d'énergie potentielle est un hyperplan de dimension 3N-1. Le taux de transition peut être défini alors comme étant le flux à travers cet hyperplan.

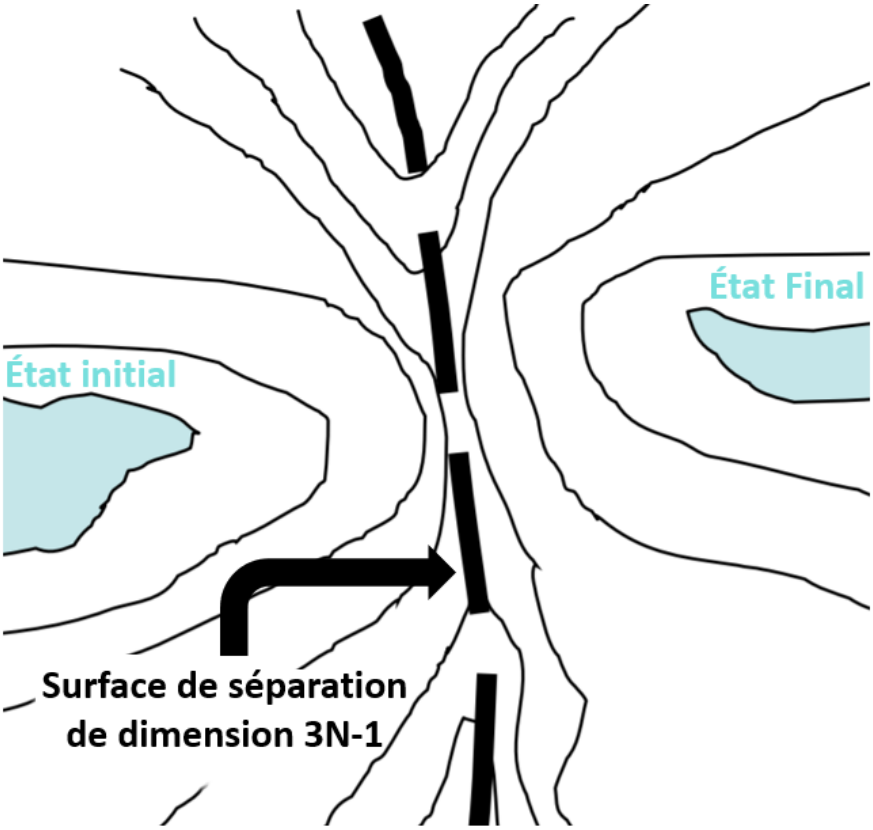

Figure 2.1. Surface d'énergie potentielle dans le cadre de la TST. La figure montre le lien entre l'état initial, le col et l'état final.

Vineyard [35] a montré que le taux de transition associé au saut d'un défaut s'écrit sous la forme :

$$\Gamma = \tilde{r} \exp\left[\frac{-\Delta F}{k_B T}\right], \tag{2.9}$$

où $\tilde{r}$ est une fréquence effective qui dépend des vibrations atomiques dans la zone entre le minimum et le point de selle, ΔF est l'énergie libre qu'il faut fournir pour passer d'un minimum local à un autre voisin et qu'on appelle également l'énergie libre d'activation, k_B est la constante de Boltzmann et T est la température absolue.

En tenant compte de la relation entre l'énergie interne E et l'énergie libre F ($F = E - TS$), l'expression devient :

$$\Gamma = \tilde{r} \exp\left[\frac{\Delta S}{k_B}\right] \exp\left[\frac{-\Delta E}{k_B T}\right]. \tag{2.10}$$

En posant $r^* = \tilde{r} \exp\left[\frac{\Delta S}{k_B}\right]$, on obtient :

$$\Gamma = \qquad r^* \exp\left[\frac{-\Delta E}{k_B T}\right]. \tag{2.11}$$

r^* est appelée fréquence d'essai, relative aux vibrations atomiques aux alentours du minimum initial et du point de selle. Si le cristal est formé par N atomes contenus dans un espace tridimensionnel, ceci implique 3N degrés de liberté pour le cristal et 3N variables pour l'énergie potentielle. La figure 2.1 montre une représentation schématique de la surface d'énergie potentielle (SEP). Pour calculer la fréquence d'essai, il faut évaluer l'intégrale de chemin sur l'ensemble de la SEP entre le minimum initial et le point de selle. Le calcul exact de cette intégrale est computationnellement très coûteux, ce qui implique la nécessité d'une approximation adéquate. Par conséquent, Vineyard a approximé l'énergie potentielle à des formes quadratiques à cause des faibles vibrations dans le bassin. Le calcul du taux de transition dans le cadre de cette approximation s'écrit alors :

$$\Gamma = \left(\frac{\prod_{i=1}^{3N} \nu_i}{\prod_{i=1}^{3N-1} \nu_i'} \right) \exp\left[\frac{-\Delta E}{k_B T}\right] \tag{2.12}$$

où (ν_i) et (ν'_i) représentent les fréquences modales de vibration au minimum et au point de selle respectivement.

2.5. Les méthodes standards de Monte Carlo cinétique

Les méthodes Monte Carlo, apparues vers la fin des années 1940, avaient comme but de résoudre certains problèmes calculatoires en utilisant des nombres aléatoires. Le nom de ces méthodes est inspiré d'un jeu pratiqué au cartier Monte-Carlo à Monaco. Le but de cette section n'est pas d'expliquer la méthode Monte Carlo (appelée également méthode Metropolis) mais plutôt les méthodes Monte Carlo cinétique (KMC) qui visent à simuler l'évolution d'un processus au cours du temps d'un état à un autre.

2.5.1. Historique

Dans les années 1960, les chercheurs ont pensé à profiter de la méthode Monte Carlo Métropolis pour faire évoluer dynamiquement les systèmes d'un état à un autre. La KMC a était appliquée pour la première fois pour étudier les dégâts d'irradiation causé par les rayonnements dans les métaux de fer, cuivre et tungstène [36]. Dans les vingt ans suivants plusieurs travaux utilisant cette méthode ont été menés pour traiter différents types de systèmes et problématiques comme l'adsorption [37] et la croissance de grains et la recristallisation [38]. Malgré tous ces utilisations, c'est seulement au début des années 90 que la terminologie Monte Carlo cinétique a été utilisé pour la première fois [39]. Grâce à sa popularité ainsi que l'éventail des applications, la méthode KMC a continué de croître et est devenue désormais un outil commun pour l'étude des matériaux sur de longues échelles temporelles surtout dans les sujets reliés aux dégâts de l'irradiation.

2.5.2. Principe

Dans les méthodes de KMC, on utilise la notion de taux de transition (telle que décrite dans la section 2.4) qui dépend de la barrière d'énergie pour passer d'un état à un autre avec des incréments de temps permettant d'avoir de décrire la cinétique du système. Le calcul des taux de transition associés aux événements rares (de hautes barrières et non pas ceux

qui correspondent à des vibrations atomiques) donne accès à de longues échelles de temps comparé à ceux obtenus par les méthodes standards comme la dynamique moléculaire.

Les étapes d'une simulation en KMC peuvent être résumées comme suit :

1. Former la liste de tous les taux r_i correspondants aux transitions possibles W_i à partir de la configuration en question.
2. Calculer la fonction cumulative $R_i = \sum_{j=1}^{i} r_j$ avec i = 1,2,...,N où N est le nombre total des transitions possible.
3. Choisir un nombre aléatoire $u \in [0, 1]$
4. Trouver l'événement i pour lequel $R_{i-1} \leq uR \leq R_i$ et l'exécuter
5. Mettre à jour le temps avec $t_{nouveau} = t_{ancien} + \Delta t$ où $\Delta t = -\frac{logu}{R_N}$
6. Retour à l'étape 1

Le problème de la Monte Carlo cinétique standard comment trouver la liste les événements possibles pour des systèmes non-simples au fur et à mesure que la simulation évolue.

2.6. ART cinétique (ARTc)

ARTc est un algorithme Monte Carlo cinétique hors réseau avec construction du catalogue à la volée. La méthode ARTc a été utilisé pour étudier des systèmes cristallins[40, 41, 42] aussi bien que amorphes[43]. Dans cette section on présentera les fondements spéciales de ARTc comparé aux méthodes standard de Monte Carlo cinétique.

2.6.1. Classification topologique

La classification topologique a pour but de traiter les structures hors réseau (non cristallines) et ce en considérant la topologie aux alentours de chaque atome au lieu de chercher les évènements liés à chaque atome. Ceci permettra ensuite, en utilisant le programme NAUTY [44], d'avoir une clé associée à chaque topologie et donc un temps de calcul très réduit. Pour obtenir la topologie entourant chaque atome, on connecte les atomes se trouvant dans une sphère de rayon donné (généralement on choisi 6 Å) avec une distance de coupure précise (généralement 2.8 Å mais elle peut varier dépendamment du matériau ; généralement le choix idéal une valeur comprise entre les distance premier et deuxième voisin et ce pour

inclure seulement les atomes en premier voisin). Pour le cas des alliages, des boucles automatisées sont ajoutés afin de distinguer différentes espèces atomiques. Le graphe (qui contient environ 80 atomes pour le cas du nickel pur par exemple) est ensuite analysé par NAUTY qui donnera un identifiant pour sa classe automorphe. Cet identifiant est identique pour des topologies semblables (le cas du réseau cristallin sans défauts par exemple) et différent pour des graphes différents. Une fois que les topologies sont identifiées, ARTc lancera la recherche des événements et ce par la méthode ARTnouveau qui sera le sujet de la prochaine section. La figure 2.2 illustre schématiquement le fonctionnement de NAUTY.

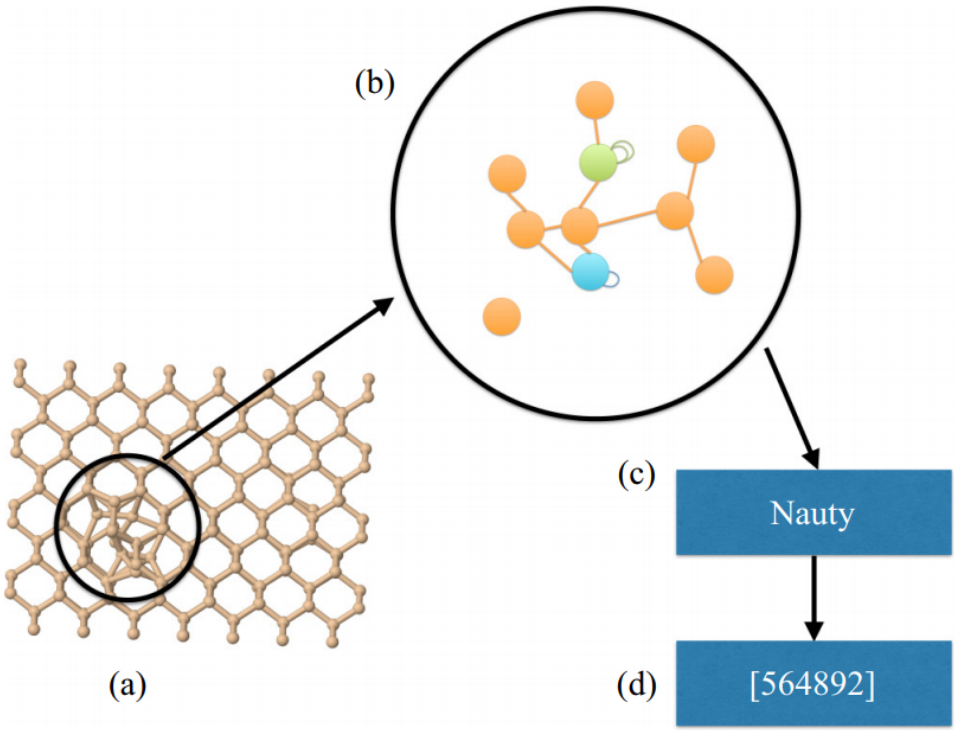

Figure 2.2. Classification topologique utilisant NAUTY[40]. (a) Les atomes situés dans une sphère d'un rayon donné autour d'un atome central sont extraits du système. (b) Les bords sont dessinés entre des paires d'atomes au-dessous d'une distance de coupure. (c) Le graphe résultant est analysé par NAUTY et (d) caractérisé par un identifiant unique.

2.6.2. ARTnouveau (ARTn)

Comme on l'a indiqué dans la partie 2.5, le problème de la Monte Carlo cinétique standard c'est la détermination des événements en trouvant les énergies d'activation associées.

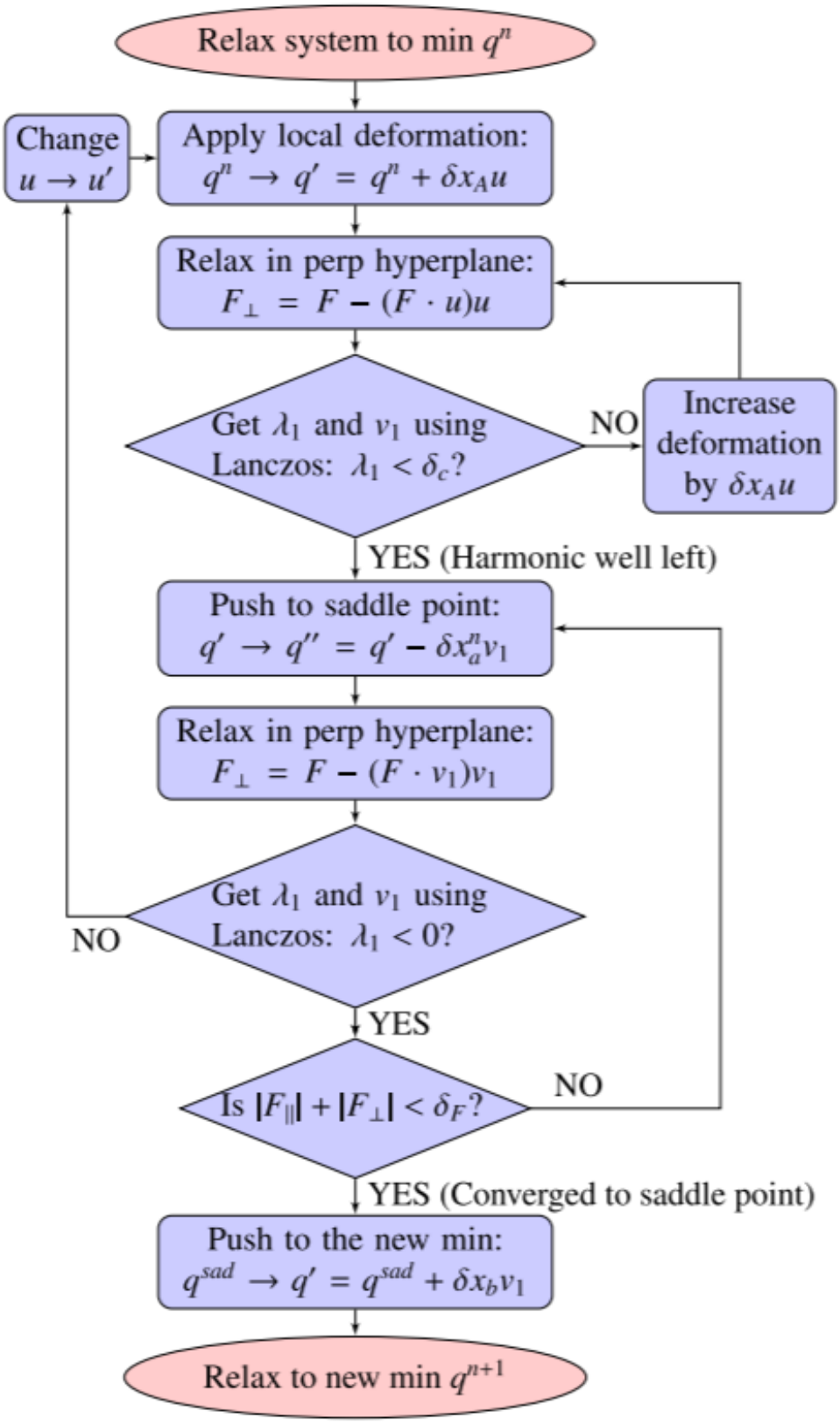

Figure 2.3. Organigramme de la méthode ARTnouveau[45].

Plusieurs méthodes ont été proposées permettant de trouver les chemins connectant un minimum local à ses voisins.

L'organigramme de ARTn est présenté dans la figure2.3.

Trois étapes constituent la base de la méthode ARTn :

1. **Activation :** Un atome ainsi que ses voisins sont légèrement déplacés (avec un certain champ de déplacement $\delta x_A u$) dans un certain nombre de directions aléatoires à partir d'un minimum local q^n. Ceci est poursuivi jusqu'à ce que la première valeur propre de signe négatif de la matrice Hessienne (nom attribué en mathématiques à la matrice des dérivées secondes d'une grandeur donnée, dans notre cas c'est l'énergie potentielle) apparaisse. D'habitude, la valeur utilisée de δx_A est entre 0.1 et 0.2 Å.
2. **Convergence vers le point de selle :** Tout en minimisant les forces dans l'hyperplan qui lui est perpendiculaire, le système suit cette direction correspondante à la valeur négative trouvée et qui permet de sortir du bassin.
3. **Relaxation :** Une fois que le système a convergé vers le point de selle (quand la condition de convergence imposée est vérifiée), la configuration est légérement poussé à partir du point de selle q^{sad} et l'énergie est minimisée pour atteindre un nouveau minimum q^{n+1}.

2.6.3. Applications de ARTc et limitations

Au cours des derniers 10 ans et un peu plus même, malgré qu'elle est toujours en développement, ARTc a été utilisée dans l'étude de plusieurs types de défauts dans différents types de matériaux cristallins et amorphes. Pour les systèmes cristallins, ARTc a été utilisé pour déterminer la contribution des lacunes dans la relaxation du silicium amorphe[43]. Concernant les cristaux, plusieurs matériaux ont été étudié. Par exemple, la cinétique détaillée des défauts intrinsèques[40] ainsi que des impuretés de lithium dans du silicium cristallin [46] a été étudié récemment montrant une richesse inattendue de leur dynamique pour un système aussi simple que le silicium. ARTc a été également utilisée pour comprendre la mobilité des atomes de carbone dans des joints de grains de fer [47]. À propos des travaux qui font l'objet de cette thèse, nous avons étudié la diffusion des défauts intrinsèques dans le nickel pur [42],

les effets du mouvement des défauts ponctuels dans les alliages ordonnés (le deuxième article dans cette thèse) et dans l'alliage désordonné de NiFe. Malgré l'applicabilité et le grand succès de ARTc dans plusieurs problématiques reliées aux défauts dans les matériaux, ARTc présente certaines limitations, comme toutes les méthodes numériques d'ailleurs. Un des problèmes de ARTc c'est le piégeage occasionnel du système dans les barrières non-diffusives que, malgré le développement de la méthode bac-MRM[48] (méthode du taux moyen de construction automatique par bassin inspiré de celle de Puchala[49]), reste un défi majeur pour automatiser la résolution. Ce problème apparait plus dans le traitement des interstitiels dont les barrières de diffusion sont très faibles. Un autre problème de ARTc, bien que très récemment des membres du groupe du professeur Normand ont essayé de résoudre, c'est de pouvoir traiter des boites non orthorhombiques ce qui permettra d'étudier les matériaux soumis à des conditions extrêmes comme des contraintes mécaniques. Aussi, une des améliorations à rajouter pour ARTc c'est d'inclure d'autres grandeurs physiques comme le facteur de compressibilité.

2.7. Conclusion

Dans ce chapitre, nous avons décrit les principales méthodes de simulations de la diffusion des défauts ponctuels dans les matériaux. Nous avons énuméré les limitations de la dynamique moléculaire après l'avoir décrit. Bien que les méthodes Monte Carlo cinétique standard permettent d'enlever ces limitations, nous avons montré qu'ils présentent certaines limitations quant au catalogue des transitions possibles ainsi que pour trouver les énergies d'activation associées. ARTc permet d'avoir une description exhaustive de l'évolution des défauts dans les matériaux. Dans les prochains chapitres, nous allons présenter nos résultats obtenus sous forme d'articles. Nous avons étudié dans le premier, le deuxième et le troisième article la diffusion des défauts ponctuels dans du nickel pur, dans les alliages ordonnés à base de nickel et dans l'alliage désordonné de NiFe, respectivement.

Chapitre 3

STUDY OF POINT DEFECTS DIFFUSION IN NICKEL USING KINETIC ACTIVATION-RELAXATION TECHNIQUE

3.1. Objectifs

Le but de cet article est d'étudier la cinétique exacte des défauts ponctuels intrinsèques dans le nickel pur. Dans la première partie de l'article on a fait une analyse, à travers la monolacune et la bilacune et la monointerstitiel, pour sélectionner le potentiel le plus adéquat entre quatre possibles pour le nickel, et ce en comparant les valeurs des énergies de migration obtenues avec celles obtenues en théorie de la fonctionnelle de la densité (DFT) et expérimentalement. Dans la deuxième partie, on a étudié la diffusion des agrégats de deux à cinq lacunes et interstitiels.

Mots clés : Nickel, défaut intrinsèque, ART cinétique, mécanismes de diffusion, paysage énergétique

Auteurs dans l'ordre : Sami Mahmoud, Mickael Trochet, Oscar A. Restrepo, Normand Mousseau

Journal : Cet article a été publié dans le journal "Acta Materialia" (5-year impact factor : 6.174). Référence : 144, 679-690 (2018)

3.2. Contributions des auteurs

— Sami Mahmoud (SM) a effectué toutes les simulations, l'analyse des données et la rédaction de l'article.

— Mickael Trochet (MT) a aidé dans la conception des outils d'analyse.

— Oscar A. Restrepo (OAR) a aidé dans l'interprétation des résultats.

— SM, MT et NM ont participé à la rédaction de l'article.

— NM a supervisé tout ce travail.

3.3. abstract

Point defects play a central role in materials properties. Yet, details regarding their diffusion and aggregation are still largely lacking beyond the monomer and dimer. Using the kinetic Activation Relaxation Technique (k-ART), a recently proposed off-lattice kinetic Monte Carlo method, the energy landscape, kinetics and diffusion mechanisms of point defect in fcc nickel are characterized, providing an exhaustive picture of the motion of one to five vacancies and self-interstitials in this system. Starting with a comparison of the prediction of four empirical potentials – the embedded atom method (EAM),the original modified embedded atom method (MEAM1NN), the second nearest neighbor modified embedded atom method (MEAM2NN) and the Reactive Force Field (ReaxFF) –, it is shown that while both EAM and ReaxFF capture the right physics, EAM provides the overall best agreement with ab initio and molecular dynamics simulations and available experiments both for vacancies and interstitial defect energetics and kinetics. Extensive k-ART simulations using this potential provide complete details of the energy landscape associated with these defects, demonstrated a complex set of mechanisms available to both vacancies and self-interstitials even in a simple environment such as crystalline Ni. We find, in particular, that the diffusion barriers of both vacancies and interstitials do not change monotonically with the cluster size and that some clusters of vacancies diffuse more easily than single ones. As self-interstitial clusters grow, moreover, we show that the fast diffusion takes place from excited states but ground states can act as pinning centers, contrary to what could be expected.

3.4. Introduction

Point defects play an important role in materials science as their presence can affect physical and mechanical properties such us electron mobility, conductivity, ductility, strain resistance and more [50, 51]. Yet, in spite of their importance, many details are still missing regarding the simplest atomistic mechanisms such as those involving point defect diffusion, mobility and clustering.Because following the kinetics at this level is difficult experimentally, we have to rely largely on computational approaches to capture the atomic details of these mechanisms. For this, however,we need a proper description, using either ab initio approaches or accurate empirical potentials, as well as comprehensive sampling methods [52]. For full benefits, these two requirements must be brought together as only comprehensive sampling methods can make good use of high quality physical description and vice versa.Such requirements are easier stated than realized, however, as ab initio methods are too costly to apply to large systems, preventing extensive strain-free sampling, while empirical potentials, fitted to a small number of properties, often lack in accuracy when applied to generic configurations or non-tested mechanisms. We are interested, here, in fully characterizing the energy landscape and kinetics of small assemblies of self-defects in the simple bulk fcc Ni systems. To realize this study on the required scale, the use of ab initio approaches is not feasible so it is necessary to turn to empirical potentials developed for Ni crystalline environment. Much effort has gone, over the years, into developing general empirical potentials for such simple fcc metals [53]. Daw and Baskes proposed, many decades ago [26, 31], a semi-empirical approach based on Rose's universal scaling law [27], that attempts to replicate,at the classical level, some features of the electronic density interaction. Over the years, a number extensions to EAM were introduced. For example, a supplementary angular term has been added to describe non-fcc metals, leading to the modified embedded-atom method (MEAM) [54, 28, 55, 56]. The original MEAM formalism works very well for a large range of materials but suffers from various structural instabilities and a fundamental difficulty in reproducing surface reconstructions. Lee et al [29, 57, 58] introduced a modification of the

original MEAM formalism to extend the range of the potential and the many-body screening, leading to the second nearest-neighbor MEAM (MEAM2NN), that describes correctly physical properties of many materials. More recently, a totally different approach was taken to develop a framework for a universal empirical potential that incorporates a bond-order approach and a self-coherent charge distribution [30]. Over the last decade,the Reactive Force Field (ReaxFF) has received considerable interest due to its flexibility and its overall excellent capacity at reproducing physical properties [59, 60]. While some of these potentials have been out for a long time,they have not been extensively compared on their capacity at describing self-defects thermodynamic and kinetic properties.Because defect kinetics can be relatively slow, standard methods such as molecular dynamics are not ideal for comparing the sevarious models. This is why we turn, here, to the kinetic Activation-Relaxation Technique (k-ART), a unique off-lattice kinetic Monte-Carlo algorithm with on-the-fly cataloging [61, 48]. K-ART has been shown to provide efficient and extensive sampling of energy landscapes as it incorporates exactly all elastic effects at both minima and saddle points for a precise kinetic description of complex materials ranging form defects in metals to long-time evolution of amorphous materials [43, 62, 63, 64, 65]. In this paper, we use k-ART to compare self-defect formation energy and diffusion properties of five vacancies and interstitials in nickel, a simple fcc metal, using four empirical potentials: EAM,MEAM1NN, MEAM2NN and ReaxFF. Assessing these four potentials for the one and two vacancies and one self-interstitial atom (SIA)systems, we find that both EAM and ReaxFF recover the fundamental physical properties obtained experimentally or predicted by ab initio calculations. Results obtained using EAM, however, are in overall better agreement with experiment results than those obtained with ReaxFF. Focusing on EAM, we characterize the diffusion mechanisms and pathways for small self-defect aggregates,providing a complete picture of the fundamental diffusion mechanisms in nickel and identifying a number of mechanisms that had not be observed before. Moreover, we show that diffusion of vacancy clusters is

faster than single vacancy, even for relatively large clusters, although the trend is not monotonic. For interstitials, the situation is more complex and we demonstrate that the diffusion direction is affected by the clusters size confirming recent experiment analysis [66].

3.5. Methods

3.5.1. Potentials

To facilitate the comparison of the effects of various forcefields on the defect kinetics in Ni, we use a version of k-ART coupled to the LAMMPS (Large-scale Atomic/Molecular Massively Parallel Simulator) library [67]. Four Ni potentials are considered in this study:the Embedded Atom Method (EAM), the original Modified Embedded Atom Method (MEAM), the MEAM based on the second-neighbor formalism (2NN) and the Reax forcefield (ReaxFF). EAM parameters are those of the universal function for nickel system used the first time by Foiles et al [31] to compare properties of pure metals. MEAM1NN parameters are those of Ni4 that reproduces the best available experimental results in comparison with Ni1, Ni2 and Ni3 parameter sets in nickel system in the studies of Baskes [68] and Cherne et al. [69] MEAM2NN parameters are taken from Lee et al's [58] work. ReaxFF parameters, developed by Zou et al, [60]have been found to give in good agreement with DFT calculations for pure nickel systems.

3.5.2. Kinetic ART

All simulations are performed using the kinetic activation relaxation technique (k-ART) [61, 48, 70] (figure3.1), an off-lattice kinetic Monte Carlo method based on the activation relaxation technique(ART nouveau) [71, 72] for event searching and the topological analysis package NAUTY [44] for generic classification. While k-ART is described in more details elsewhere [43, 45], the basic algorithm can be summarized in the following steps:

1. Starting with a system relaxed in a local minimum, the local topology associated with each atom is calculated using NAUTY;for Ni, the graph includes all atoms within a 6 Å radius of the central atom, representing around 79 atoms, with vertices drawn

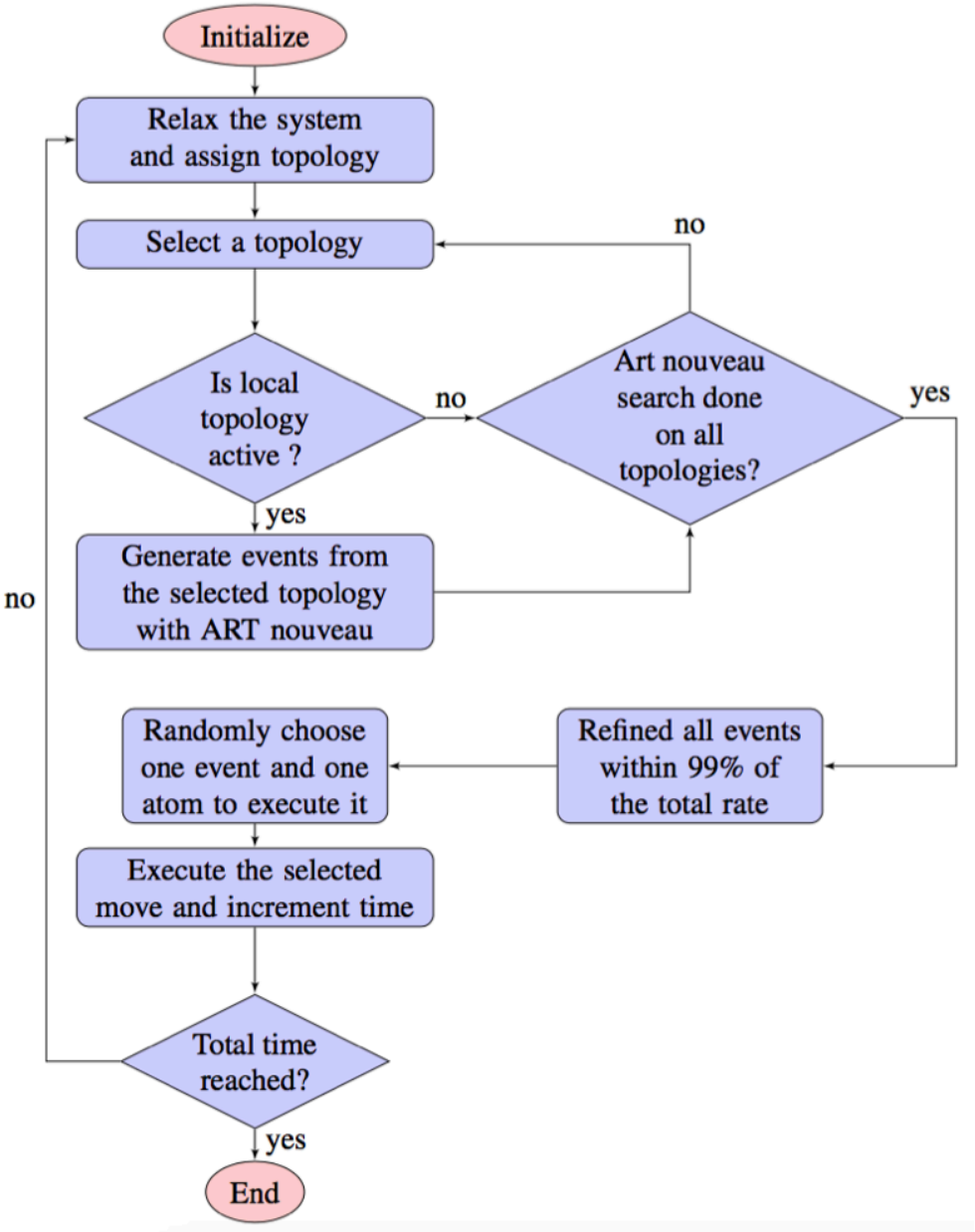

Figure 3.1. Kinetic Activation Relaxation Technique (kART) principle.

between those within 2.6 Å of each other. This connectivity graph is sent to NAUTY which returns a unique identifier characteristic of its automorphic group.

2. If the topology is present in the event catalog, associated event sare loaded into the active event list; if not, 50 ART nouveau searches are launched to identify diffusion mechanisms and pathways associated with this topology with additional searches performed for frequently found events to ensure that the catalog is complete. We

can assess the completeness of the catalog by comparing events found in independent runs on the same system. In the current work, we find that 50 searches is more than sufficient for all systems except for monovacancy,where we used 100 searches. Not counting events associated with the perfect crystal or with a barrier above 5 eV, a single vacancy in Ni is associated with two events for each potential as it will be indicated later in monovacancy section. In all cases,events are reconstructed to ensure that the saddle point connects two nearby minima.

3. A first evaluation of the KMC timestep is made using the rates of events available for the current conformation. All events with an occurrence probability of 1 in 10 000 or more are then fully reconstructed and their transition state is relaxed to ensure that elastic and configurational effects are exactly taken into consideration. Once this is done, specific rates and the overall KMC timestep are recalculated.
4. A event is selected following the standard KMC algorithm [73],the time and the configuration is updated and the algorithm goes back to step B. Following the standard practice with KMC, a constant pre-exponential factor is used. This approximation was shown to be valid for close-packed metallic systems [74, 75].

K-ART provides an extensive representation of the energy landscape surrounding each local minimum, describing in full detail the local activated barriers and connected nearby energy minimums. While this information is essential for constructing a reliable evolution pathway, it also offers a rich view of the system's structure and potential kinetics. Because it uses an on-the-fly event searching approach and topological classification for cataloging, k-ART can be applied to complex materials and is not restricted to crystalline conformations. Over the last few years, it has been applied to systems such as defects in crystalline metals and semiconductors [63, 40], amorphous [43] and ion bombarded silicon [48, 65] and metallic alloys [64].

3.5.3. Simulated system

Vacancies are created by removing atoms from crystalline sites while interstitials are formed by inserting atoms in the central octahedral site of selected fcc cells. All simulations are launched from a fully-relaxed local minimum. Simulations are run for a minimum of 100 and up to 10 000 KMC steps, not including intrabasin jumps, or flickering states, that are resolved analytically using the basin-autoconstructing Mean Rate Method (bac-MRM) [48] built upon Puchala et al.'s Mean-Rate Method [49]. The simulation box is selected after testing convergence on both defect types using EAM potential. Following Ref., [76], convergence is assumed when the energy difference between the first and the last values of formation energy for a specific system in three successive increasing volumes evolves by less than 0.01 eV. A complete table describing this evolution is presented as supplementary material. It shows that even for relatively simple systems such as those studied here, a cubic fcc box of at least a $9 \times 9 \times 9$ cells (2916 crystalline sites) is necessary to ensure convergence for all systems. In the following, volume is optimized to ensure zero pressure at T = 0 for each potential and simulations are run at T = 600K. Since the event catalog is generated at 0 K, the choice of simulation temperature does not affect the list of events, the catalog nor the reconstructed diffusion mechanisms. However, it allows the system to sample by itself a wider range of pathways, making it more straightforward to demonstrate the richness of energy landscape.

3.5.4. Analysis

The formation energy for n vacancies (v) or interstitials (i) is given by:

$$E^F_{nv,i} = E_{N-n} - (E_N \times \frac{N-n}{N}) \tag{3.1}$$

where E_N is the total energy of a perfect crystalline system with N nickel atoms and E_{N-n} is the system's total energy with n vacancies or interstitials. The binding energy of n vacancies (v) or interstitials (i) is given by:

$$E^B_{nv,i} = nE^F_{1v,i} - E^F_{nv,i} \tag{3.2}$$

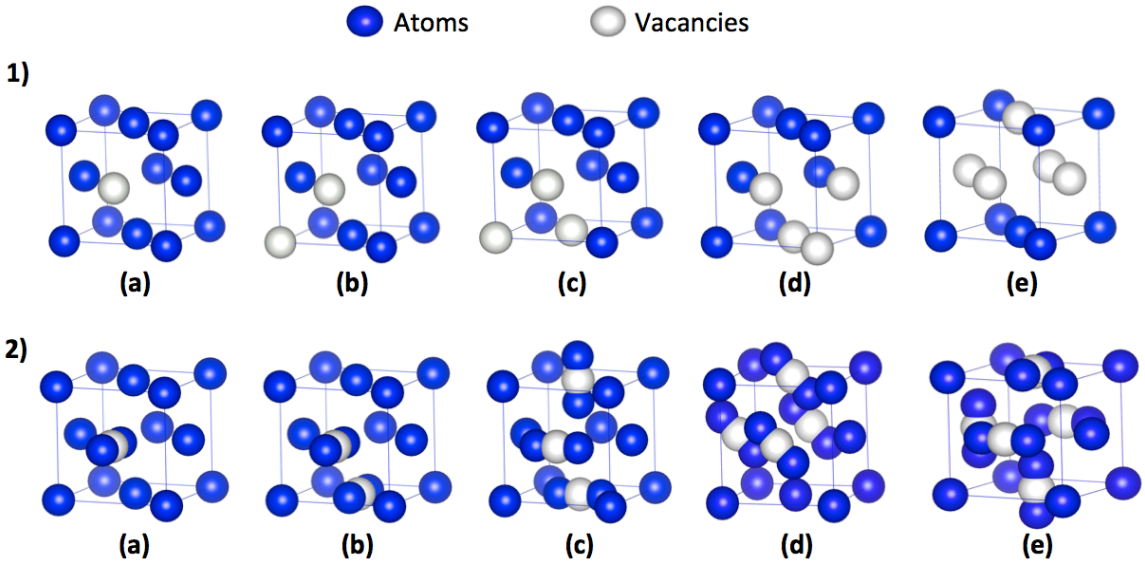

Figure 3.2. Schematic illustration of lowest-energy states for one to five self-defects in nickel using EAM potential. 1) Ground states for vacancies and 2) self-interstitials. a), b), c), d) and e) present the structure with one, two, three, four and five mono-self-defects for each case.

In all KMC simulations, runs begin with an energy minimizationusing the Fast Inertial Relaxation Engine (FIRE) method. In thesesimulations, we use a CPU with a 12-core nodes composed of twoprocessor Intel Westmere-EP X5650 hexa-cores, @2,667 GHz. To give an idea of the speed of the simulation, it takes 7 min, 9.36 h,16.23 h and 75 h using EAM, MEAM1NN, MEAM2NN and ReaxFF potentials, respectively, with 12 nodes to run 100 k-ART steps in the case of a single vacancy, which corresponds to a simulation time between 0.5 and 8 ms, depending on the exact energy barrier predicted by each potential.

3.5.5. Comparing potentials

Because large simulation cells are required to explore the energy landscape of even small ensembles of self-defects, it is not possible to proceed with ab initio description. We therefore compare first the four empirical potentials described above for simple systems for which ab initio and experimental results are available: the mono and di-vacancy as well as the self-interstitial.

Monovacancy diffusion is studied with each potential (EAM,MEAM1NN, MEAM2NN and ReaxFF) over 100 k-ART steps, with the complete event catalog obtained before the

Table 3. I. Formation (E^F_{1v}), migration for direct vacancy jumps to first ($E^m_{1v(1nn)}$) and activation energies for second ($E^a_{1v(2nn)}$) nearest neighbor sites in nickel. Comparison between values obtained in this work and other works is also presented.

Method	$E^F_{1v}(eV)$		$E^m_{1v(1nn)}(eV)$		$E^a_{1v(2nn)}(eV)$
	This work	Other works	This work.	Other work	This work
EAM	1.63	1.60[77]	1.07	1.08[31]	4.28
MEAM1NN	1.46	1.48[68]	1.22	1.22[68]	4.44
MEAM2NN	1.56	1.51[77, 58]	1.25	-	4.25
ReaxFF	1.92	-	1.35	-	4.83
DFT	-	1.62[78] ,1.42[79]	-	1.51[78]	-
Experience	-	1.74[80]	-	1.3-1.5[81], 1.32[66]	-

first step. We obtain the same diffusion mechanisms for all potentials. The vacancy diffuses from a crystalline position to one of the twelve first nearest-neighbor lattice sites by crossing a saddle position situated halfway between nearby lattice sites. The migration and formation energies for this mechanism obviously depend on the specifics of the potentials and are listed in Table3. I. As expected we recover the previously calculated formation energies for each potential to within a few 0.01 eV, with the difference largely due to size and convergence effects. Migration barriers associated with first-neighbor jumps are much more precise as finite-size effects are,to first order, the same at the minimum and the transition state.We also report in Table3. I the energy barriers associated with a direct jump to the second nearest-neighbor sites for the mono-vacancy. To our knowledge, this mechanism, associated with a high-energy barrier that varies between 4.25 and 4.83 eV depending on the potential, had not been reported previously. Its transition point corresponds to an atom moving by a half-lattice parameter in the $\langle 100 \rangle$ direction and demonstrates the capacity of k-ART to provide extensive event cataloging.

As also reported in Table 3. I, DFT calculations and experiments present a range of formation energies for the monovacancy, with EAM and the two MEAN potentials providing values that are be-tween the limits set by DFT and experiments. EAM predicts a formation energy compatible with DFT and within 0.11 eV of the measured value, closest to experimental value of 1.74 eV[73].ReaxFF, for its part, is 0.3-0.5 eV above DFT and over-estimates the experimental value by 0.18 eV. The monovacancy diffusion barrier energy is found experimentally to be between 1.3 and 1.5 eV [81] compared with the DFT value at the lowest

limit (1.29 eV [78]). Here ReaxFF predicts a barrier within the experimental range, 0.06 eV above DFT prediction, while both MEAM potentials are slightly below, at 1.22 eV and EAM underestimates the barrier by about 0.23 eV.

To further differentiate potentials, we turn to divacancies. Simulations are started with two vacancies distant by 12.2 Å. It takes 34KMC steps and 95ms using EAM potential to bring the two vacancies in nearest-neighbor position, representing the ground state for this potential. The formation energy in the ground state varies from 2.89 to 3.59 eV depending on the forcefield as indicated in Table 3. II, in general agreement with DFT predictions that estimate the formation energy to be 2.86 eV [78], except for ReaxFF that overestimates that value by 0.73 eV.

Figure 3.3 gives the binding energy as a function of distance for the four potentials, showing two very different behaviors. For MEAN1NN and MEAM2NN, the divacancy is unstable in first and second neighbor positions, with the ground state in fourth neighbor (more stable by 0.36 eV with respect to first neighbor,with a 0.19 eV binding energy). EAM and ReaxFF, for their part,show a more physical and very similar picture, with the binding energy decreasing smoothly with distance and a ground state in first neighbor position, associated with a bonding energy of 0.23and 0.29 eV, respectively, in agreement with experiment (0.33 eV[82]) and a very slight repulsion at the third and fourth neighbor,with the long-range interactions dying faster for EAM. DFT, for its part, largely underestimates the binding energy of divacancy system with respect to experiment and predicts 0.01 eV in nearest-neighbor position [78]. This mismatch is likely associated with the small 108-atom system used, insufficient to hide the long-range elastic interactions with the PBC images.

Barriers connecting the various configurations are shown in Table 3. III for the EAM potential. Similar tables for ReaxFF, MEAM1NN,MEAM2NN potentials are presented in supplementary material.Since MEAM potentials provide the wrong ground state for the divacancy, this defect kinetics is discussed here only for EAM and ReaxFF. The dominant diffusion process for both EAM and ReaxFF is the diffusion by rotation. This latest takes place when one atom diffuses in one of its 1nn vacancy while keeping the divacancies in its

Table 3. II. Diffusion proprieties of the divacancy in nickel using various potentials. Diffusion coefficient D and formation energy E_{2v}^F in the most stable configuration at T = 600 K, with a KMC prefactor of 10^{13} Hz.

Potential	$D(10^{-10}cm^2s^{-1})$	$E_{2v}^F(eV)$
EAM	4875	3.03
MEAM1NN	0.41	2.89
MEAM2NN	6093	3.29
ReaxFF	3.16	3.59

Table 3. III. Relative configuration (ΔE) and barrier energies for pathways between the five dominant bound states for the divacancy complex using EAM potential (x nn). All barriers are associated with an atom jumping over a 1nn distance, except for the barrier labeled with star where the jump is to 2nn. Energies are in eV

To \ From	1nn	2nn	3nn	4nn	5nn
ΔE	0	0.20	0.23	0.23	0.23
1nn	0.68	1.03	0.89	0.87	-
2nn	1.23	-	1.01	-	1.07
3nn	1.11, 4.40*	1.04	1.05	1.01	-
4nn	1.10	-	1.01	-	1.07
5nn	-	1.07	-	1.07	-

.

ground state. The energy barrier for this mechanism is found to be 0.68 and 0.96 eV for EAM and ReaxFF, respectively.

The four potentials provide the same ground state for the self-interstitial, with the additional atom sharing a site by forming a dumbbell centered on a lattice site with the two atoms positioned at a distance of $3/5a_0$ (2.12 Å) in the $\langle 100 \rangle$ direction. Formation energy for the four potentials is relatively similar as indicated in Table 3. IV, between 4.21 and 4.78 eV, above the DFT results of 4.07 eV[83]. These latter results are obtained on a 108-atom cell and could be affected by long range elastic effects associated with the insertion of an interstitial in a close-compact network.

These potentials differ, however, in their diffusion pathways. EAM identifies three different mechanisms shown in figure 3.4. In the first mechanism, shown in figure 3.4a A, an atom leaves the dumbbell by jumping to a first neighbor site to form a new dumbbell in a perpendicular direction with respect to the initial dumbbell crossing an energy barrier of

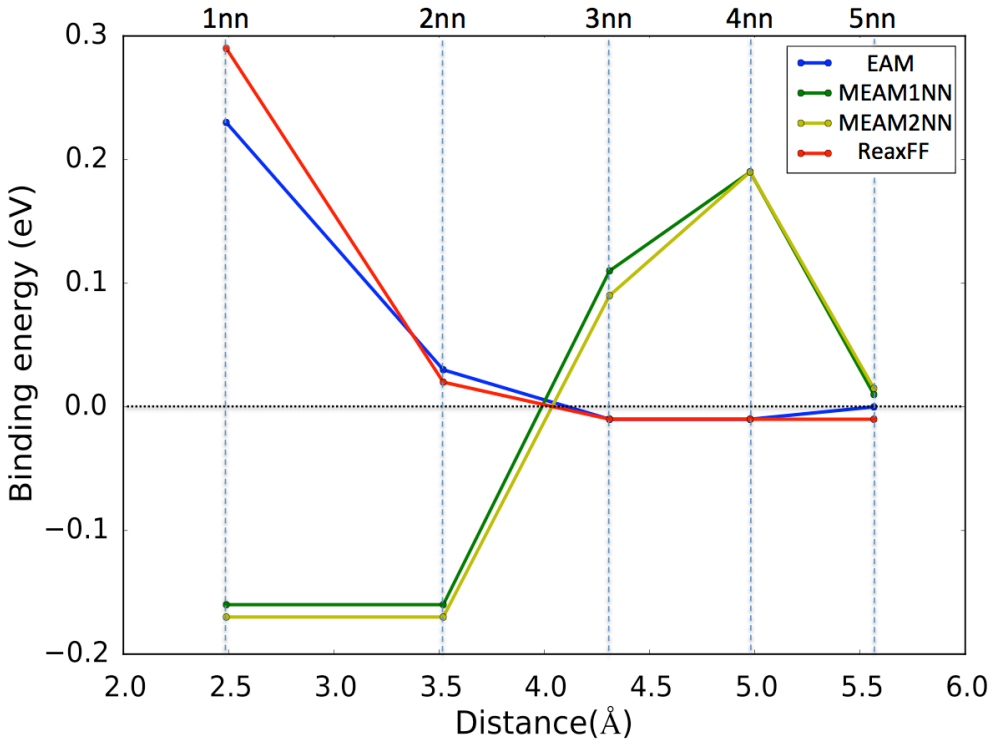

Figure 3.3. Binding energy for divacancies in nickel as a function of first (1nn) to fifth (5nn) nearest-neighbor distance between vacancies for various potentials.

0.14 eV. At the saddle, the diffusing atom is situated in a position between the tetrahedral and octahedral sites. This is in agreement with DFT calculations [83] that show a similar mechanism with an energy barrier of 0.14 eV and with experimental results that estimate the energy barrier for this transition to be 0.15 eV. The second mechanism (B) is similar to the first one but the atom in saddle configuration is situated nearer to the octahedral site with an energy barrier of 0.17 eV. The third diffusion mechanism for the nickel SIA is associated with a saddle point at the octahedral site with a 0.35 eV barrier and it's shown in figure 3.4a C.

ReaxFF, as shown in figure 3.4b B, reproduces EAM's first mechanism where the atom is in the saddle configuration but is situated 0.1 Å closer to the nearest unoccupied octahedron site, with a 0.25 eV barrier, 0.10 eV above DFT and experiments. The second mechanism, shown in figure 3.4b D, is not observed with EAM. It corresponds to a rotation of the dumbbell followed by a shift of one atom of its constructing atom to recreate a dumbbell in

Table 3. IV. Formation and migration energies of 1SIA in nickel using different potentials. The considered formation energy is relative to ⟨100⟩ dumbbell. Energies are in eV

Method	Formation energy (eV)		Migration energy (eV)	
	This work	Other works	This work	Other works
EAM	4.54	5.05[31]	0.14	0.14[31]
MEAM1NN	4.37	4.24[68]	0.18	0.28[68]
MEAM2NN	4.21	4.88[58]	0.27	-
ReaxFF	4.78	-	0.25	-
DFT	-	4.07[83]	-	0.14[84], 0.15[85], 0.18[77]
Experience	-	-	-	0.15[86], 0.16[66]

the same initial direction but in the nearest position. The energy barrier of this mechanism is high, at 0.59 eV.

Although 1NN and 2NN MEAN forcefields predict elastic constants more precisely than EAM [58], they do not reproduce the single vacancy, divacancy and the self-interstitial energetics accurately when compared with DFT and experiments. EAM and ReaxFF,for their part, show the right overall physics, although they each suffer from some inaccuracies over these three defects. Nevertheless EAM provides surprisingly superior results to ReaxFF. In the rest of the paper, we therefore use EAM for all our calculations.

3.6. RESULTS

We now consider the energy landscape and diffusion mechanisms of vacancy and self-interstitial clusters, with two to five self-defects, using EAM potential.

3.6.1. Vacancy clusters

Simulations for the two to five vacancies are started with the defects placed at a large enough distance from each other to ensure minimal interaction.

3.6.1.1. *Divacancy*

As discussed above, vacancy pairs form rapidly into dimers with the two point defects at a first nearest-neighbor distance from each other. From the ground state, the dominant diffusion mechanism,with a 0.68 eV barrier, is a rotation that involves migration of one atom in a nearest-neighbor site while keeping the dimer in 1nn conformation (1nn-dimer), in

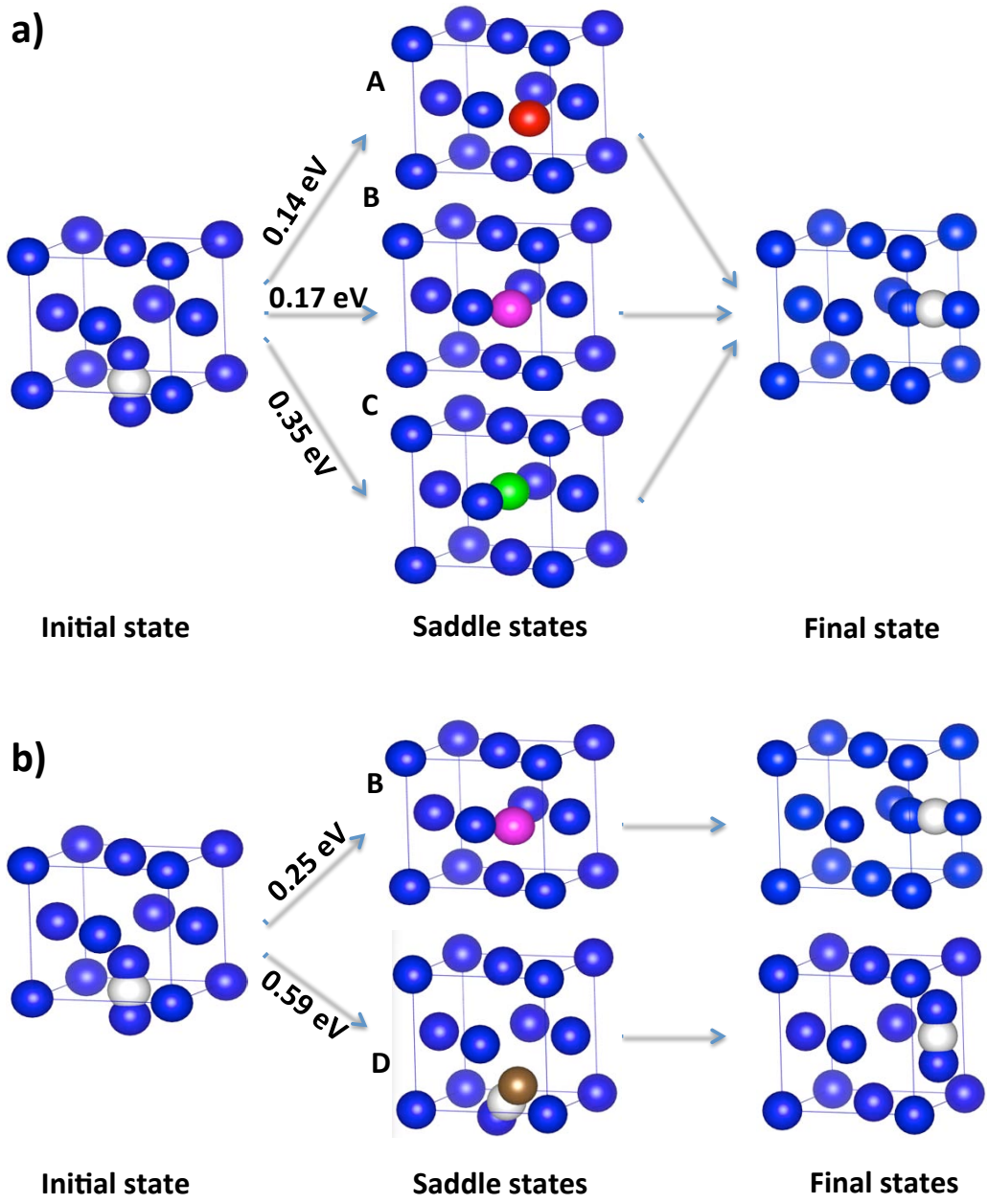

Figure 3.4. Mono-self-interstitial of nickel diffusion mechanisms using a) EAM and b) ReaxFF potentials. A,B,C,D are the possible saddles for each mechanism. A: the atom is in a position between the octahedron and tetragonal sites (This state is obtained by both EAM and ReaxFF potentials with energy barriers of 0.14 and 0.25 eV, respectively). B: same as for A but the atom is nearest to the octahedron site. C: the saddle configuration as the diffusing atom is in the octahedron position. D: the dumbbell turns in the $\langle 111 \rangle$ direction before rotating and shifting to create a new dumbbell in the same initial direction and in nearest neighbor site. The interstitial atom is indicated in white at the minimum position and various colors at the saddle. Ni atoms in crystalline position are in blue.

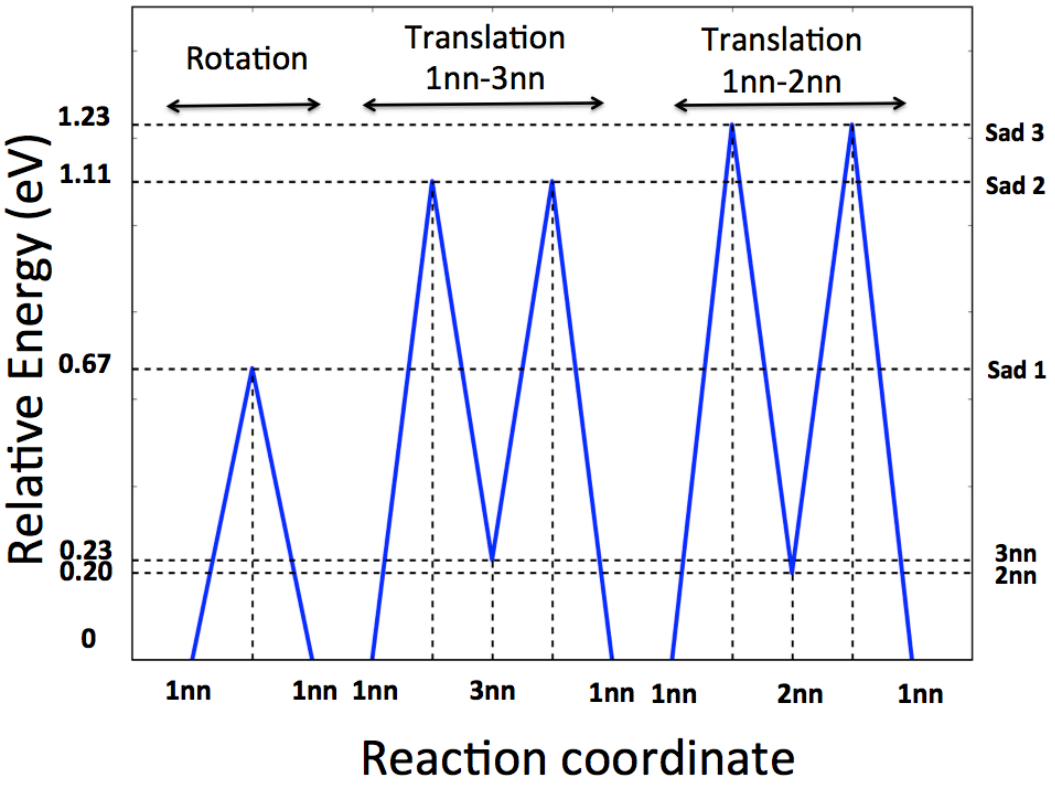

Figure 3.5. Dominant diffusion mechanisms for divacancies in nickel. Energies for saddles points (sad1, sad2 and sad3) and meta-stable (meta1 and meta2) are shown in figure for each mechanism. Rotation takes place through a one-step mechanism moving one atom by a 1nn distance to a 1nn vacancy site. Translation takes place through the diffusion of one atom into a 1nn vacancy site forming dimer of vacancies in 3nn and 2nn distance. The diffusion of a second atom then reforms a dimer of vacancies in 1nn.

agreement with experimental results and DFT calculations [78]. Divacancies can also diffuse through pure translation, where a vacancy migrates to a nearest-neighbor site forming a dimer of vacancies in third neighbor position (3nn-dimer) with a 1.11 eV barrier. This conformation is metastable,0.23 eV above the ground state, and reforms into a 1nn-dimer crossing a 0.89 eV barrier. From the 3nn-dimer, reconstruction of the 1nn-dimer is the most probable move (see Table 3. III) as the barrier further separating the vacancies is 1.01 eV, implying a probability of 91% at T = 600 K to reform the 1nn-dimer. Other less probable breaking mechanisms going through an intermediate 2nn-dimer are also possible. A detailed description of the energetics of the rotation and translation mechanisms is given in figure with the transition details between the first five states provided in table 3. III.

3.6.1.2. *Trivacancy*

The three isolated vacancies aggregate to form the ground state in 0.25 ms and 190 KMC steps, with the three vacancies in first neighbor (1nn) position, forming an equilateral triangle as indicated in figure 3.2. This cluster is characterized by a binding energy of 0.68 eV (0.23 eV per vacancy) as measured from the three isolated vacancies. Since divacancy diffusion is faster than the monovacancy, the initial formation of a dimer is relatively slow (taking 0.14 μs). Once a divacancy is formed, it rapidly finds its way to the remaining monovacancy. As clusterization takes places, the system visits a rich space of configurations, with 227 different k-ART topologies visited out of the 1217 found.

Due to fcc symmetry, the trivacancy cluster can diffuse through rotation of the cluster, with one vacancy jumping to a first neighbor site, without breaking the triangle, crossing a barrier of only 0.35 eV. The cluster is stable and can be broken only by crossing barriers of 0.84 and 0.86 eV, corresponding to jumps of one of the vacancies into 3nn and 2nn position, respectively, as measured from the remaining divacancy. Along these less probably pathways, the trivacancy complex diffuses by transiting between ground and excited states situated at 0.23 and 0.19 eV above the fundamental state.

3.6.1.3. *Tetravacancy*

Starting from four isolated vacancies, the ground state for the tetravacancy is reached in about 4 μs and 102 KMC steps. Aggregation occurs in steps, with the formation a rapidly diffusing divacancy that absorbs a third vacancy, with the cluster moving to the remaining vacancy consecutively. The ground state is characterized by four vacancies forming a regular tetrahedron with edges of 1nn distance between each pair of vacancies as indicated in figure 3.2. Binding energy for the ground state, as measured from four isolated vacancies, is 1.36 eV, or 0.34 eV per vacancy. 3610 topologies were identified by kART, with 674 of them visited, showing the rapid increase in complexity with the number of defects.

The shortest diffusion mechanism for the tetravacancy complex is described in figure 3.7. Diffusion takes place in four steps by the migration of one vacancy that jumps to 1nn

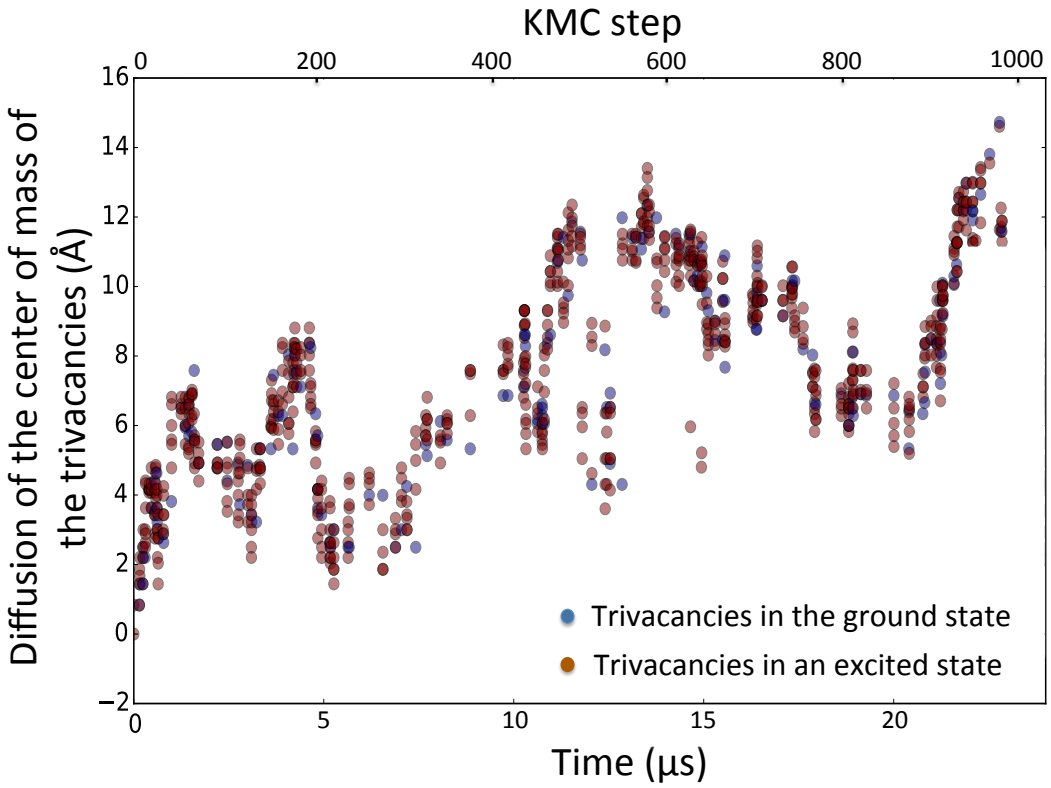

Figure 3.6. Center of mass diffusion as a function of time for trivacancies in Ni. Diffusion and time are measured from the position of the first occurrence of ground state. Blue and brown symbols corresponds to trivacancies in fundamental and excited states respectively.

positions at each step. The first jump is energetically expensive with a barrier of 1.07 eV; with such high barrier, the tetravacancy ground state is largely a pinning center with a two microseconds diffusion timescale at 600 K. Once this barrier is crossed, the diffusion goes on rapidly crossing barriers of 0.26, 0.51 and 0.64 eV to a new ground state situated in another corner of the Ni unit cell as indicated in figure 3.7.

A second important diffusion mechanism for tetravacancy system includes the same initial transition as in the first mechanism. The system then jumps to higher energy state leading to four vacancies further than that in the first mechanism in the second step, crossing a 0.70 eV of energy barrier that brings the system to a state 0.20 eV above the ground state, corresponding to the second excited state in the tetravacancy system. With two successive inverse transitions to those in the two second steps, the ground tetrahedron is reformed. The migration barrier associated with mechanism is equal to 1.13 eV.

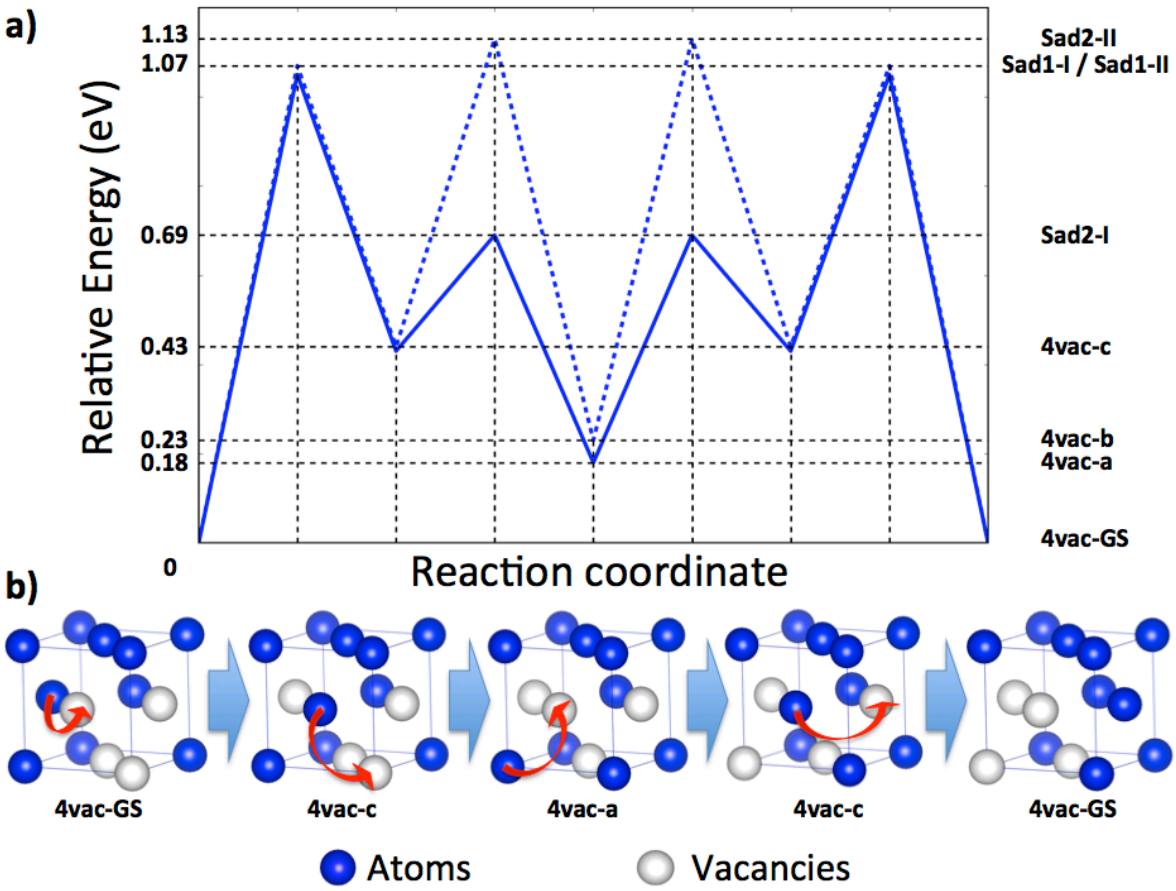

Figure 3.7. Tetravacancy diffusion mechanism in nickel from ground state. a) Energy landscape for the dominant (continuous blue line I) and the second diffusion mechanisms (dotted blue line II). b) Atomistic representation of the dominant diffusion mechanism. States 4vac-GS, 4vac-a, 4vac-b, 4vac-c are ordered from the most to the least stable states along the pathway. Red arrows indicated the changes between conformations.

3.6.1.4. *Pentavacancy*

Due to the complexity of the tetravacancy diffusion mechanisms and the low mobility of the monovacancy, the aggregation into a pentavacancy of five isolated vacancies is relatively a slow process.Since the energy landscape for both the monovacancy and tetravacancy systems has been explored, we therefore start the exploration of this more complex system with the five vacancies already aggregated.

The ground state (GS) for this system forms an equilateral pentahedron in $\langle 100 \rangle$ direction with a square base and an edge of 1nn distance and 2nn length for the diagonals, with a binding energy of 1.91 eV or 0.38 eV per atom (figure 3.2). As in the case of tetravacancies,

diffusion takes place by a successive migrations of one vacancy into a 1nn crystalline position. The first move, from the ground state, requires crossing a 0.58 eV energy barrier. The shortest diffusion mechanism, described in figure 3.8, takes approximatively 5 ns. This mechanism allows the diffusion of the fundamental pentahedron through a rotation into a new direction as defined by a line passing from the center of mass and the summit of the cluster. This mechanism diffuses the pentavacancy system by about 1.97 Å in around 2 ns.

A second mechanism, with a 0.66 eV of energy barrier, is related to the migration of the atom witch is symmetric to the summit of the pentahedron through the base to one of its vacancy cites. This mechanism is non diffusive but leads to a same-cell rotation of thepentahedron into to a new perpendicular ⟨100⟩ direction.

A 5-step diffusion mechanism is also observed. A 1nn atom in the parallel plane to the base of the pentahedron and passing from summit first migrates to the summit, after crossing a barrier of 0.71 eV, leading to a deformed pentahedron. This state is situated at0.50 eV from the GS. Then, by crossing a barrier of 0.21 eV to reach the first excited state of this system (0.29 eV from the GS). Starting from this configuration, the four vacancies cross a symmetric barrier of 0.56 eV, leading to an overall migration barrier of 0.85 eV.

A number of mechanisms with energy barriers higher than 0.97 eV are also found but, being rare, they are not discussed here.

3.6.2. Self-interstitial clusters

We now turn to systems counting from two to five SIA to explore diffusion processes as a function of cluster size.

3.6.2.1. *Di-self-interstitial*

Simulation of the two self-interstitial (SIA) system is started with the defects separated by 4.98 Å corresponding to the distance between fourth nearest neighbors in crystalline fcc nickel. These defects come rapidly in close contact and in less than 0.4 ps reach the ground state corresponding to the formation of two parallel ⟨100⟩ (or equivalent) dumbbells in nearest neighbor position.

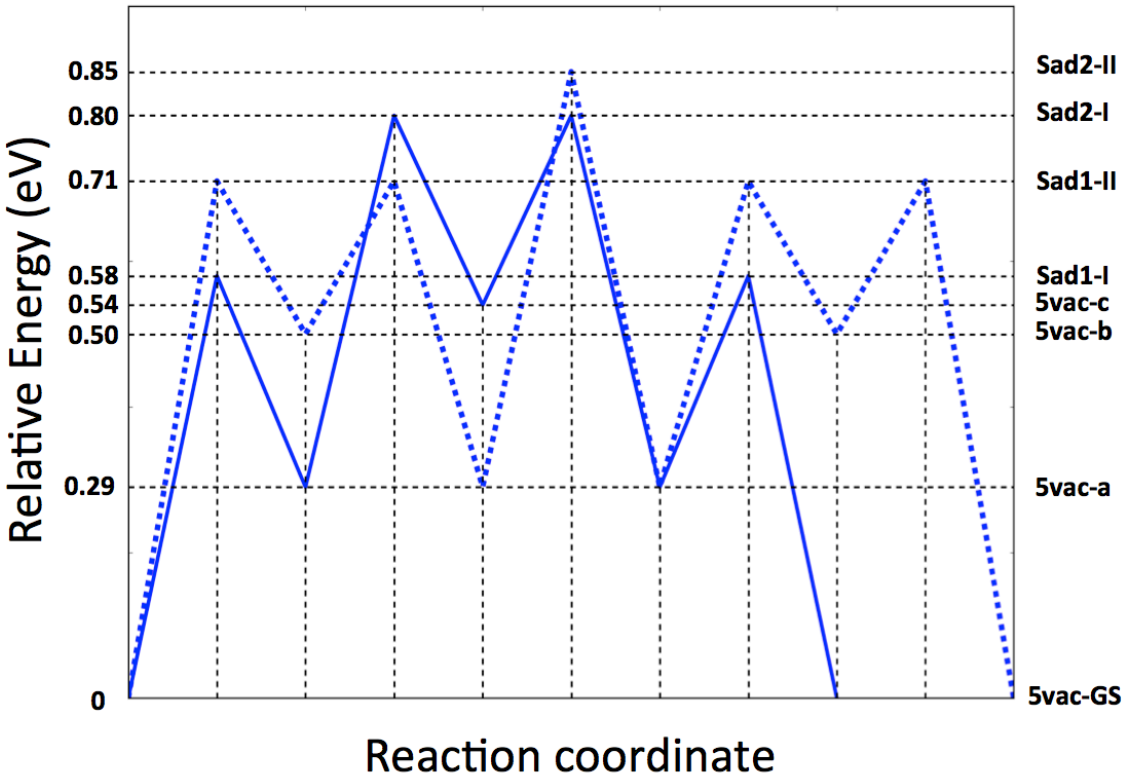

Figure 3.8. Pentavacancy diffusion mechanisms in nickel from the ground state. Energy landscape for the shortest mechanism (continuous blue line and index I) and the second diffusion mechanism (dotted blue line and index II). States 5vac-GS, 5vac-a, 5vac-b, 5vac-c are ordered from the most to the least stable states along the pathway.

Figure 3.9 presents the three most frequent diffusion mechanisms for the 2SIA system. The dominant one takes place over three steps through the ⟨110⟩ configuration, following the crowdion motion as reported in Zhao's et al work [87]: First, a simultaneous rotation of the two dumbbells from the ⟨100⟩ GS to a ⟨110⟩ orientation is achieved by crossing a barrier of 0.19 eV characterized by the two dumbbells turned 22.5 degrees from the ⟨100⟩ direction. Going over a second barrier, at 0.06 eV, the dimer jumps to a nearby site,maintaining its ⟨110⟩ orientation and then can relax into the ground state through a 0.05 eV barrier. This diffusion mechanism is in agreement with Zhao et al.'s [87] 0.12 eV barrier.

K-ART also identifies a second low-energy diffusion mechanism,with a 0.27 eV barrier, that moves the 2SIA by two successive 1SIA shift-rotations leading to the ground state again. At 600 K, and considering the fact that there is 24% of probability to cross a single0.20 eV barrier, this mechanism should occur about 12% of the time.

A third low-energy diffusion mechanism with a barrier of 0.29 eV is also observed. This mechanism takes place in only one step with a dumbbell rotating in perpendicular position versus as the other makes a 1SIA shift-rotation to reconstruct the 2SIA-GS as a final configuration. At 600 K, this mechanism should still occur about 17% of the time.

Rarer mechanisms, with barriers of 1.3 eV and higher, are also identified but, given their very low probability, are not discussed here.

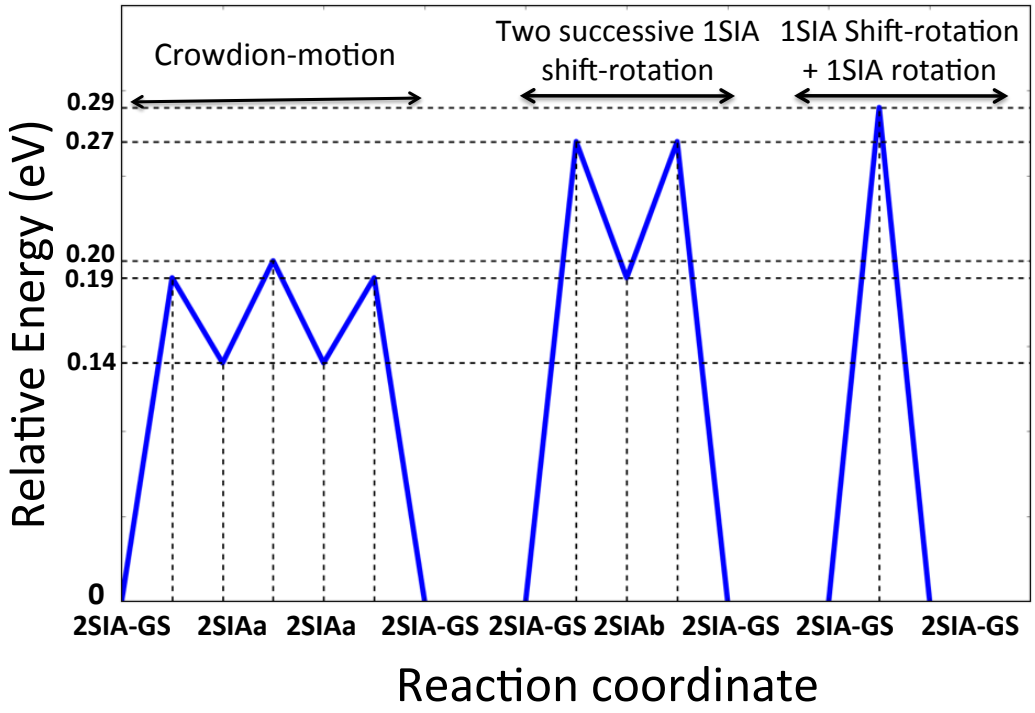

Figure 3.9. The three dominant diffusion mechanisms for 2SIA in nickel. The first two states above the ground state (2SIA-GS) are referred to as 2SIAa and 2SIAb, respectively. GS corresponds to two parallel dumbbells oriented along the ⟨100⟩ direction (or equivalent) in 1nn position. In 2SIAa, the dumbbells are parallel in the ⟨110⟩ direction (or equivalent) in 1nn position and 2SIAb is associated with the dumbbells in 1nn position but perpendicular to each other in ⟨110⟩ directions.

3.6.2.2. *Tri-self-interstitial*

The 3SIA simulation starts with two interstitials 4.98 Å apart and the third one 9.96 Å away from the first two. We find that the most stable configuration for the 3SIA system

Table 3. V. Relative configuration energies (E) (top line) and barrier energies for pathways between the five dominant bound states for the 4SIA system. Energies are in eV.

To \ From	3SIA-GS	3SIAa	3SIAb	3SIAc
ΔE	0	0.02	0.06	0.08
3SIA-GS	0.14	0.06	0.29	0.27
3SIAa	0.08	0.13	0.54	-
3SIAb	0.37	0.60	0.05	-
3SIAc	0.38	-	-	-

in nickel is when the dumbbells are all in first nearest neighbor, except for one dumbbell where the distance is equal to 2nn, with two parallel and the third one perpendicular to them in $\langle 100 \rangle$ and equivalents as indicated in figure 3.2 . This configuration is reached after 31 KMC steps from the beginning of the simulation, corresponding to 0.37 ps. The dominant diffusion process for this system, with a 0.14 eV barrier, takes place by a crowdion motion as in the case of 2SIA by translation after rotation from the $\langle 100 \rangle$ to $\langle 110 \rangle$ direction for the three dumbbells as reported in Zhao's et al work [49]. Figure 3.10 shows the configurations associated with the 3SIA. Seven of them are found to dominate, representing more than 96% of all accepted configurations. The most important state is the 3SIAb involved in the dominant diffusion mechanism with a barrier of 0.05 eV as indicated in Table 3. V. The 3SIAb-3SIAb transition is related to the crowdion motion corresponding to a diffusion following the $\langle 110 \rangle$direction. The transitions between 3SIA-GS and 3SIAa and conversely, with barriers of 0.08 and 0.06 respectively, are not a diffusion mechanism but result in a change in the dumbbell's orientation.

3.6.2.3. *Tetra-self-interstitial*

Starting at distances between 7.04 Å and 12.19 Åor each other, the four interstitials aggregates after 28 KMC steps and 62 ns.

The most stable configuration for 4SIA places all the dumbbells in the $\langle 110 \rangle$ direction or equivalents and in 1nn distance except for one pair with a 2nn distance as indicated in figure 3.11. The formation energy for 4SIA-GS is equal to 12.08 eV or 3.02 eV per SIA. The

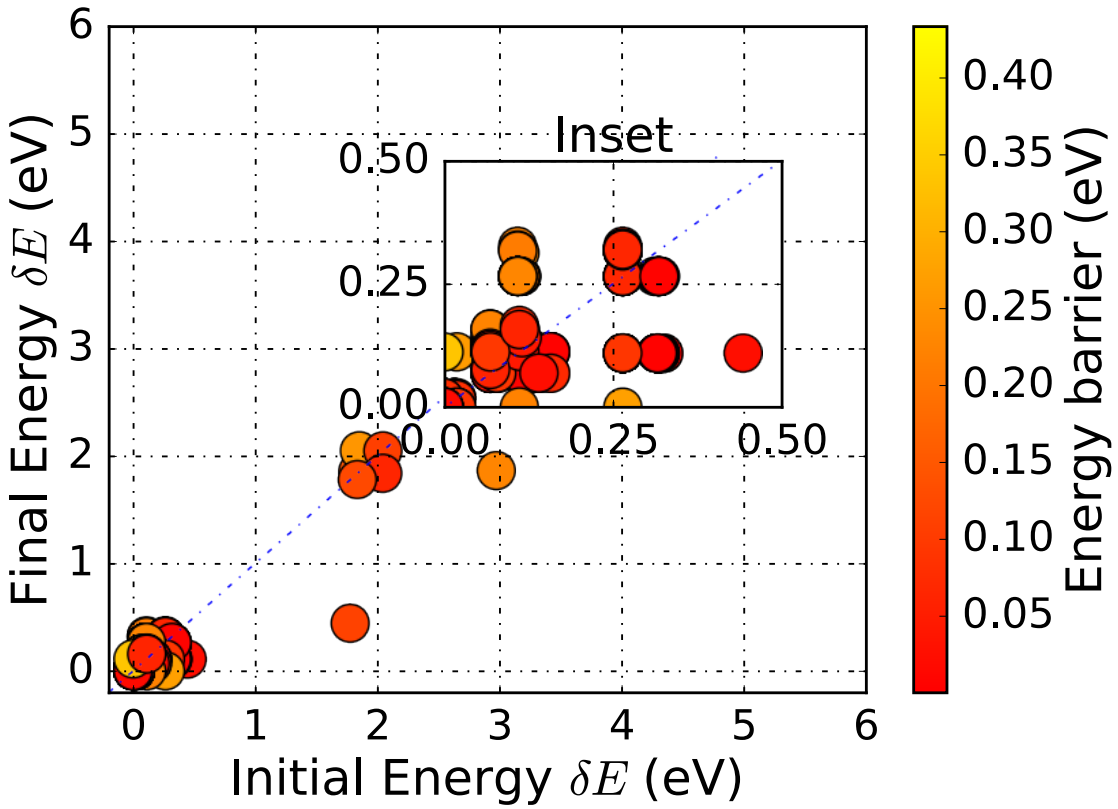

Figure 3.10. Representation of all k-ART accepted activation events for the tri-self-interstitial atoms system for a 1000 KMC steps simulation. All initial and final energies are measured from 3SIA-GS, the ground state. Inset: zoom-in between 0 and 0.50 eV. Symbols are color-coded according to the scale on the right.

binding energy connecting dumbbells forming the 4SIA-GS cluster is equal to 5.99 eV or 1.50 eV per atom.

The diffusion kinetics of the 4SIA-GS structure system is dominated by very low-barrier mechanism, only 0.004 eV, which is in a good agreement with MD-simulation result [87]. This low barrier in comparison with that of other transitions indicated in Table 3. VI implies that only this diffusion mechanism, which is related to the crowdion motion as reported in Zhao's [87] work, will be selected predominantly.

The five interstitials are placed initially at distances between 10.56 Å to 15.23 Å. They aggregate and reach the ground state after 0.5 ns (24 KMC steps). Once aggregated, the pentavacancy cluster diffuses quickly. The 5SIA ground state corresponds to the five dumbbells all within 1nn distance except for two pairs in 2nn position, distributed in different

Table 3. VI. Relative configuration (ΔE) (top line) and barrier energies for pathways between the five dominant bound states for the 4SIA system. Indexes refer to the number of active dumbbells in the diffusion process (for example 0.92_{2d} means diffusion with an energy barrier of 0.92 eV in witch two dumbbells are moving). Energies are in eV

To \ From	4SIA-GS	4SIAa	4SIAb	4SIAc
ΔE	0	0.62	0.83	0.91
4SIA-GS	0.004_{5d}, 0.89_{4d}, 1.27_{4d}	0.31_{4d}	0.14_{4d}	-
4SIAa	0.93_{4d}	1.46_{4d}	-	-
4SIAb	0.90_{4d}	-	-	-
4SIAc	0.92_{2d}	-	-	-

.

equivalent $\langle 100 \rangle$ directions and a binding energy of 7.67 eV or 1.53 eV per atom. The GS and the three first excited states of 5SIA are presented in figure 3.11 and are identified 5SIA-GS, 5SIAa, 5SIAb and 5SIAc from the most to the least stable configuration, respectively. States 5SIAa and 5SIAb are very close in energy but are not the same, as is shown in the supplementary material.

While the GS is characterized by close dumbbells distributed in $\langle 100 \rangle$ directions (and equivalents), excited states place all dumb-bells in $\langle 110 \rangle$ directions. Transition barriers between these states are shown in Table 3. VII. Since dumbbells in 5SIA-GS and the other are distributed differently, transitions between the ground and one of the excited states require a collective movement of all dumbbells either by rotation or translation or both, which explain the 0.61-eV barrier found for this system, much higher than for one to three SIA.Once relaxed into excited state, diffusion takes place easily by transiting between different states. The most dominant diffusion mechanism is the crowdion motion corresponding to the 5SIAa-5SIAa transition with an energy barrier of 0.09 eV, in agreement with those mentioned by Zhao et al [87]. Transitions between 5SIAa and 5SIAc with low energy barriers and movement of only one dumbbell are non diffusive mechanisms and corresponds to an oscillations between these two states. Diffusion along $\langle 100 \rangle$ direction is slow and requires a high activation barrier at least 1.09 eV as indicated in Table 3. VII. Despite being a simple system, with only 5SIA, k-ART was able to identify hundreds of barriers relating only the four considered states. In the case of GS-GS transition, for example, k-ART identifies 9 possible barriers corresponding to different mechanisms that ranges from 1.09 eV to 3.25 eV.

Table 3. VII. Relative configuration (E) (top line) and barrier energies for pathways between the five dominant bound states for the 5SIA system. Indexes means the number of moved dumbbells in the diffusion process. Energies are in eV

To \ From	5SIA-GS	5SIAa	5SIAb	5SIAc
ΔE	0	0.04	0.06	0.12
5SIA-GS	1.09_{2d}, 2.13_{4d}, 3.25_{5d}	0.56_{5d}	0.16_{5d}	0.59_{5d}
5SIAa	0.61_{5d}	0.09_{5d}	1.55_{5d}	0.03_{1d}, 4.36_{4d}
5SIAb	0.23_{5d}	1.57_{5d}	0.56_{2d}	-
5SIAc	0.71_{5d}	0.11_{1d} ,4.40_{4d}	-	-

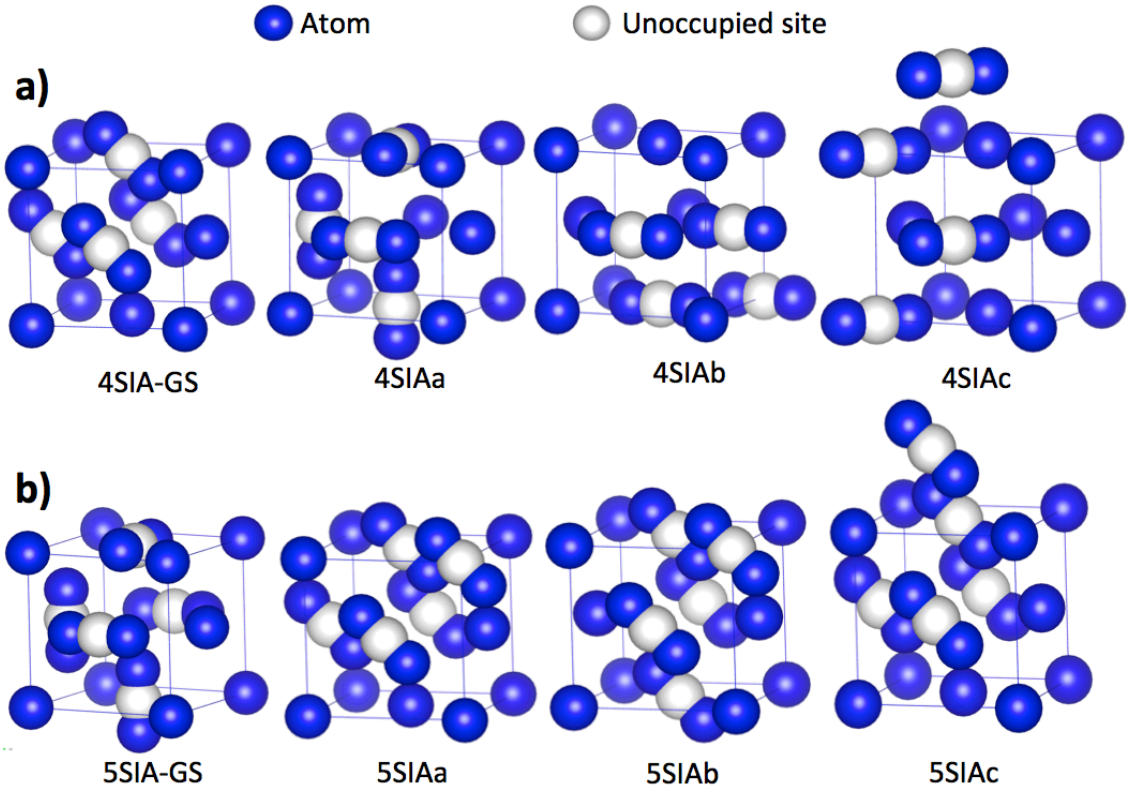

Figure 3.11. Most stable configurations for a) four and b) five SIA in nickel. Indices a to d refernce to configurations ordered starting from the most stable state for each system.

3.7. Discussion and conclusion

Points defects play an important role in determined the properties of materials [50, 51, 66] and understanding how they aggregate and move through crystals remain a major challenge as experimental approaches fail to provide the necessary detailed microscopic information. Direct calculations can compensate experimental limitations in the case of simple point

defects but the rapidly increasing complexity of the energy landscape of even small clusters requires automated search tools that have become available only relatively recently [88].

Following the characterization of points defects in bcc iron [63, 88] we turned to fcc systems, looking at the energy landscape associated with crystalline Ni containing one to five vacancies and self-interstitials to identify trends in defects diffusion and aggregation. To ensure the relevance of this study, we first compared four empirical potentials - EAM [31], MEAM1NN [68, 69], MEAM2NN [58] and ReaxFF [60] - with experimental and ab initio results for simple defects, one and two vacancies and one self-interstitial. While both MEAM potentials describe incorrectly the di-vacancy energetics, ReaxFF and EAM are in generally good agreement with experiment and DFT calculations. Overall, EAM provides the best accord, although it underestimates the mono-vacancy diffusion barrier by 20-25% and is the potential we used for the characterization of points defects in Ni.

We describe in detail the energy landscape of one to five vacancy clusters, finding a non-monotonic diffusion rate as a function of size. As for k-ART study of bcc Fe [63],we find that the trivacancy diffuses particularly rapidly, with a barrier of only0.35 eV, compared to 0.68 and 1.07 eV, for the di and tetravacancy clusters, due to the underlying crystalline symmetry that allows the cluster to move directly from ground state to ground state. While pentavacancy cluster diffusion is much slower than tetravacancy in Fe, it is the opposite in fcc Ni, with an overall diffusion barrier lower by about 0.27 eV pentavacancy. The overall energy landscape for vacancies in fcc system, however, appears to be much richer than for bcc, likely due to the local environment surrounding these point defects.

Even though diffusion occurs on widely different time scale for various clusters, it is often accompanied by a change in the diffusion direction and can involve many steps. The fastest diffusion pathway for tetra and pentavacancy clusters, for example, requires crossing four barriers associated with as many single vacancy jumps. This suggests that the 1D vacancy cluster diffusion observed in Au by Matsukawa and Zinkle requires much larger clusters to set in than studied here [89].

Interstitial diffusion in compact lattices is complex, with the number of barriers and mechanisms increasing rapidly with the number of self-defects [88]. For fcc metals, simulations have shown that small self-interstitial clusters diffuse very rapidly along the $\langle 110 \rangle$ direction, although details of these mechanisms were not provided [66, 87]. With k-ART, it is possible to reconstruct in detail the energy landscape surrounding the various clusters. While the diffusion barrier for a single interstitial is already low, at 0.15 eV, it drops to 0.08 eV for the 3SIA cluster and even to 0.004 eV for 4SIA,essentially ensuring a free diffusion across the crystal, with the help of the crowdion mechanism, which involves a collective rotation of dumbbells, from the $\langle 100 \rangle$ to the $\langle 110 \rangle$, followed by a jump in the same direction. As the cluster size increases, this collective rotation from the ground state into an excited state becomes costlier, as observed already for the 5SIA cluster, which requires crossing a 0.61 eV barrier to realign all dumbbells. From this point, however,diffusion remains very rapid, with barriers of 0.09 eV. Since the fast diffusing state is only 0.04 eV above the GS, its occurrence probability is high. This suggest a similar behavior for larger SIA clusters,where the ground state might gain in stability but with fast diffusing excited states with a sufficiently lifetime to dominate SIA kinetics, explaining experimental observations for this type of defects [25,53]. The picture that emerges for SIA diffusion in simple fcc metals appears more straightforward than that observed in bcc Fe, where diffusion barriers for small SIA clusters increase with cluster size and are associated with fairly complicated moves [88] in spite of a similar richness in terms of number of available states.

Using k-ART, we have provided here a detailed characterization of point defect clustering for system counting from one to five vacancies and self-interstitials. These results represent a strong basis to further work at relating these mechanisms with results obtained on larger clusters that involve important mechanisms such as stacking fault tetrahedra [90, 91] that occur for clusters with more than 5 vacancies and can greatly affect the mechanical properties of metals. As shown experimentally, self-defect diffusion is largely influenced not only by the crystalline lattice but also by the nature of the alloys. Interstitials, for examples, diffuse much more slowly in NiFe and even pure Fe than in pure Ni, while vacancies gain in diffusivity.

Much work remains to understand these differences. Extensive methods, such as k-ART, make it possible, at last, to turn our attention to these systems.

3.8. Code availability

Various ART nouveau implementations are available freely for download from http://normandmousseau.com. The k-ART code is available from the authors upon request

Acknowledgment

This work has been supported by the Canada Research Chairsprogram and by grants from the Natural Sciences and EngineeringResearch Council of Canada (NSERC) and the Fonds Quebecois de laRecherche sur la Nature et les Technologies (FQRNT). We aregrateful to Calcul Quebec for generous allocations of computerresources.

Chapitre 4

LONG-TIME POINT DEFECT DIFFUSION IN ORDERED NICKEL-BASED BINARY ALLOYS : HOW SMALL KINETIC DIFFERENCES CAN LEAD TO COMPLETELY LONG-TIME STRUCTURAL EVOLUTION

4.1. Objectifs

Le but de cet article est d'étudier les effets de la diffusion des monolacunes et interstitiels sur la stabilité des structures hautement ordonnées d'alliages binaires à base de nickel. Nous avons considéré initialement des cristaux ordonnés en $L1_0$ qui consiste à un empilement alterné des monocouches de nickel et un autre élément comme alliage (fer ou cobalt ou cuivre) contenants des monolacunes ou des monointerstitiels. Nous avons essayé de voir si on obtient une physique similaire ou différente quant à l'effet du mouvement des monodéfauts pour des métaux contenant des éléments possédants une taille similaire.

Auteurs dans l'ordre : Sami Mahmoud, Normand Mousseau

Journal : Cet article a été publié dans le journal " Materialia". (5-year impact factor : Not available yet). Référence : 4, 575-584 (2018)

4.2. Contributions des auteurs

— Sami Mahmoud (SM) a effectué toutes les simulations et l'analyse des données.

— SM a rédigé l'article.

— Normand Mousseau (NM) a participé à la rédaction de l'article.

— NM a supervisé tout ce travail.

4.3. abstract

In this paper, we characterize the effect of defect kinetics on the stability of ordered nickel-based binary alloys, NiFe, NiCo and NiCu, using the kinetic Activation-Relaxation Technique (k-ART), an unbiased off-lattice kinetic Monte Carlo method with on-the-fly catalog building, that can provide kinetic pathways over second scales taking full account of chemical and elastic effects. We generate the full energy landscape surrounding vacancy and self-interstitial diffusion for $L1_0$ NiFe, an alloy with promising magnetic properties, with those of model $L1_0$ NiCo and NiCu, and combine this information with unbiased long-time kinetic simulations to characterize the link between specific microscopic diffusion mechanisms and overall phase stability. Our simulations demonstrate an unexpected richness and diversity: even though these alloys display similar proprieties like atomic radius, single vacancy and interstitial diffuse along totally different pathways that explain the relative stability of ordered structure.

4.4. Introduction

With their low expansion at high temperatures and their high resistance to corrosion, nickel based alloys play an important role in high-tech industries such as aerospace and nuclear energy. As demand for more sophisticated materials grows and new manufacturing methods are developed, some of these alloys are also attracting more and more attention for new applications across a wider range of industrial sectors. This is the case, in particular, for chemically-ordered alloys, such as FeNi, that can be grown by Alternate Monoatomic Layer deposition[92] or Molecular Beam Epitaxy (MBE) [93] making them good candidates for applications such as spintronics[94] and inexpensive permanent magnets[95].

These possible applications have caused a renewed fundamental interest to characterize the NiFe and related binary alloys both experimentally [23, 66, 96] and numerically [97, 98], providing new insights regarding the link between defect kinetics and stability in these systems. While the reported order-disorder transition transition temperature in tetrataenite ($L1_0$ NiFe) is 593 K, Bordeaux *et al.* showed that the slow disordering, characterized by a 3.1 eV activation energy, pushes the kinetic transition to much higher temperatures. Yet, Geng *et al.* showed that room temperature mechanical milling can overcome these barriers and lead to the production of nanocrystalline $L1_0$ NiFe from the disordered phase. Comparing vacancy diffusion between ordered and disordered NiFe, TiAl and CuAu, in high temperature molecular dynamics, find that, for ordered systems, the antisite creation rate is highly composition dependent.

These works underline the importance of understanding the slow kinetics associated with the general class of $L1_0$ alloys and, more particularly, NiFe alloys, by capturing the detailed kinetics of vacancy and mass diffusion in these materials. Yet, the slow defect diffusion has made it difficult to characterize the nature of point defect diffusion in these alloys by standard techniques, such as molecular dynamics, and how it differs from that, much better understood, observed in perfect systems. [42] To overcome this limitation, we revisit this problem using the kinetic Activation Relaxation Technique (k-ART)[99, 45], an off-lattice kinetic Monte-Carlo methods with unbiased on-the-fly event catalog construction capabilities, to describe in details the kinetic of point defects and their associated energy landscape in Ni-based alloys comparing, in particular, with their behavior in pure iron[63] and nickel[42] gained recently, with the same technique.

More precisely, in order to understand the link between point defect kinetics and structural evolution and kinetic stability, we consider three ordered $L1_0$ model systems — NiFe, NiCu and NiCo —, where only $L1_0$ NiFe is found experimentally to be thermodynamically stable. The full energy landscape associated with single point-defect diffusion is reconstructed for each system and long-time k-ART simulations are launched to generate kinetic trajectories at 300 K, far away from the NiFe order-disorder transition, to better establish the

inherent differences and similarities between the alloys. We also characterize the landscape and kinetics of these alloys under interstitial diffusion as even though the evolution of these alloys seems mostly controlled by vacancies, the preparation of $L1_0$ NiFe phase through ion bombardment [100] or mechanical milling[96] will generate interstitials that will play a role in the phase ordering.

In this work, long-time k-ART simulations are performed using empirical potential to fully characterize the diffusion kinetics and energy landscape of single vacancies and interstitials in $L1_0$ NiFe, NiCo and NiCu alloys. As potentials need to be validated for the type of problem studied, we first compare three sets of parameters for NiFe based on the Embedded Atom Method formalism (EAM)[31] developed by Bonny and collaborators to identify the most appropriate set of parameters. Simulations show that the energy landscape surrounding the defects and the associated kinetics vary greatly as a function of alloy composition, leading to leading to very different consequences on the structural evolution of these alloys and opening the door to design more stable and even self-annealing materials through kinetic control.

4.5. Methods

4.5.1. Kinetic-Activation Relaxation Technique (k-ART)

The kinetic activation relaxation technique (k-ART)[99, 45, 42] is an off-lattice kinetic Monte Carlo method based on the activation-relaxation technique (ART nouveau)[71, 72] for event searching and NAUTY[44] for topological analysis and generic classification. The flowchart in figure 4.1 shortly explains the k-ART method. While details about k-ART can be found elsewhere [99, 48, 70], its basic principles can be summarized briefly as follows.

After classical local energy minimization of the total structure using FIRE (Fast Inertial Relaxation Engine)[101], k-ART characterizes the local topological environment surrounding each atom with the help of NAUTY. For this, all atoms contained within a sphere of a given radius (6 Å for the current system) are extracted. A graph is generated by drawing edges between all atoms within a cut-off distance of 2.8 Å of each other, corresponding roughly to including first-neighbors only. Additional self loops are added to distinguish between

the various atomic species. The graph, containing about 80 vertices, is then sent through NAUTY to extract an identifier associated with its automorphic class. If the topology is known and cataloged, generic events associated with it are placed in event tree, otherwise 50 ART nouveau searches are launched to identify its associated events; additional searches are added in some cases to ensure the completeness of the catalog. To ensure that the events correspond to connected sets of minimum-saddle-minimum states, a relaxation is performed in both direction form the saddle point.

After identifying all events, a first evaluation of the time to the next event is performed according to transition state theory [102] with a constant 10 THz prefactor. All barriers in the tree with an occurrence probability of one in 10 000 or higher are reconstructed and fully relaxed to ensure that all elastic events are exactly included. After this relaxation, the time step is evaluated again and the clock moved forward following the Poisson distribution characterized by this time step. An event is then selected at random with a probability proportional to its rate and the system is ready for the next step. To prevent being trapped by events with low-energy non-diffusive barriers known as flickering states, we use the basin-accelerated mean-rate method (bacMRM) [48], which solves analytically intra-basin kinetics. Since the right kinetics is maintained, it is possible to adjust the threshold for defining flickering states depending on alloy nature and defect type without affecting the result. In the case of vacancies, with high migration energy for all systems, this threshold is set at 0.5 eV. For interstitials, with migration energy and oscillations activation energies are small (around 0.05 eV), the bacMRM threshold is set to 0.01 eV.

4.5.2. Simulated systems

We consider three NiX alloys — NiFe, NiCo and NiCu — all at a 50-50 percent concentration in both fcc solid solution and $L1_0$ structure. The simulated systems are cubic boxes of 4000 atoms, a size sufficient to ensure that defect diffusion is not affected by boundary effects, relaxed at zero pressure; lattice parameters for these three cells are indicated in Table 4. I. Simulations are performed at 300 K, as indicated below. Vacancies of Ni or/and X are created by removing one atom of the given species. Interstitial atoms, for their part, are

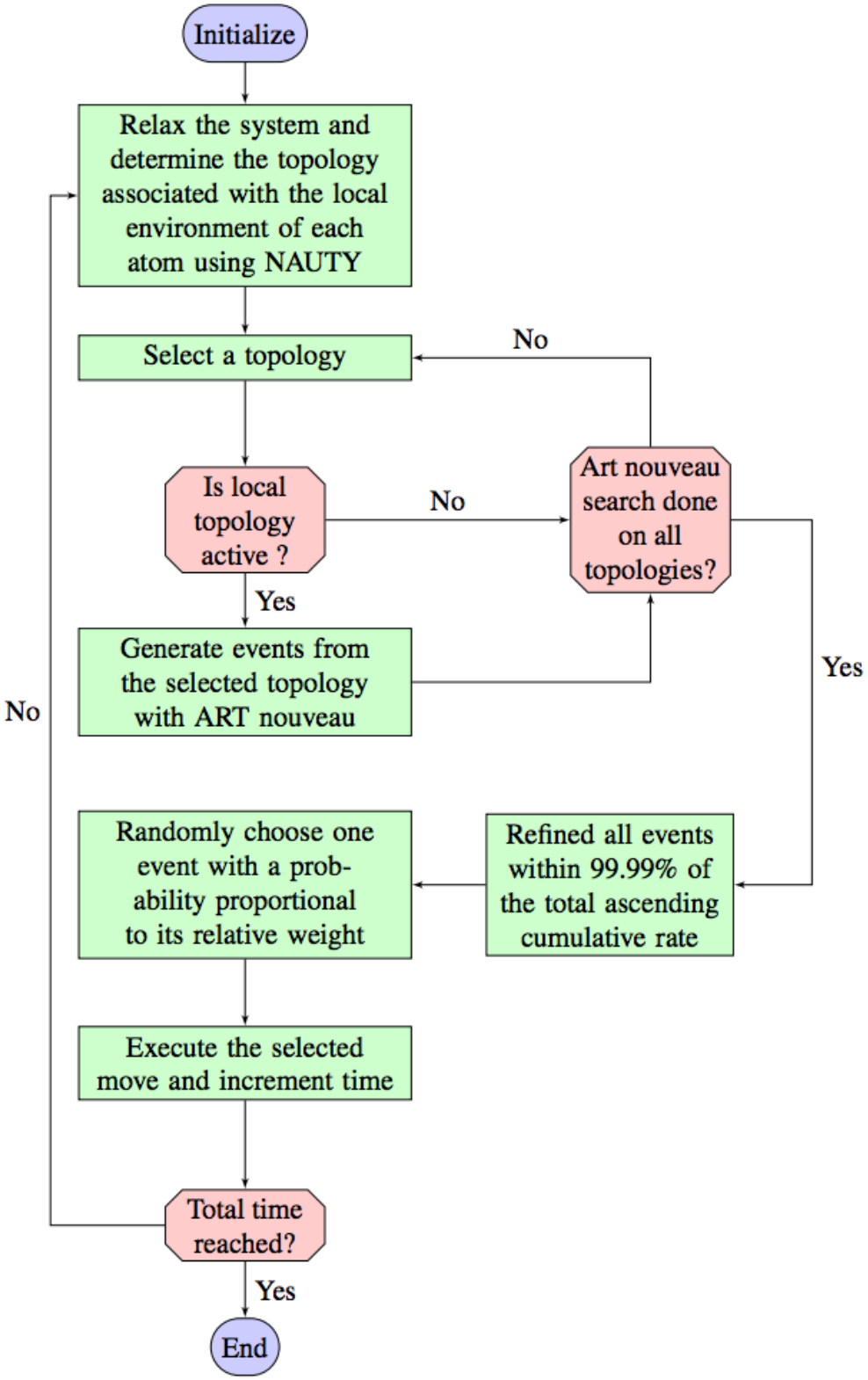

Figure 4.1. Flowchart of k-ART.

Table 4. I. Lattice parameters of pur metals considered for comparison and alloys (NiFe, NiCu and NiCo) used in this study. d is the interatomic distance.

Metal	a	b	c	d	Crystal structure	reference
pure Ni	3.5200	3.5200	3.5200	2.48	fcc	[[42]]
pure Fe	2.8665	2.8665	2.8665	2.87	bcc	[[105]]
pure Cu	3.6147	3.6147	3.6147	2.56	fcc	[[106]]
pure Co	2.5071	2.5071	4.0695	2.51	hcp	[[107]]
NiFe	3.5790	3.5790	3.5790	2.53	$L1_0$ fcc	[[97]]
NiCu	3.5594	3.5594	3.6483	2.52	$L1_0$ tetragonal	[[104]]
NiCo	3.5250	3.5250	3.5250	2.49	$L1_0$ fcc	[[97]]

placed initially in an octahedral site and, after minimization, form a dumbbell with one of their neighbors, either the same type or not.

For the $L1_0$ structure, Ni and X atomic layers are stacked alternatively along the $\langle 100 \rangle$ direction. It has been shown experimentally[93, 95] and from DFT calculation[103] that the NiFe-alloy $L1_0$ structure is stable. While this is not the case for the two other alloys,[92, 104] comparing diffusion pathways of point defects in these three cases contributes to providing an explanation for the observed difference in stability in addition to serving as a reference system for understanding diffusion in solid solutions.

4.5.3. Choice of parameters for the interaction potential

To select the best available forcefield for our simulation, we first compare various parameter sets optimized by Bonny and collaborators within the embedded-atom method framework for NiFe[108, 109, 110], NiCo [111] and NiCu[112] systems.

Because NiFe alloy has received more attention than the two other systems, we focus on this alloy to establish the best potential, comparing three sets of parameters with available DFT results. Table 4. II shows results obtained with three potentials for vacancy diffusion barriers in three different first nearest-neighbors (1nn) environments as well as recent DFT calculations[97, 98]. Bonny's 2013 EAM potential introduces an unphysical two-step mechanism for monovacancy diffusion where the vacancy, starting from the crystalline position, finds a first minimum halfway on the path to the 1nn site localized in the same plane nature. This mechanism is observed for both Fe and Ni vacancies with barriers of 0.87 and 1.05 eV

Table 4. II. Migration energy of one vacancy in NiFe alloy as a function of first nearest-neighbor (1nn) environment composed by (n, m) elements where n and m are the number of Ni and Fe respectively. Considered cases here are (8,4) $\mapsto$ (8,4) for the diffusion of Fe vacancy in Fe plane, (4,8) $\mapsto$ (4,8) for the diffusion of Ni in Ni plane and (8,4) $\mapsto$ (5,7) for the jump of Fe vacancy from the Fe to the Ni plane. All vacancy diffusion mechanisms consist of direct 1nn jump except for values with an asterisk that correspond to a two-step diffusion to 1nn position. All values are in eV.

	Bonny2009	Bonny2011	Bonny2013	DFT
(8,4)↦(8,4)	0.75	1.00	0.77*	0.87[98]
(4,8)↦(4,8)	1.07	1.32	0.55*	1.05[98]
(8,4)↦(5,7)	1.12	1.22	1.09	1.07[97], 1.31[98]

respectively as indicated in Table 4. II. Bonny's 2009 EAM potential under-estimates the intraplanar in Fe layer and the interplanar diffusion barriers by 0.12 and 0.19 eV respectively compared to Chakraborty's[98] DFT results. Since DFT calculations between various groups disagree for the interplanar diffusion (8,4) $\mapsto$ (5,7), we take as reference the average between the two values; here again, Bonny's 2011 potential presents the best value. Finally, Zhao *et al.*[97] have compared the distribution of formation energies in random alloys as a function of first-neighbor environment for DFT and empirical potential and concluded that, although imperfect, Bonny's 2011 offer the best agreement with *ab initio* results. Overall, therefore, Bonny's 2011 EAM potential offers reasonable accuracy and better relative energies than the other empirical potentials and is selected here for the treatment of NiFe alloy.

4.5.4. Formation energy

The formation energy $E^{conf}_{f1SIA}(NiX)$ for a mono-self-interstitial (1SIA) in NiX (X is Fe or Cu or Co) alloy is calculated as follow:

$E^{conf}_{f1SIA}(NiX) = (E^{conf} - (E_p \times \frac{(n+1)}{n}))$,

where E^{conf} is total energy of the system in the considered configuration, E_p is the energy of the perfect crystal with n atoms (4000 in our case). According to this definition, a state with lower $E^{conf}_{f1SIA}(NiX)$ is more stable.

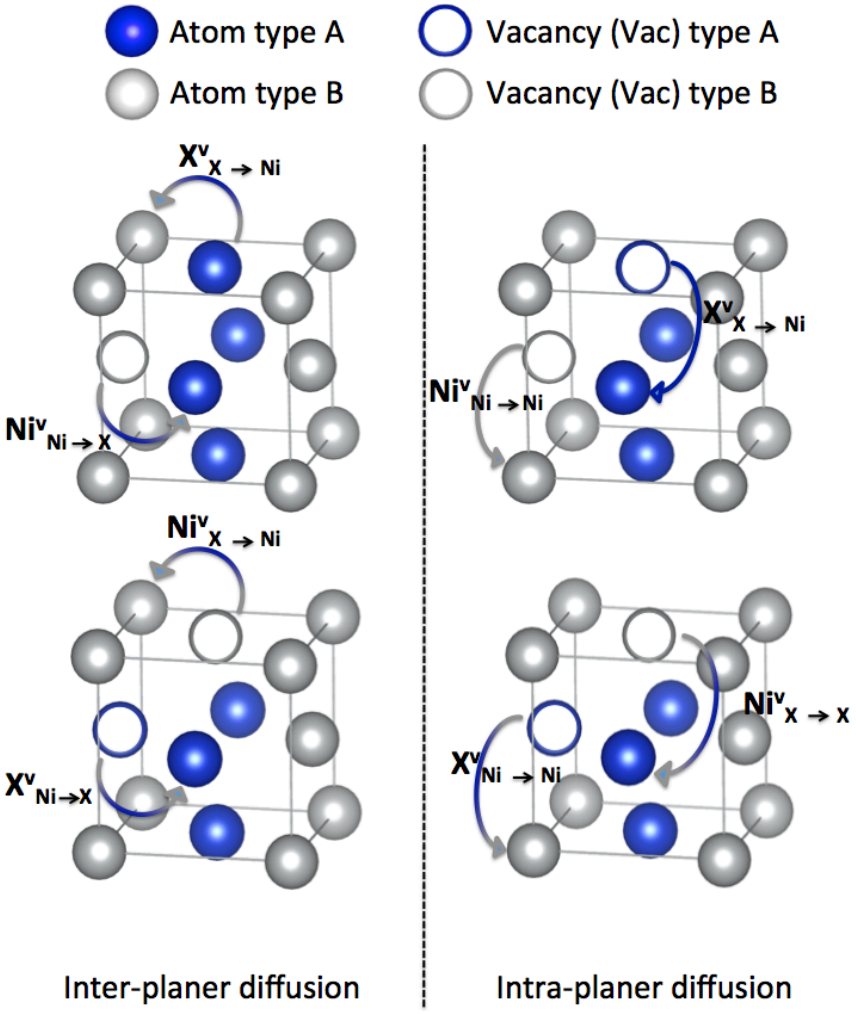

Figure 4.2. Interplanar and intraplanar diffusion pathways of a vacancy diffusing in fcc $L1_0$ alloys. While intraplanar jumps are symmetric, this is not the case for interplanar diffusion that generates antisites, as indicated on the left-hand-side panel.

4.6. Results and discussion

4.6.1. Vacancy diffusion

To characterize monovacancy diffusion in $L1_0$ structure, we need information on the eight barriers presented in figure 4.2. Four barriers are associated with intraplanar migration depending on the plane and vacancy types, and four others determine the interplanar ones that depend on vacancy type and the initial and final hosting plane. Table 4. III presents all k-ART generated barriers for the three alloys.

We first focus on the NiFe case. For this alloy, the lowest barrier, at 0.81 eV, corresponds to a nickel vacancy jump from the Ni to the Fe plane. Once in this plane, the Ni vacancy diffuses preferably in Fe plane with a barrier of 1.03 eV. Indeed, although the jump to the Ni plane is only slightly higher, a 1.13 eV, Ni vacancy intraplanar diffusion in the Ni plane involves crossing a much higher energy barrier, at 1.32 eV, 0.25 eV greater than for pure Ni[42]. A Ni vacancy, therefore, would create a single Fe antisite in the Ni, before diffusing in the Fe sublayer. To avoid obscuring the results, we will label the various sites caused by an initial vacancy by the initial defect (here Ni vacancy), understanding, for example, that it means an Fe antisite with Fe vacancy when it is in the configuration just described.

We observe a similar behavior for the Fe vacancy, which diffuse preferably in the Fe layer, crossing a barrier of 1.00 eV. The Fe vacancy will only rarely jump to the Ni layer, as it requires an energy of 1.22 eV, with diffusion in this layer ever higher, at 1.25 eV due to the presence of an antisite in the Fe layer.

The integrated effect of this landscape surrounding a monovacancy in the $L1_0$ NiFe alloy, obtained by long-time k-ART simulations, is presented in figure 4.3(a). The graph shows an evolution dominated by intraplanar diffusion in the Fe layer (Y and Z directions), with almost no interplanar motion as that the vacancy diffuses in an environment dominated by Ni atoms (4 Fe in plane and 8 Ni out of plane). This conclusion is confirmed by the right-handed panel (figure 4.3(d)). This figure presents the events generated along the pathway as dots positioned as a function of the initial energy (measured with respect to the ground state, x-axis), the final energy (y-axis) and the energy barrier (colored according to the right-handed color code). We see, for example, that for symmetric events, at $(0, 0)$, the connecting barrier is light yellow or 1.32 eV; similarly, an event starting in a state at 0.3 eV above GS, can reach the ground state $(0.3, 0)$ after crossing a 1.22 eV barrier. This plots shows all 2500 accepted events generated during the 4.5 million second (1250 hours) run at 300 K, with a typical rate of 2.2×10^{-7} s^{-1}. The small number of differently positioned points on the graph indicates that only a few different states are visited, and that the system does no show structural evolution, remaining essentially ordered as the vacancy diffuses around, restricted

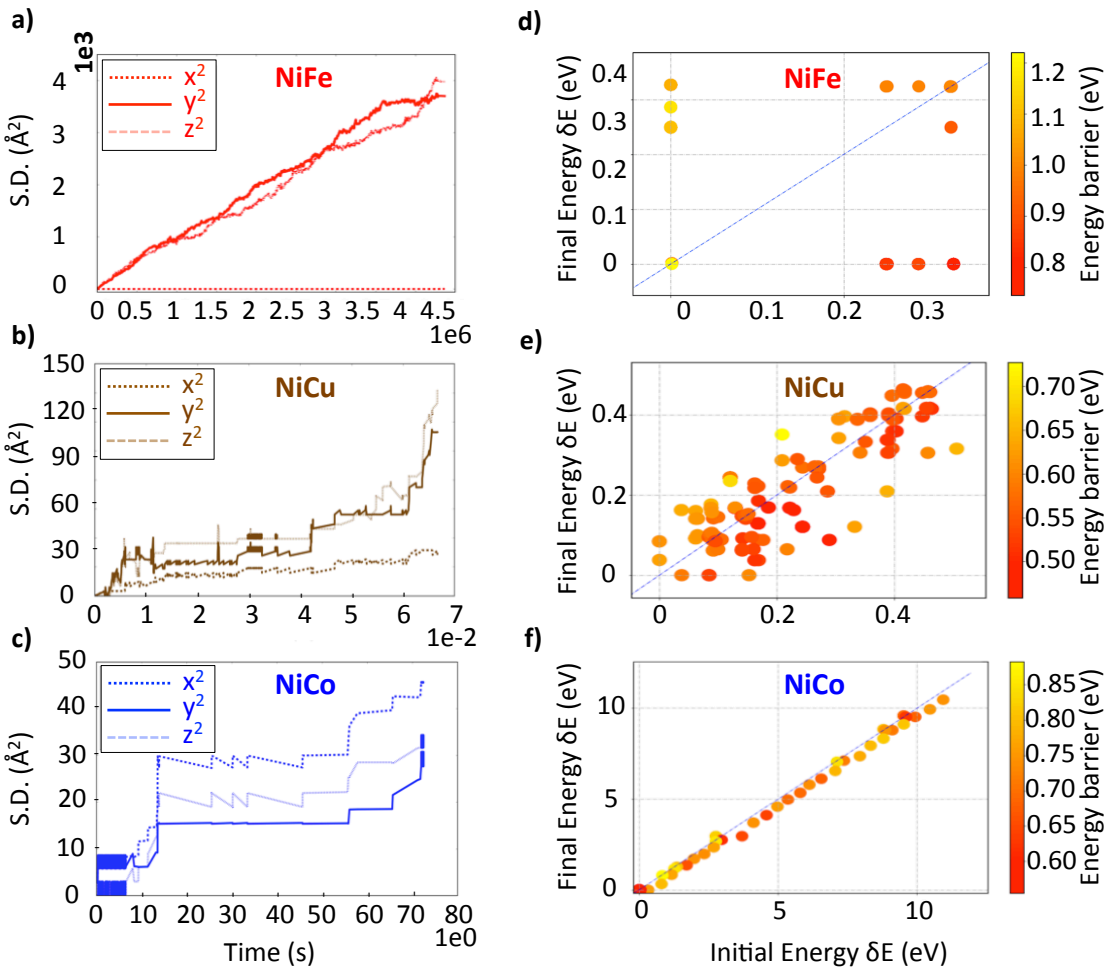

Figure 4.3. Diffusion of vacancy in ordered $L1_0$ NiFe, NiCu and NiCo alloys. Left-hand-side panels (a,b,c): Square displacement (S.D.) as a function of time and lattice directions (y and z represent the elemental planes, with x, pointing in the normal direction); right-hand-side panels (d,e,f): final energy of each accepted event as a function of initial energy, as measured from the ground state. The symbol color indicates the energy barriers as defined by the scale on the right-hand side of the graph.

essentially to the Fe planes. As temperature increases, however, as observed experimentally, the relative probability between the jumps in different orientations is reduced and leads to disordering. As temperature is raised to 600 K, for example, near the experimental order-disorder temperature, interlayer jumps takes place every 100 to 300 μs (not shown), while no interlayer jump was observed in a 10^6 s run at 300 K .

Vacancy diffusion in the $L1_0$ NiCo alloy is opposite to that of the NiFe case. From Table 4. III, the fastest move for the Ni vacancy is towards the Co sublayer, with a 0.77 eV barrier, compared with 1.07 eV for Ni intra-layer diffusion. Once in the Co layer, the

vacancy is more likely to diffuse in plane (1.04 eV barrier) than to come back to the Ni layer (1.20 eV). However, the Co vacancy will preferably move to the Ni plane, with a 0.75 barrier, rather than diffuse intraplane (with a barrier of 1.19 eV). Once in the Ni plane, however, it can move easily within the plane, with a 0.83 eV barrier. For NiCo, therefore, a vacancy will first move to the other plane, creating an antisite, then diffuse intraplane until it moves away from this antisite and prefers, then, to cross into a new plane, leading to the multiplication of antisites and the disordering of planar structure.

This analysis is confirmed by looking at the long-time diffusion of a monovacancy in the $L1_0$ NiCo alloy, starting from a perfectly ordered system as presented in the left-handed panel of figure 4.3(c). Diffusion shown here is over 70 s and 1200 steps is almost perfectly isotropic, as indicated by a similar diffusion along the three axes. Looking at the event's characteristics (figure 4.3(f), we note that, contrary to both NiFe and NiCu, for which the system's total energy does not evolve over the simulation time scale, for NiCo, the total energy drops by more than 10 eV, over 70 s, as the vacancy diffuses around and disorders the alloy, crossing barriers that vary by at most 0.30 eV, as a function of the local environment, in agreement with recent DFT result that show antisites are energetically favored in this alloy [113].

The diffusion behavior of vacancy in NiCu alloy is also different from the two other alloys. For this system, the evolution of this point defect takes place almost isotropically, as indicated in figure 4.3(b), because of similarities in barriers between the various mechanism and thus specific pathway dominates: the lowest barriers correspond to a migration of Ni vacancy from Cu to Ni plane and intraplaner Cu vacancy in Cu plane with barriers of 0.53 and 0.57 eV respectively. The migration of Ni or Cu vacancy from a layer to another one of different type require crossing 0.65 eV, higher than for the two other mechanisms, but still much lower than for the two other alloys, and lower also than for pure copper with an activation energy equal to 0.74 eV [114]. Figure 4.3(e) shows that, contrary to NiCo, disordering does not lower the total energy but takes place for entropic gains. As for NiCo,

Table 4. III. Migration energies of single vacancy in L_{10} fcc nickel binary-based alloys. Notation is a bit similar to Kröger-Vink's ones (Exemple : $Ni^v_{X\to Ni}$ is the barrier for the Ni vacancy (v) to diffuse from the X plane (Fe or Co or Cu) to the Ni plane).

Alloy \ Barrier	$Ni^v_{Ni\to X}$	$Ni^v_{X\to Ni}$	$Ni^v_{Ni\to Ni}$	$Ni^m_{X\to X}$	$X^v_{X\to Ni}$	$X^v_{Ni\to X}$	$X^v_{X\to X}$	$X^v_{Ni\to Ni}$
NiFe	0.81	1.13	1.32	1.03	1.22	1.22	1.00	1.25
NiCu	0.65	0.53	0.89	0.56	0.65	0.84	0.57	0.94
NiCo	0.77	1.20	1.07	1.04	0.75	1.22	1.19	0.83

however, the 1246 events taking place over 80 s in NiCu cross barriers that vary as a function of local chemical environment, leading to the scatter observed in figure 4.3(b).

4.6.2. Interstitial diffusion

For the three alloys considered, the interstitial atom shares a crystalline site with a lattice-atom, forming a dumbbell with a formation energy that is influenced by the dumbbell composition, orientation and its insertion plane, for a total of 12 theoretical different conformations for each alloy, as shown in Table 4. IV, that provides the formation energy for these various configuration. For NiFe alloy, all twelve dumbbells can be stabilized. This is not the case for the other alloys: the CuCu dumbbell perpendicular to the Ni monolayer in NiCu as well as the NiCo dumbbells, either perpendicular to Co layer or in the Ni layer layer, and rather flip directly into a different orientation or form a different dumbbell. As seen from this table, dumbbells are easiest to form in NiCu, often by a considerable margin, while they are much less sensitive to environment for NiFe : 1SIA formation energies for NiCu, NiFe and NiCo alloys are in the range of [1.22 eV,3.44 eV], [3.14 eV,4.48 eV] and [3.00 eV,6.17 eV] respectively. For the three alloys, the NiNi dumbbell is always more stable than dumbbells composed of Ni and the alloying element in agreement with recent *ab initio* calculations [115]. They show relatively narrow energy range as a function of their position (Ni or X plane) and orientation, except for NiNi with a parallel orientation in the Ni plane for NiCo, that is 0.77 eV above the NiNi dumbbell with a parallel orientation in the Co plane.

Table 4. IV. Formation energies of mono-interstitial in $L1_0$ alloys as a function of dumbbell composition, orientation and belonging plane. Letters p and h followed by an atom type means perpendicular and horizontal to the atom type plane, respectively. The presence of an asterisk (*) means that the dumbbell is unstable and that the energy given is for the nearest metastable state the system relaxes into. All values are in eV.

Dumbbell composition	$NiNi$ dumbbells				NiX dumbbells				XX dumbbells			
Belonging plane and orientation	pNi	hNi	pX	hX	pNi	hNi	pX	hX	pNi	hNi	pX	hX
NiFe	3.14	3.38	3.32	3.59	3.82	3.90	3.62	3.63	4.48	4.26	3.72	4.27
NiCu	1.36	1.22	1.39	1.40	2.40	1.98	2.02	2.31	2.92*	2.84	2.86	3.44
NiCo	4.09	3.32	3.00	3.48	5.50	3.34*	4.46*	5.54	5.06	4.89	5.80	6.17

After characterizing the thermodynamical properties of 1SIA in the three alloys, we turn to their kinetics and its effects on their structure. As shown in figure 4.4, the direction of 1SIA dumbbells migrations is alloy dependent, leading to many more possible pathways, as suggested in Table 4. V, which displays the activation barriers for SIA diffusion in NiFe. Because of the complexity of the energy landscape associated with the structure, however, many pathways — transition or final states — that would be present in pure Ni FCC are not found here: starting from the expected final state, the system relaxes in only a restricted number of configuration. For NiFe, (figure 4.5), the dominant diffusion movement is a translation-rotation (also named shift-rotation[97]) mechanism in the Ni plane with an energy barrier of 0.23 eV, starting from a dumbbell parallel to the Ni plane. The perpendicularly oriented dumbbell, corresponding to the ground state, requires an additional 0.52 eV to turn. Making a translation-rotation to reach the NiNi$\langle 010 \rangle_{Ni}$ (or NiNi$\langle 001 \rangle_{Ni}$) is easier than the direct translation from Ni plane to its nearest Ni plane that cost 0.62 eV as energy barrier (not shown in the table). Starting from NiNi$\langle 010 \rangle_{Ni}$, the complex can diffuse easily by successive translation-rotation to reach NiNi$\langle 001 \rangle_{Ni}$ (or vice versa) in Ni layer after crossing 0.23 eV. The NiNi$\langle 010 \rangle_{Ni}$ dumbbell (or NiNi$\langle 001 \rangle_{Ni}$) can also translate-rotate to form NiFe$\langle 010 \rangle_{Fe}$ after crossing 0.27 eV. At 300 K, as shown in figure 4.4(a), over a 10^{-7}s, the interstitial, diffuses essentially in the Ni layer, a preference that decreased significantly with temperature: from 300 to 600 K, near the order-disorder temperature, the ratio between diffusion rates in the type layers falls from about 1 to 1000 to 1 to 30. At 300 K, the system diffuses mostly between states above GS — only 1 % of the events are directly connected to the GS (where the systems spends 56 % of the simulation time). Most of the diffusion — about

70 % of the jumps — takes place along the the meta1-meta1 pathway defined in figure 4.5, with a 3.1 Å averaged displacement between minima. About 15% of the transitions take place through the meta1-meta2 pathway, with jumps of 3.0 Å. From meta2, the transition symmetry prevents the NiFe$\langle 001 \rangle_{Fe}$ dumbbell to move directly to the ground state, it must therefore go back to the meta1 state a step performed 14% of the time.

For NiCu, interstitial diffusion is also dominated by translation-rotation mechanisms with migration barriers much lower than for NiFe : between 0.03 and 0.16 eV, as indicated in Table 4. VI. 1SIA diffusion is therefore much faster than the case of NiFe alloy, taking place on picosecond timescale at 300 K, similar to interstitial diffusion in pure Cu (0.11 eV) [87]. Contrary for NiFe, however, all diffusion directions are almost equivalent and barriers do not depend strongly on the dumbbell composition; this is reflected, in part, in the different subset of accessible pathways for the 1SIA than observed in NiFe. The first observed mechanism that does not correspond to a translation-rotation is a direct translation in $\langle 100 \rangle$ (or equivalent), with 0.39 eV barrier, significantly higher than the dominant ones. As shown in figure 4.4(b), diffusion in z direction is less probable than in plane due to a slightly larger distance between atoms for this direction than in the others. With these barriers, 1SIA diffusion in NiCu is therefore almost isotropic contributing to the disordering of the crystal.

For NiCo, NiNi crowdion motion dominates the diffusion as indicated in figure4.5. Starting from the GS characterized by $\langle 100 \rangle_{Co}$ NiNi dumbbell, the defect go to a $\langle 001 \rangle_{Ni}$ NiNi dumbbell conformation (0.32 eV above GS and characterized by a perpendicular dumbbell in Co layer) through a translation-rotation after crossing a 0.43 eV barrier (Table 4. VII). Once in $\langle 001 \rangle_{Ni}$, the dumbbell of NiNi adopts a crowdion configuration along the $\langle 011 \rangle_{Ni}$ direction (0.30 eV above GS), after crossing a small 0.03 eV barrier and can then diffuse rapidly in the same direction (Ni plane) crossing small 0.04 eV barriers or moving between $\langle 011 \rangle_{Ni}$-crowdion and $\langle 001 \rangle_{Ni}$ dumbbell states with a limiting barrier of 0.05 eV which corresponds to a timestep of few picoseconds per jump. While these states are well above GS, moving NiNi$\langle 001 \rangle_{Ni}$ dumbbell back to $\langle 100 \rangle_{Ni}$ is harder than the 0.11 eV would let expect as this jump can only take place in the presence of a Ni antisite in the Co layer, as the NiCo

Table 4. V. Activation barriers of SIA diffusion by translation-rotation mechanism in NiFe alloy depending on dumbbell composition and plane belonging. Barriers connecting in an unstable state are not indicated. Symmetrically-possible transition that do not exist due to instability of the initial or/and the final state, or because of the need for a non-available antisite in one of states are indicated as n/e. All values are in eV.

To \ From		Ni plane			Fe plane		
		NiNi	NiFe	FeFe	NiNi	NiFe	FeFe
Ni plane	NiNi	0.23	n/e	n/e	0.27	0.03	-
	NiFe	n/e	n/e	0.16	n/e	0.16	0.44
	FeFe	n/e	0.15	n/e	n/e	n/e	0.24
Fe plane	NiNi	0.31	n/e	n/e	n/e	n/e	n/e
	NiFe	0.27	0.15	n/e	n/e	n/e	n/e
	FeFe	n/e	0.50	0.38	n/e	n/e	n/e

not only because it requires a higher barrier (0.11 eV), but also it requires the existence of a neighbor Ni atom in Co layer to form. Without it, the NiNi crowdion must go in a NiCo dumbbell in Co plane that is 2.54 eV above GS. At 300 K, once in meta1 state, the jump to meta2 is observed 14% of transitions (see figure 4.5). The other transitions, mostly connecting meta1 to meta1, involve the $\langle 011 \rangle$ diffusion of the NiNi dumbbell associated with a 2.53 Å displacement of the center of mass through crowdion motion in Ni layer; over the full simulation, we observe only two jumps connecting the meta2 state to the ground state. The lifetime of the $\langle 011 \rangle_{Ni}$-crowdion is equal to 2 picoseconds; due to high instability of the NiCo system, a many flickering states are observe.

Kinetically, therefore, CoCo and NiCo dumbbells transform into $\langle 001 \rangle_{Ni}$ NiNi dumbbells, generating Co antisites, that cost 1.21 eV, to reach the GS. From this point, diffusion is Ni dominated and restricted to the Ni plane, maintaining the $L1_0$ crystalline structure, irrespective of the initial interstitial. Due to symmetry of the system, a NiNi$\langle 001 \rangle$ cannot translate-rotate to form the NiCo$\langle 100 \rangle$, since this structure is unstable (Table 4. IV). The GS can therefore only be reached in the presence of a Ni antisite in the Co layer. These barriers explain why, if disordering NiCo lowers its energy, as seen previously, this does not take place through interstitial diffusion on the $10^{-}7$s timescale generated here at 300 K (figure4.4(c) and (f)).

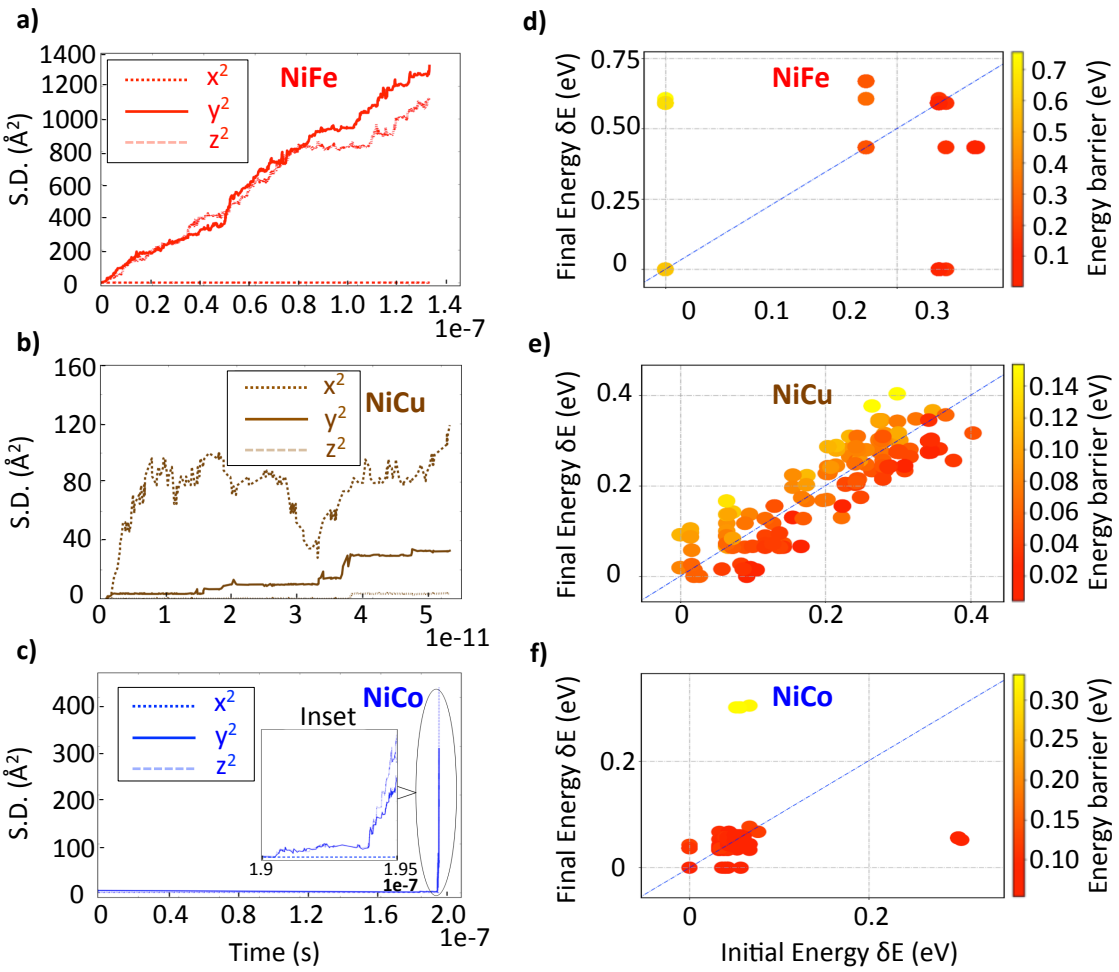

Figure 4.4. Diffusion of interstitial in ordered $L1_0$ NiFe, NiCu and NiCo alloys. Left-hand side panels (a,b,c): square displacement (S.D.) in Åas function of time and directions; right-hand-side panels (d,e,f): final energy as a function of initial energy, measured from the ground state. The symbol color indicates the energy barriers as defined by the scale on the right-hand side of the graph.

4.7. Discussion

Over the last few years, there have been significant efforts at characterizing the stability and evolution of metallic alloys[116, 66, 115] . In particular, the possibility of growing $L1_0$ NiFe, an alloy that presents promising magnetic properties, has caused many groups to address its stability and the role of self-defect in the order-disorder transition[23, 97, 96, 98]. Running short high-temperature molecular dynamics simulations, above the order-transition temperature, for example, Chakraborty *et al.* identify a few barriers for vacancy for NiFe and show that disordering takes place at various rates in different alloys.

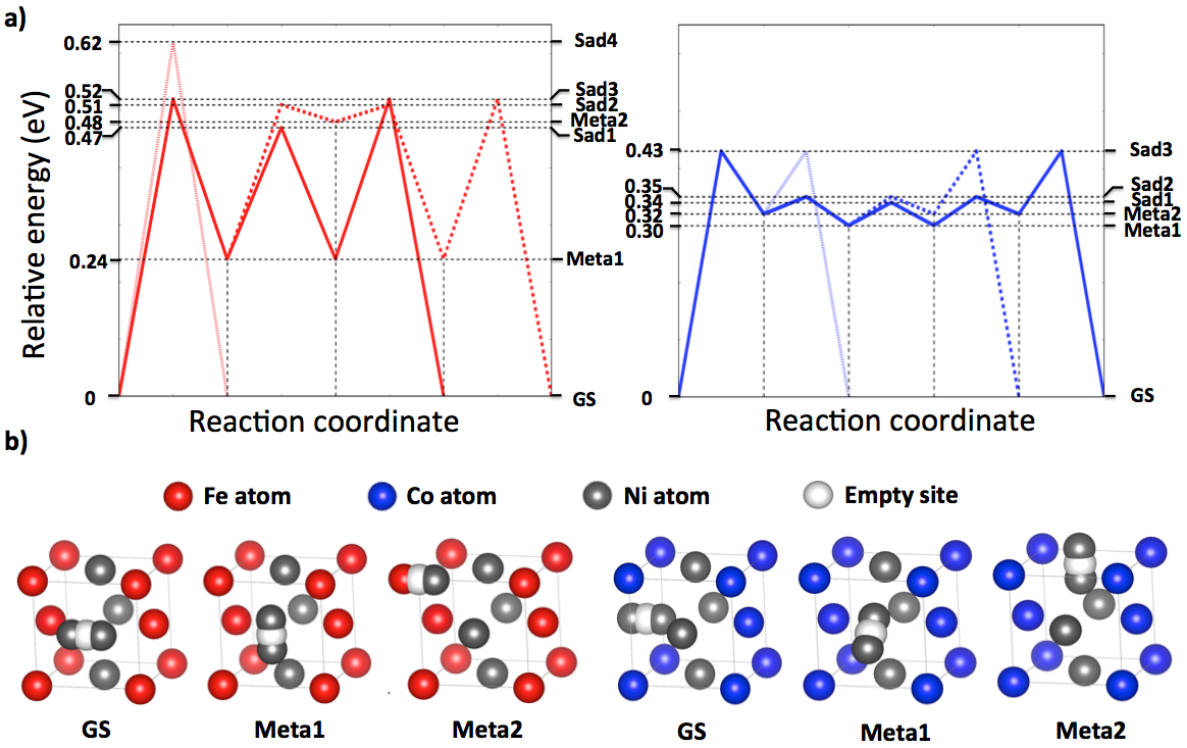

Figure 4.5. Shortest self-interstitial diffusion pathways in ordered NiFe (red) and NiCo (blue) alloys. a) The first (continuous line), the second (dotted line) and the third (dashed line) dominant mechanisms. b) Atomic arrangement in the ground (GS), metastable (Meta1 and Meta2) and saddle (Sad1 and Sad2 and Sad3 and Sad4) states. Dumbbells can be seen as two atoms connected by an empty site

Table 4. VI. Activation barriers of SIA diffusion by translation-rotation mechanism in NiCu alloy depending on dumbbell composition and plane belonging. Barriers connecting in an unstable state are not indicated. Symmetrically-possible transition that do not exist due to instability of the initial or/and the final state, or because of the need for a non-available antisite in one of states are indicated as n/e. All values are in eV.

To \ From		Ni plane			Cu plane		
		NiNi	NiCu	CuCu	NiNi	NiCu	CuCu
Ni plane	NiNi	n/e	n/e	n/e	0.04	0.16	n/e
	NiCu	n/e	n/e	n/e	n/e	0.03	0.08
	CuCu	n/e	n/e	n/e	n/e	n/e	n/e
Cu plane	NiNi	0.21	n/e	n/e	n/e	n/e	n/e
	NiCu	0.03	0.11	n/e	n/e	n/e	n/e
	CuCu	n/e	0.05	n/e	n/e	n/e	0.05

To fully understand the kinetic role of self-defects in the ordered phase, however, it is necessary to reconstruct in more details the energy lansdscape and follow the evolution of

Table 4. VII. Activation barriers of SIA diffusion by translation-rotation mechanism in NiCo alloy depending on dumbbell composition and plane belonging. Barriers connecting in an unstable state are not indicated. Symmetrically-possible transition that do not exist due to instability of the initial or/and the final state, or because of the need for a non-available antisite in one of states are indicated as n/e. All values are in eV.

To \ From		Ni plane			Co plane		
		NiNi	NiCo	CoCo	NiNi	NiCo	CoCo
Ni plane	NiNi	n/e	n/e	n/e	0.43	2.41	n/e
	NiCo	n/e	n/e	n/e	n/e	0.15	0.12
	CoCo	n/e	n/e	n/e	n/e	n/e	n/e
Co plane	NiNi	0.11	n/e	n/e	n/e	n/e	n/e
	NiCo	0.19	0.20	n/e	n/e	0.13	0.14
	CoCo	n/e	0.79	n/e	n/e	0.39	n/e

these defects on appropriate time scale, that can be well beyond the reach of molecular dynamics. Using the kinetic Activation-Relaxation technique, we reconstructed the detailed energy landscape and kinetics of three fcc $L1_0$ alloys — NiFe, NiCo and NiCu — around single vacancies and self-interstitials (see Table 4. VIII, for a summary).

Starting with the $L1_0$ NiFe phase, which is stable below 600 K, we find that the monovacancy diffuses preferentially in the Fe planes, due to the slightly larger size of Fe atoms with respect to Ni. Since the Ni layer is under tension, the vacancy rapidly jumps into the Fe lattice, creating an antisite, that lowers the tension while also diminishing the compression in the Fe layer. Being confined, predominantly, in the Fe layer, vacancy diffusion does not affect the chemical arrangement of this structure, directly contributing to the observed stability of this crystal structure from DFT calculations[103] and experimental evidence[93, 95].

For NiCo and NiCu alloys, for which the $L1_0$ phase is not observed experimentally, the chemical order is not conserved because of quasi-isotropic diffusion of vacancy. While NiCo disordering is dominated by energy relaxation, however, the evolution is NiCu is purely entropic.

Interstitial diffusion is also dramatically different in the three alloys and are coherent with the effects of vacancy diffusion. Contrary to vacancies, however, despite their similarities in terms of atomic size, interstitial migration pathways differ between alloys. Indeed, dumbbells

in NiFe and NiCo alloys prefer to diffuse in Ni layers while the diffusion is quasi-isotropic in NiCu. This quasi-isotropy leads to a 3D diffusion of single defects in NiCu alloy, similar to what is observed in pure metals[42]. The $L1_0$ NiCu is therefore unstable under the diffusion of single vacancies and interstitials.

To a first approximation, vacancy and interstitial diffusion results can be explained by the size difference between the alloying elements[117]. Since Fe, Cu and Co are larger than Ni atoms, we could expect, if no other factor comes into play, the NiNi$\langle 001 \rangle$ to present the highest stability as it makes us of the additional space along orientation. Fe being significantly larger than Ni, it is also natural to see, at low temperature, the vacancy move and diffuse predominantly in the Fe plane and dumbbells be confined to the Ni plane, making NiNi more stable than NiFe and FeFe dumbbells. Similarly, since size mismatch between Cu and Ni is only 2.5 per cent, and both pure metals adopt the same fcc structure, we expect that both vacancy and and interstitial will move relatively isotropic fashion. The same logic should apply to NiCo alloys since size mismatch between Co and Ni is even smaller than between Cu and Ni. Electronic differences, here, as captured by the EAM potential, as supported by the agreement between our results and recent DFT calculation [113], seem to play a more important role, with the energetic largely favoring random configurations.

The complex self-interstitial diffusion mechanisms, observed in both in NiFe and NiCo, however, are multi-step processes that involve long-distance motion through metastable states that are not directly captured by a simple characterization of the energy barriers around GS configurations (figure 4.5). Self-interstitial diffusion is particularly intricate for NiCo, where diffusion from the first excited state, 0.30 eV above GS, is almost barrier-less. Moreover, we find that, for this system, the kinetics of SIAs plays against the thermodynamics: while solid solution NiCo is more energetically favorable than $L1_0$, the energy barriers considerably reduce the disordering through SIA motion.

We can compare this with the NiCu system, were diffusion is a single-step quasi-random process and takes place with translation-rotation mechanism. The quasi-random criteria is explained by the almost equal low diffusion barriers in different directions.

Table 4. VIII. Effect of single defect kinetics on ordered nickel-based alloys at 300 K.

Disorder the alloy ? / Single defect type	NiFe	NiCu	NiCo
Thermodynamically stable	Yes	No	No
Vacancy	No	Yes	Yes
Interstitial	No	Yes	No

The atomic-thin network of tension and compressions zones created by size mismatch in the layer compounds is determinant the alloys' structural evolution: in NiFe, for example, defect motion is essential constrained to atomic plans while, for NiCo, for example, vacancy diffusion is mostly perpendicular to these planes, with macroscopic consequences. Indeed, this in-Fe-plane movement behavior, for example, implies that, in fcc $L1_0$ NiFe alloy, the dislocation glide a very low-probability process and the climb is a dominant one. However, because of higher probability of inter-plane plane diffusion in NiCo alloy, the climb encouraged against the glide.

In addition to the influence and effect of the presence of other defect type such as dislocation in pure[118] and composed metals[66], we show in our study that he symmetry and the order of the structure can play a major role in the movement dimensionality of point defects: For NiFe at room temperature, the alternated monolayer structure forces point defects to diffuse uniquely in one layer and thus the order is not affected by vacancy and interstitial diffusion, in agreement with experiment[100]; as expected, of course, raising the temperature eventually leads to an order-disorder transition. Self-defect diffusion, on the other hand, leads to the destabilisation, albeit through difference mechanisms, of the layer compound for both NiCu and NiCo, even at room temperature.

This study for the diffusion of single point defects allows us to understand some physical aspects not reported before, not only in $L1_0$, in other ordered structures such $L1_1$ and $L1_2$. This selective vacancy diffusion in NiFe, for example, play a role in the observed stabilization by Ni of the austenite phase.[119]

4.8. Conclusion

We have shown from longtime scale simulations using k-ART method that diffusion of point defects in apparently very similar nickel-based binary alloys — NiFe, NiCo and NiCu — shows different behavior that generate a diverse set of structural evolution pathways for the three systems. Focusing on $L1_0$ alloys, a highly ordered layered structure, allows us to fully characterize the energy landscapes of each system and assess the stability under self-defect diffusion. Through unbiased kinetic simulations performed on experimentally-relevant timescales, we have demonstrated that the movement of single vacancies does not affect the stability of ordered NiFe alloy due to in-Ni layer diffusion behavior. On the contrary, with different but quasi-isotropic movement, monovacancies rapidly destabilize NiCo and NiCu.

Interstitial diffusion is even richer: our results indicate a dominant bidimensional diffusion in NiFe alloy just was with the vacancy, and an isotropic tridimensional movement by translation-rotation mechanisms in NiCu and NiCo. However, while self-interstitial diffusion follows a straightforward mechanism, this is not the case for NiCo, which involves multiple intermediate steps.

We have shown here the richness associated the diffusion of point defects in newly relevant symmetric materials[93, 95] with the help of methods that lift timescale limitations of standard methods and allow for extensive mapping of the system's energy landscape. This approach can also be used to treat the chemical arrangement dependency in disordered structures of these alloys which can allows us to understand in details clustering defects impact, radiation damage and corrosion problems at experimental timescales. Overall, these long-time scale simulations complementary provide informations not accessible by experiment and help us understand what is provide by methods such as y high-resolution transmission electron microscopy (HRTEM)[120, 118, 66], that are limited to 2D materials. Our results show a very rich and unexpected structural evolution led by size-mismatch as well as electronic constraints that cannot be obtained through a simple characterization of defect ground or even local energy barriers. These effects are profound and need to be further evaluated in the case of disordered structures as well as more complex alloys as we try to understand the

physical original or clustering defects impact, radiation damage and corrosion problems in experimentally relevant conditions. They raise also the possibility to use this knowledge to design more stable or even self-annealing materials.

4.9. Code availability

Various ART nouveau implementations are available freely for download from `http://normandmousseau.com`. The k-ART and ART nouveau more recent codes are available from the authors upon request.

4.10. Acknowledgments

This work has been supported by the Canada Research Chairs program and by grants from the Natural Sciences and Engineering Research Council of Canada (NSERC) and the Fonds Québécois de la Recherche sur la Nature et les Technologies (FQRNT). We are grateful to Calcul Quebec for generous allocations of computer resources. We also thank M. M. Rahman and Roger Gaudreault for the important discussions that we did about this paper.

Chapitre 5

LONG-TIME DIFFUSION OF A SINGLE VACANCY IN DISORDERED NIFE ALLOY : CHEMICAL ENVIRONMENT DEPENDENCY AND EFFECT ON VACANCY MIGRATION.

5.1. Objectifs

Le but de cet article est d'étudier la cinétique des monolacunes dans des alliages désordonnés. L'alliage choisi pour déterminer le comportement migratoire des monolacunes est le NiFe qui est très utilisé dans l'industrie. Dans la première partie, nous avons trouvé que la diffusion des lacunes est fonction de la composition chimique de son environnement immédiat. Dans la deuxième partie, nous avons cherché à décrire en détail la surface d'énergie potentielle et par conséquent les chemins de diffusion et les connexions entre eux.

Mots clés : NiFe, alliage désordonné, monolacune, ART cinétique, paysage énergétique

Auteurs dans l'ordre : Sami Mahmoud, Normand Mousseau

Journal : Cet article n'est pas encore été publié à la date de dépôt de la thèse.

5.2. Contributions des auteurs

— Sami Mahmoud (SM) a effectué toutes les simulations, l'analyse des données et la rédaction de l'article.

— Normand Mousseau (NM) a aidé dans la rédaction de l'article et a supervisé tout ce travail.

5.3. ABSTRACT

Radiation damage in metals can produce point defects and disorders the crystal structures. Studying the diffusion of point defects and specially vacancies in disordered alloys still a challenge because of the timescale limitation of standard methods such molecular dynamics. With k-ART, a recently proposed off-lattice kinetic Monte Carlo method with on-the-fly catalog building, we study the diffusion of a single vacancy in disordered NiFe alloy. We first identify the migration behavior of a single vacancy depending on the chemical composition of its nearest neighbors on long simulated times. Then, we characterize in detail the diffusion pathways of a single vacancy which allows us to get thorough description of monovacancy diffusion behavior in such alloys.

5.4. Introduction

The NiFe solid-solution alloys are widely used in industry because of their beneficial properties. They are considered as a maraging steels (iron alloys) because of their high mechanical strength[121]. NiFe alloys, such as invar, also possess a high hardness feature[122] and a very low thermal expansion[123], making them useful for the aerospace industry and, more commonly, in measurement apparatus using bimetallic strips[124], such as seismic creep gauges. Because of this technological interest in a range of environments, these binary alloys also represent in interesting model for characterizing the kinetics and energy landscape associated with point defects in this class of materials.

Indeed, point defects play an important role in influencing the physical properties of materials, especially their mechanical ones[125, 126]. For example, the irradiation of materials causes atomic displacements from perfect crystalline sites, leading to the creation of interstitials and vacancies[127]. While point defects, especially vacancies, are also known to control the kinetics of the solid-solid order-disorder transition in alloys such as NiFe, it was

shown recently that the details of their kinetics is closely linked with the stability of ordered phases in metallic alloys [24].

Characterizing points defects kinetics is challenging, particularly in disordered alloys. Direct experimental probes are not available for mapping the energy landscape; at best is it possible to extract average diffusion rates that cannot provide information on the specific environments. Computational modeling is also challenging. As migration barriers are generally high for these methods, high temperature simulations are required for standard methods such as molecular dynamics to produce any results, as they reach, at best, the microsecond timescale. These approaches are, however, unable to access the appropriate time scale for the more experimentally relevant temperature range, that go down to room temperature in certain cases, such as systems under irradiation [128, 129, 130].

New simulation methods, such as the kinetic Activation Relaxation Technique (k-ART), an off-lattice kinetic Monte Carlo algorithm with on-the-fly catalog building [61, 48], are changing the situation and made it possible to describe in detail the energy landscape for these complex systems and follow the diffusion kinetics on the physically relevant timescale. They make it possible fully reproduce and understand the microscopic kinetic of defects as a function of their local environment, and map the most likely diffusion pathways in these disordered environments.

In this paper, we use k-ART to characterize the diffusion behavior of a single vacancy in disordered NiFe alloy described with an embedded-atom potential. We describe in detail the environment-depend diffusion barriers and kinetics and link these results to recent work on defect diffusion in ordered NiFe alloy [24]. Through the generation of long-time kinetic trajectories we identify the most likely migration pathways and show the dynamic richness that results from this simple disorder.

5.5. Methods

5.5.1. Kinetic Activation Relaxation Technique

While the kinetic Activation Relaxation Technique (k-ART) is described in detail in previous works[61, 45, 42], we present its flowchart in figure 5.1, that can be summarized as follows: Starting from structure in a local energy minimum reached using FIRE (Fast Inertial Relaxation Engine)[101], the local topological environment that surrounds each atom is determined with NAUTY[44]; a graph is generated by linking atoms contained in a sphere with a radius of 6 Å and a cut-off distance of 2.8 Å which ensures the inclusion of first-neighbor atoms only. To distinguish between the various atomic species in the generated graph, self-loops are added to certain chemical species. The generated graph, which contains about 80 vertices for the chosen sphere radius, is sent to NAUTY that returns a key characteristic of the automorphic class to which it belongs. If the associated topology is already known and cataloged, events are copied in the event tree for this configuration. If the topology is new, then events are generated with ART nouveau, an unbiased open-ended saddle point search algorithm, [71, 72] to populate the catalog. For our systems, 25 ART nouveau searches are launched but additional searches are added, when symmetry is found, to ensure the completeness of the catalog of events. To ensure detailed balanced, the reversibility of each event is checked: energy minimization from the saddle point must find both the final and initial minimum, after a small push in the appropriate direction.

Once all events are identified, the transition state theory [102] is applied to make evaluate the rate associated with each even time. The KMC prefactor is considered constant and is set to 10 THz. All energy barriers with occurrence probability of one in 10 000 or more are reconstructed and fully relaxed to ensure the inclusion of elastic events (specific event). The rarer events are simply recopied in the tree as generic event, without reconstruction. Time for the next event is drawn from a Poisson distribution based on the total rate[131]. As the clock is advanced, an event from the tree is chosen randomly with a probability relatively to its rate. After this step, an event is finished and the algorithm starts over for the next step.

In some cases some low-energy events, corresponding to flickering non-diffusive mechanisms, appears and — the progression of the system. To avoid them, we use the basin-accelerated mean-rate method (bacMRM) [48] which solves analytically them. In our simulations, a threshold of 0.5 eV is set to do not consider these flickering states without affecting the real kinetics.

5.5.2. Force calculation and simulated system

We consider solid solution fcc NiFe alloys, as shown in figure 5.2 a), at a 50-50 percent concentration. Cubic boxes of 4000 atoms are used, a size sufficient to ensure that it does not affect the boundary for the defect diffusion, and relaxed at zero pressure. The lattice parameter is equal to 3.5790 Å according to Zhao *et al.*'s work [97]. The system is then relaxed at zero pressure. Forces are calculated from Bonny's potential[109] based on embedded atom method[31]. In previous work, we showed that, for this alloy, Bonny2011's potential is the most accurate in terms of energy barriers for vacancy diffusion in fcc ordered structure[42] as compared with two similar potentials — Bonny2009[112] and Bonny2013[110]. All simulations are run at $T = 300K$, well below the order-disorder transition temperature [23].

We run three simulations in the same disordered NiFe alloy, with the vacancy initially positioned on sites with different chemical distribution in the first-neighbor (1nn) shell. This allows to explore a richer set of environments and to confirm results of the generality of the observations. Each environment is described by a pair (n, m) of 1nn atoms where n is the number of Ni neighbors and m is referred to the number of Fe atoms. Initially, the vacancy is surrounded by (3,9), (5,7) and (4,8) for the first, second and third path respectively. The total simulation time in each run is one hour (3600 seconds) corresponding to 235, 510 and 1315 steps for the first, second and third path respectively, non-counting the oscillations taking place in the flickering basins.

5.6. Results

Figure 5.2(b) shows the mean square displacement (M.S.D.) of the vacancy as a function of time for the three independent runs each of 3600 s. In spite of the disordered nature of the

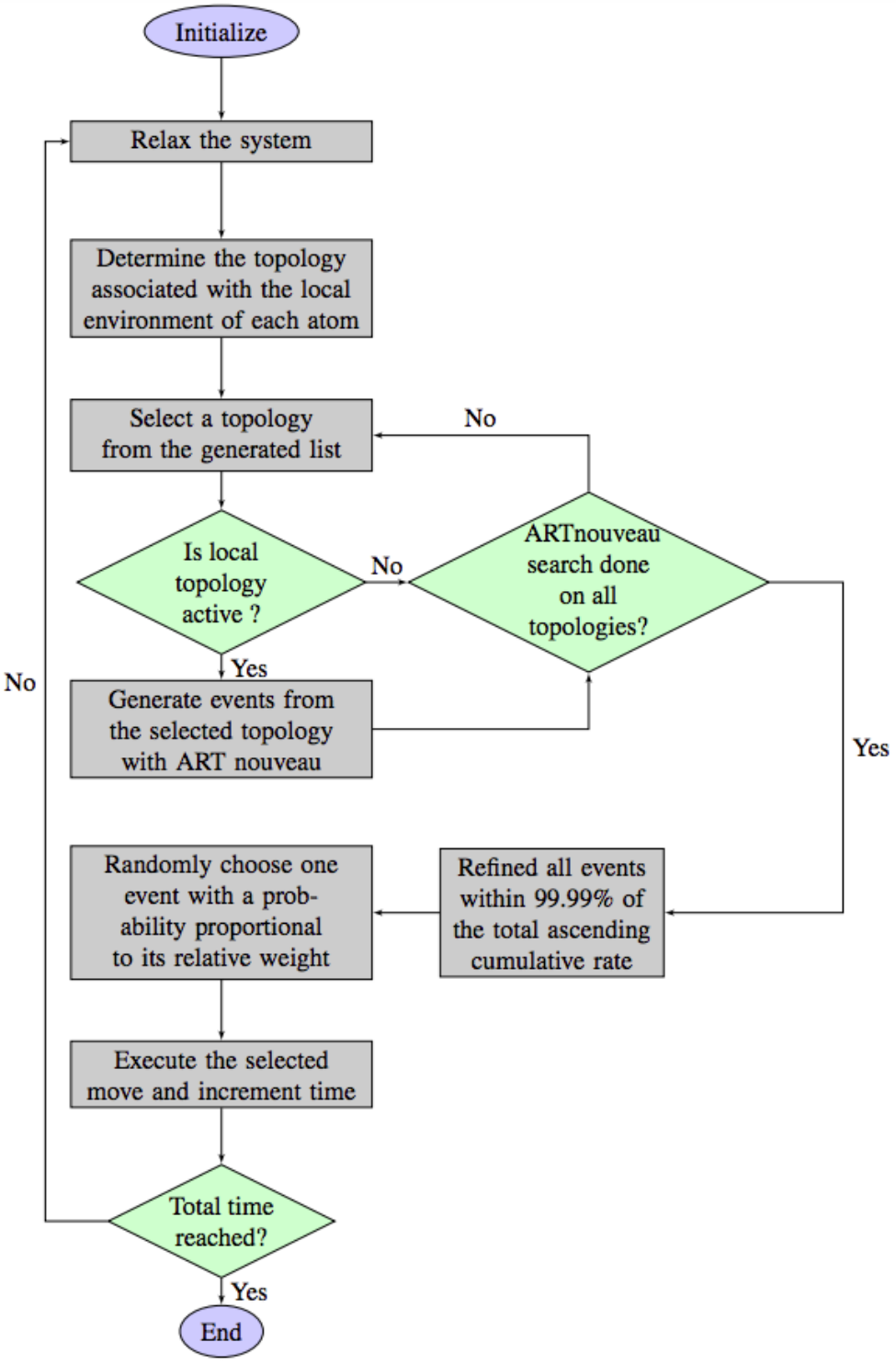

Figure 5.1. Flowchart of kinetic Activation Relaxation Technique.

system, we observe a very similar behavior over hundreds of steps as the vacancy explored the energy landscape of each system. Indeed, from the plot M.S.D. in function of time, we calculate the diffusion coefficient using Einstein formula $D = \frac{\langle R^2 \rangle}{6t}$. Averaging the diffusion

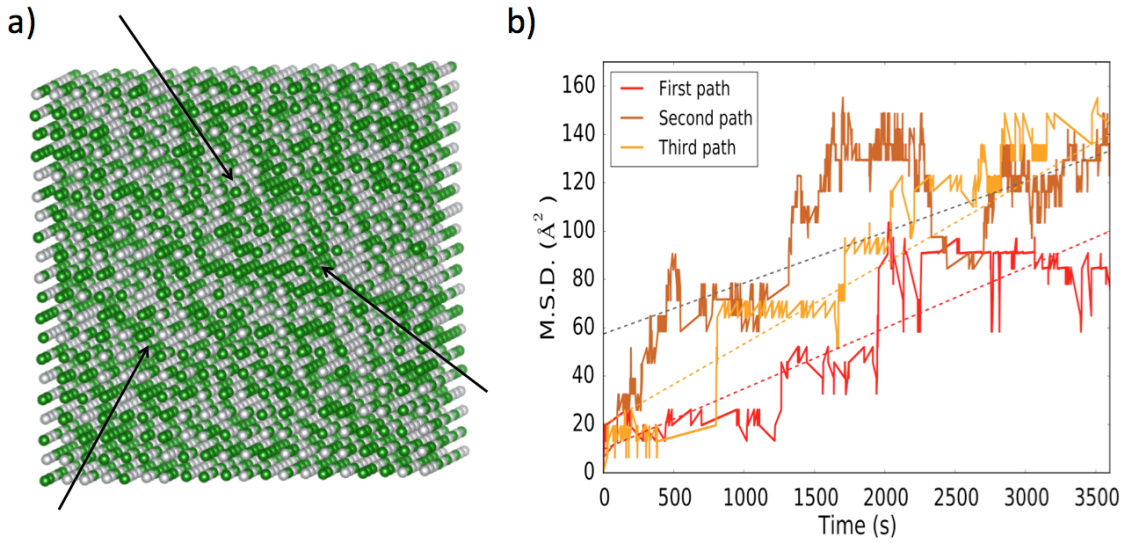

Figure 5.2. Diffusion of a single vacancy in disordered NiFe alloy. a) Three initial positions are considered (indicated by the black arrow) and atoms of Ni and Fe presented by green and gray spheres respectively. b) Mean Square Displacement (M.S.D.) in function of time for the three considered paths that differ by the initial atomic composition of first nearest neighbor of the vacancy. The simulated time for the three paths is equal to one hour (3600 seconds). Diffusion coefficients are calculated according to Einstein formula $D = \frac{\langle R^2 \rangle}{6t}$ (D is the diffusion coefficient and R is the mean square displacement) and are equal to 2.5× 10^{-18} $cm^2 s^{-1}$, 2.1× 10^{-18} $cm^2 s^{-1}$ and 3.3× 10^{-18} $cm^2 s^{-1}$ for first, second and third path respectively.

coefficient over the three paths, we get a value of 2.6× 10^{-18} $cm^2 s^{-1}$. This value is around 10^4 lower than that obtained at T=500K from k-ART simulations[132].

The vacancy diffusion is dominated by the local environment defined mostly by the nearest neighbor chemical composition and arrangement. Figure 5.3, for example, that repeats the diffusion pathways, but with coloring that indicates the local chemical environment for each jump, shows that trapping and diffusive zones are conditioned by the number of Ni and Fe atoms surrounding the vacancy. In the first path (panel (a)), for example, environments (2,10)-(5,7) trap the vacancy over 500 to 1000 seconds, with limiting barriers of 0.88 and 0.68 eV, respectively.

The same environments trap the vacancy for run 3 (panel (c)), as the vacancy oscillates between compositions with color orange and sky blue corresponding to (2,10) and (5,7) respectively in time intervals between 1800 and 2100 seconds, with escaping barriers of 0.88 eV, similar to run 1, as presented in figure 5.4. These environments, however, are not visited

in run 2 (panel (b)). Here, the vacancy is trapped, rather, in a symmetric zone composed of two nearby (3,9)-(3,9) environments, separated by a 0.92 eV barrier also observed in run 3 between 50 and 400 seconds.

Regions (2,10)-(4,8) appears to be trapping ones in the third path in time interval [800, 1600] seconds, with connecting and escaping barriers of 0.74 and 0.83 eV, respectively. This behavior is also observed in the second path between 120 and 350 seconds. In the first and third path, the most present state is the (2,10) with a 45 and 39% respectively from to total of observed states. In the second path, however, the (2,10) state is not dominant and appears only in around 4% of time. In total (2,10) state in then a station state for to the vacancy diffusion in disordered NiFe alloy.

Figure 5.4 shows a flowchart for the single vacancy diffusion paths starting from the reference state (2,10). The flowchart in the form of a tree shows red and black branches related to diffusive and non-diffusive trajectories respectively through different states. We notice that the state (3,9) is always an intermediate state related to diffusive trajectory. (7,5) and (4,8), however, constitute a well that blocks the vacancy diffusion which can be explained by their very low energy. The station state (2,10) is mostly associated to a trapping path which leads nowhere for the vacancy. It is important to notice that the difference in barriers for some similar events is associated to the difference in atom arrangements for similar pair compositions. For example, in the tree presented in figure 5.4, we see that there are two different barriers (0.88 and 0.91) associated to the same event in which the vacancy jumps from (2,10) to (5,7).

5.7. Discussion

The results obtained from studying the vacancy migration behavior in disordered NiFe alloy show a complexity of the diffusion even for a single defect. We have shown that the vacancy is highly trapped in some specific environments. It diffuses, however, very fast in others. The diffusion trend is not monotonous with the species ratio of Ni and Fe surrounding the vacancy. In our simulations, despite the fact that the NiFe alloy is

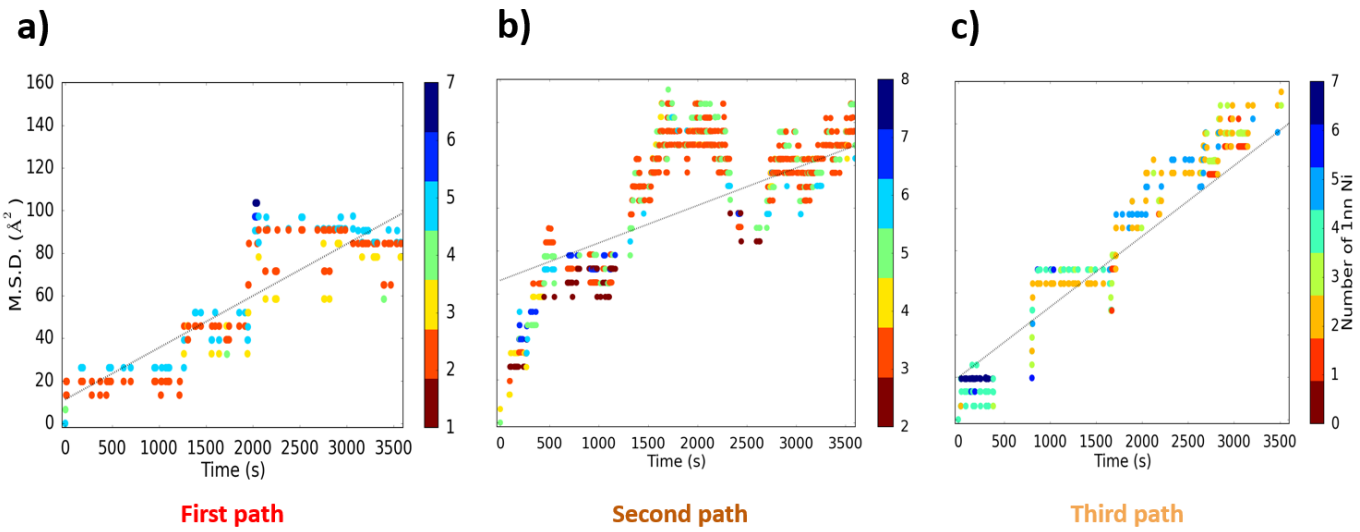

Figure 5.3. Chemical composition of the twelve first nearest neighbors to the vacancy in the a) first, b) second and c) third path in NiFe alloy according to figure 5.2. The number of the Ni atom is indicated with a color bar for each path.

equitably composed by Ni and Fe atoms, there is not a lot of observed surroundings in which the number of Ni atoms dominates compared to Fe which means that the vacancy prefers to stay in Fe dominating environments. This is similar to the case of ordered structures of NiFe alloy [24]. In addition, we have shown through a long-time simulation up to one hour of simulated time that diffusion behavior depends on regions not only states. This is confirmed in the case of state characterized by the pair (2,10) which can be either trapping or diffusive center depending on neighboring states in the energy landscape. After showing the different pathways in figure 5.4, we can notice the complexity of the diffusion mechanism. By comparing a few migration energy barriers to those obtained from DFT calculations in a few paths, our results shows a good agreement. For example, the diffusion barrier between states (5,7) and (6,6) was in the range of [0.93,0.97]eV with Zhao et al's DFT calculations[97] who has checked a few migration energies in disordered NiFe alloy. In our case, the range was [0.87,0.95]eV. For the migration between (7,5) and (6,6) the energy barrier in Zhao et al's[97] work was in the range of [0.97,1.17]eV in perfect agreement with our case which is equal to 1.02 eV. Different diffusion paths are shown leading to a major change in comparison to the initial region.

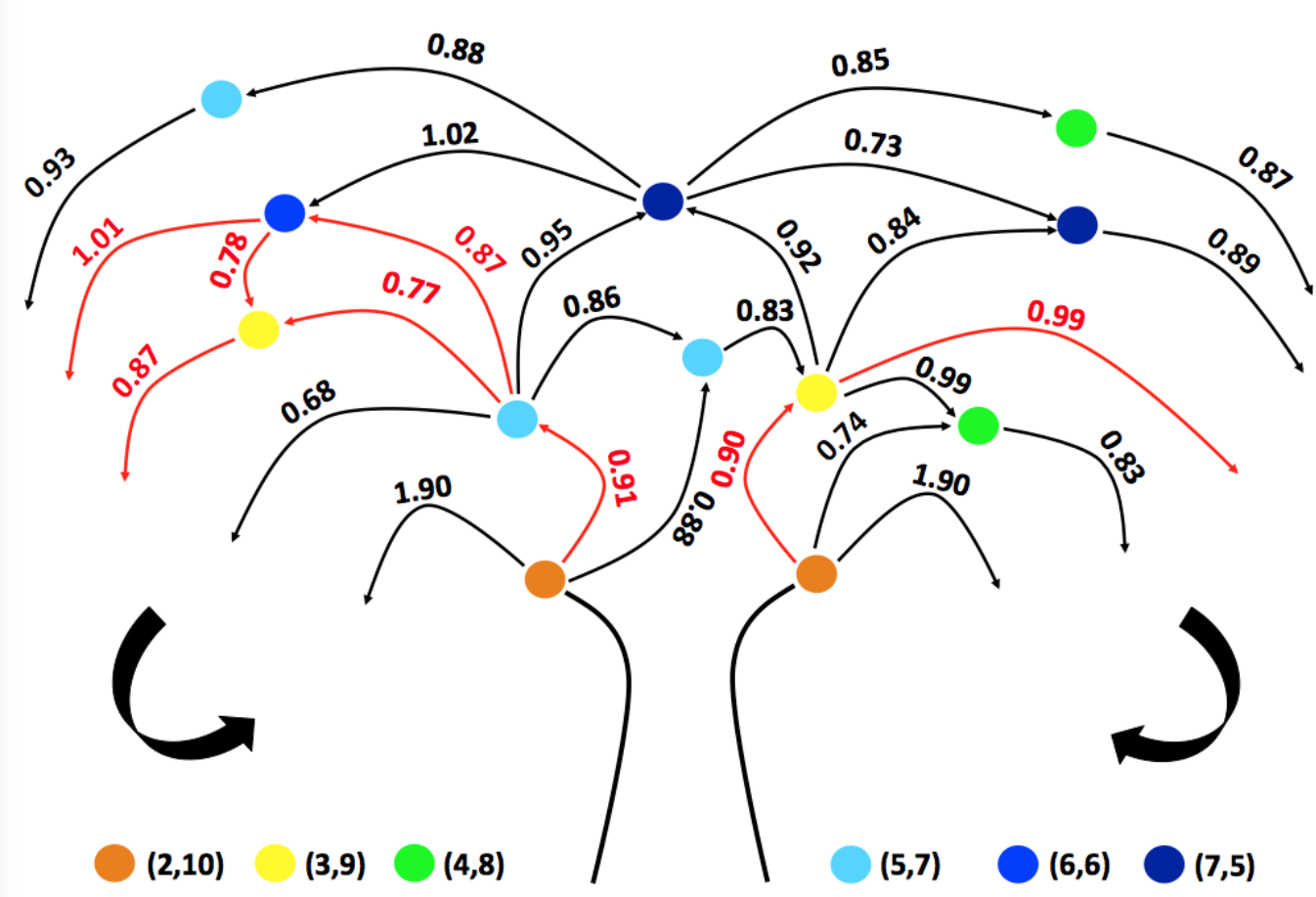

Figure 5.4. Energy pathways of single vacancy in disordered NiFe alloy. Values of energy barriers connecting states are indicated in eV. States are identified with colored circles referred to first nearest neighbors composition indexed by (n,m) with n and m are the number of Ni and Fe respectively. Red and black branches indicates a diffusive and non-diffusive paths respectively. Bold arrows indicates the end of previous cycle and the start of the new one.

5.8. Conclusion

We have shown, for a disordered NiFe alloy with a single vacancy, the dynamic richness of such simple system. The exact kinetic was determinate for this system by identifying the diffusion pathways of the vacancy depending on the chemical composition of its first nearest neighbors. We have demonstrated that these latest controls the migration behavior of the vacancy by making it diffuses fast in some cases, and block it in others. We also have the diffusion "wells" for the vacancy in the disordered NiFe. We have then demonstrate the effect of chemical composition of neighboring atoms to the vacancy on its kinetic by

offering a unique energy landscape description not allowed by other kinetic Monte Carlo methods. Our results can provide explanations to the mystery of "sluggish diffusion" observed experimentally in high entropy alloys (HEAs) [133, 134]. It will be interesting in the future to study the case of many vacancies and their aggregation as well as the chemical composition effect on the formation of stacking fault tetrahedra.

5.9. Code availability

Various ART nouveau implementations are available freely for download from `http://normandmousseau.com`. The k-ART and ART nouveau more recent codes are available from the authors upon request.

5.10. Acknowledgments

This work has been supported by the Canada Research Chairs program and by grants from the Natural Sciences and Engineering Research Council of Canada (NSERC) and the Fonds Québécois de la Recherche sur la Nature et les Technologies (FQRNT). We are grateful to Calcul Quebec for generous allocations of computer resources and the Tunisian government for the additional financial support.

CONCLUSION GÉNÉRALE

Durant cinq ans de thèse, nous avons contribué à développer ART cinétique et ce dans le but de bien comprendre certains phénomènes liés à la cinétique des défauts ponctuels dans les alliages à base de nickel.

En premier lieu, nous avons pu caractériser les mécanismes de diffusion des défauts ponctuels individuels et sous forme d'amas lacunaires et d'interstitiels dans le nickel cristallin pur. Nous avons réussi à donner une image complète quant au paysage énergétique de ces défauts ce qui nous a permis de donner une description détaillée de leur cinétique. Dans nos résultats sur les lacunes allant d'un à cinq, on a vu que les amas de lacunes diffusent plus rapidement que les monolacunes à l'exception de la tetralacune. Le comportement diffusif n'était pas monotone vis-à-vis le nombre de lacunes. En plus des amas lacunaires, nous avons étudié les interstitiels (dont le nombre varie d'un à cinq) et nous avons montré que la diffusion des agrégats d'interstitiels est très rapide, surtout pour le cas de quatre défauts. Nous avons pu identifier deux nouveaux mécanismes de diffusion des dumbbells d'interstitiels en plus de celui qui est dominant.

Dans notre deuxième partie, nous avons étudié l'effet de la diffusion des monolacunes et moninterstitiels dans des alliages à base de nickel — NiFe, NiCu et NiCo —. Pour se faire, nous avons simulé sur de longues échelles de temps le mouvement d'une lacune et d'un interstitiel dans des structures fcc hautement ordonnées $L1_0$ qui consiste à un empilement alterné de monocouches de nickel avec un autre élément. Nous avons montré que, à basse température telle que l'ambiante, la diffusion de la lacune n'affecte pas l'ordre des ces structures pour l'alliage NiFe car l'ordre global de la structure cristalline reste intact. Toutefois,

même pour une seule lacune, l'ordre peut être affecté dans les alliages NiCu et NiCo. En effet, nos simulations ont montré que la diffusion de la lacune est tridimentionnelle pour ces deux derniers alliages. Pour l'interstitiel, la structure ordonnée des alliages NiFe et NiCo n'est pas affectée par la diffusion de l'interstitiel, car elle a comportement bidimensionnel dans plan du nickel avec des mécanismes plus complexes pour le NiCo. Pour l'alliage NiCu, tout comme le cas de la lacune, la diffusion de l'interstitiel implique une instabilité de sa structure ordonnée.

Comme troisième partie, nous nous sommes intéressés au comportement de la monolacune dans des structures désordonnées de l'alliage NiFe. Nos résultats montrent une dépendance quant au comportement diffusif de la lacune vis-à-vis la composition chimique de son environnement local en premiers voisins. Nous avons pu aussi explorer la surface d'énergie potentielle de la lacune ce qui nous a permis de déterminer en détails exacts les chemins de diffusion et nous avons aussi montré la complexité et la richesse de sa dynamique. De plus, nous avons déterminé les chemins préférentiels exacts quant au mouvement de la lacune dans un tel alliage désordonné ce qui constitue une analyse approfondie et unique.

Les travaux que nous avons menés nous ont permis d'avoir une meilleure compréhension de la cinétique des défauts ponctuels dans le nickel pur ainsi que ses alliages. Nous avons eu des résultats marquants dans différents systèmes (un matériau pur, des alliages ordonnés ainsi que désordonnés). Nous avons montré que la physique est différente pour des alliages simples constitués d'éléments semblables (en termes de rayon atomique).

Les résultats qu'on a trouvés dans le deuxième article sont éminents, sauf que ça sera très important de vérifier le cas d'agrégats lacunaires, car ils peuvent avoir un comportement différent de celui des monolacunes. De même pour le troisième article, ça sera indispensable de traiter la diffusion des agrégats de lacunes dans les alliages désordonnés considérés. Il est aussi important de simuler la diffusion des interstitiels ainsi que leurs recombinaisons avec les lacunes dans les deux systèmes ordonnés et désordonnés. Aussi, il est indispensable d'étudier l'effet de la température sur la diffusion de la lacune dans les alliages désordonnés de nickel.

Comme perspective de ce travail, il serait important d'étudier des défauts plus complexes tels que des défauts d'empilement en tétraèdre qui sont observés par microscopie électronique[135] mais peu étudiés par des méthodes numériques, des dislocations et leur glissement et montée dans les structures ordonnées contre celles désordonnées, les joints de grains ainsi que leur interaction avec d'autres défauts étendus (dislocations et joints de grains) et les défauts ponctuels. Aussi, il serait possible d'étudier et donc expliquer le phénomène de "sluggish diffusion" (diffusion lente) dans les alliages de haute entropie (des alliages formés d'au moins cinq éléments métalliques).

Bibliographie

[1] G. E. Dieter and D. J. Bacon. *Mechanical metallurgy*, volume 3. McGraw-hill New York, 1986.

[2] H. Xiao and I. Baker. The relationship between point defects and mechanical properties in fe al at room temperature. *Acta metallurgica et materialia*, 43(1) :391–396, 1995.

[3] Y. Fukai. Electrical resistivity due to vacancies and impurities in aluminium : Band structure effects in the defect scattering in polyvalent metals. *Physics Letters A*, 27(7) :416–417, 1968.

[4] D. Y. Gusakova, A. V. Vedyaev, O. A. Kotel'nikova, and A. I. Buzdin. Magnetization distribution in a helicoidal structure containing a point defect. *Journal of Experimental and Theoretical Physics*, 99(6) :1207–1213, 2004.

[5] W. D. Callister Jr and D. G. Rethwisch. *Fundamentals of materials science and engineering : an integrated approach*. John Wiley & Sons, 2012.

[6] L. H. Van Vlack. *Elements of materials science and engineering*. Addison-Wesley, 1989.

[7] M Vázquez, J González, and A Hernando. Induced magnetic anisotropy and change of the magnetostriction by current annealing in co-based amorphous alloys. *Journal of magnetism and magnetic materials*, 53(4) :323–329, 1986.

[8] M. Eldrup. Application of the positron annihilation technique in studies of defects in solids. In *Defects in Solids*, pages 145–178. Springer, 1986.

[9] S. Rushbrook Williams and L. W. Barr. A radioactive tracer study of diffusion processes in lead and silver bromide. *Le Journal de Physique Colloques*, 34(C9) :C9–173, 1973.

[10] I. H. Segel. Enzyme kinetics : behavior and analysis of rapid equilibrium and steady state enzyme systems. 1975.

[11] F. Tuomisto and I. Makkonen. Defect identification in semiconductors : Experiment and theory of positron annihilation. *Rev. Mod. Phys*, 2013.

[12] S. L. Dudarev. Density functional theory models for radiation damage. *Annual Review of Materials Research*, 43, 2013.

[13] H. Jónsson, G. Mills, and K. W. Jacobsen. Nudged elastic band method for finding minimum energy paths of transitions. In *Classical and quantum dynamics in condensed phase simulations*, pages 385–404. World Scientific, 1998.

[14] G. Nandipati, N. Govind, A. Andersen, and A. Rohatgi. Self-learning kinetic monte carlo simulations of al diffusion in mg. *Journal of Physics : Condensed Matter*, 28(15) :155001, 2016.

[15] G. Henkelman and H. Jónsson. A dimer method for finding saddle points on high dimensional potential surfaces using only first derivatives. *The Journal of chemical physics*, 111(15) :7010–7022, 1999.

[16] P. M. Derlet, D. Nguyen-Manh, and S. L. Dudarev. Multiscale modeling of crowdion and vacancy defects in body-centered-cubic transition metals. *Physical Review B*, 76(5) :054107, 2007.

[17] J. P. Hirth and J. Lothe. Theory of dislocations. *John Wiley & Sons*, 1982.

[18] H. Yang, M. Huang, and Z. Li. The influence of vacancies diffusion-induced dislocation climb on the creep and plasticity behaviors of nickel-based single crystal superalloy. *Computational Materials Science*, 99 :348–360, 2015.

[19] F. C. Frank. Dislocations and point defects. *Discussions of the Faraday Society*, 23 :122–127, 1957.

[20] M. Wen, A. Takahashi, and N. M. Ghoniem. Kinetics of self-interstitial cluster aggregation near dislocations and their influence on hardening. *Journal of Nuclear Materials*, 392(3) :386–395, 2009.

[21] S. D. Mesarovic. Lattice continuum and diffusional creep. *Proc. R. Soc. A*, 472(2188) :20160039, 2016.

[22] A. H. Seville. Effects of vacancies on the physical properties of platinum. *Platinum Metals Review*, 19(3) :96–99, 1975.

[23] N. Bordeaux, A. M. Montes-Arango, J. Liu, K. Barmak, and L. H. Lewis. Thermodynamic and kinetic parameters of the chemical order-disorder transformation in l10 feni (tetrataenite). *Acta Materialia*, 103 :608–615, 2016.

[24] S. Mahmoud and N. Mousseau. Long-time point defect diffusion in ordered nickel-based binary alloys : How small kinetic differences can lead to completely long-time structural evolution. *Materialia*, 4(4) :575–584, 2018.

[25] P. B. Hirsch, R. W. Horne, and M. J. Whelan. Direct observations of the arrangement and motion of dislocations in aluminium. *Philosophical Magazine*, 7 :677—684, 1956.

[26] M. S. Daw and M. I. Baskes. Embedded-atom method : Derivation and application to impurities, surfaces, and other defects in metals. *Physical Review B*, 29(12) :6443, 1984.

[27] J. H. Rose, J. Ferrante, and J. R. Smith. Universal binding energy curves for metals and bimetallic interfaces. *Physical Review Letters*, 47(9) :675, 1981.

[28] M. I. Baskes, J. S. Nelson, and A. F. Wright. Semiempirical modified embedded-atom potentials for silicon and germanium. *Physical Review B*, 40(9) :6085, 1989.

[29] B.-J. Lee and M. I. Baskes. Second nearest-neighbor modified embedded-atom-method potential. *Physical Review B*, 62(13) :8564, 2000.

[30] A. C. T. Van Duin, S. Dasgupta, F. Lorant, and W. A. Goddard. ReaxFF : A reactive force field for hydrocarbons. *Journal of Physical Chemistry A*, 105(41) :9396–9409, 2001.

[31] S. M. Foiles, M. I. Baskes, and M. S. Daw. Embedded-atom-method functions for the fcc metals Cu, Ag, Au, Ni, Pd, Pt, and their alloys. *Physical Review B*, 33(12) :7983–7991, 1986.

[32] M. W. Finnis and J. E. Sinclair. A simple empirical n-body potential for transition metals. *Philosophical Magazine A*, 50(1) :45–55, 1984.

[33] L. Verlet. Computer" experiments" on classical fluids. i. thermodynamical properties of lennard-jones molecules. *Physical review*, 159(1) :98, 1967.

[34] H. Eyring. The activated complex in chemical reactions. *The Journal of Chemical Physics*, 3(2) :107–115, 1935.

[35] G. H. Vineyard. Frequency factors and isotope effects in solid state rate processes. *Journal of Physics and Chemistry of Solids*, 3(1-2) :121–127, 1957.

[36] J. R. Beeler Jr. Displacement spikes in cubic metals. i. α-iron, copper, and tungsten. *Physical Review*, 150(2) :470, 1966.

[37] R. Gordon. Adsorption isotherms of lattice gases by computer simulation. *The Journal of Chemical Physics*, 48(3) :1408–1409, 1968.

[38] F. F. Abraham and G. M. White. Computer simulation of vapor deposition on two-dimensional lattices. *Journal of Applied Physics*, 41(4) :1841–1849, 1970.

[39] K. A. Fichthorn and W. H. Weinberg. Theoretical foundations of dynamical monte carlo simulations. *The Journal of chemical physics*, 95(2) :1090–1096, 1991.

[40] M. Trochet, L. K. Béland, J.-F. Joly, P. Brommer, and N. Mousseau. Diffusion of point defects in crystalline silicon using the kinetic activation-relaxation technique method. *Physical Review B*, 91(22) :224106, 2015.

[41] O. A. Restrepo, C. S. Becquart, F. El-Mellouhi, O. Bouhali, and N. Mousseau. Diffusion mechanisms of c in 100, 110 and 111 fe surfaces studied using kinetic activation-relaxation technique. *Acta Materialia*, 136 :303–314, 2017.

[42] S. Mahmoud, M. Trochet, O. A. Restrepo, and N. Mousseau. Study of point defects diffusion in nickel using kinetic activation-relaxation technique. *Acta Materialia*, 144 :679–690, 2018.

[43] J.-F. Joly, L. K. Béland, P. Brommer, F. El-Mellouhi, and N. Mousseau. Optimization of the kinetic activation-relaxation technique, an off-lattice and self-learning kinetic monte-carlo method. In *Journal of Physics : Conference Series*, volume 341, page

012007. IOP Publishing, 2012.

[44] B. D. McKay. Practical graph isomorphism. 1981.

[45] N. Mousseau, L. K. Béland, P. Brommer, F. El-Mellouhi, J. F. Joly, G. K. N'tsouaglo, O. A. Restrepo, and M. Trochet. Following atomistic kinetics on experimental timescales with the kinetic Activation Relaxation Technique. *Computational Materials Science*, 100 :111–123, 2015.

[46] M. Trochet and N. Mousseau. Energy landscape and diffusion kinetics of lithiated silicon : A kinetic activation-relaxation technique study. *Physical Review B*, 96(13) :134118, 2017.

[47] O. A. Restrepo, N. Mousseau, M. Trochet, F. El-Mellouhi, O. Bouhali, and C. S. Becquart. Carbon diffusion paths and segregation at high-angle tilt grain boundaries in α-fe studied by using a kinetic activation-relation technique. *Physical Review B*, 97(5) :054309, 2018.

[48] L. K. Béland, P. Brommer, F. El-Mellouhi, J.-F. Joly, and N. Mousseau. Kinetic activation-relaxation technique. *Physical Review E*, 84(4) :046704, 2011.

[49] B. Puchala, M. L. Falk, and K. Garikipati. An energy basin finding algorithm for kinetic monte carlo acceleration. *The Journal of Chemical Physics*, 132(13) :134104, 2010.

[50] P. G. Klemens. Thermal resistance due to point defects at high temperatures. *Physical review*, 119(2) :507, 1960.

[51] R. Gul, U. N. Roy, S. U. Egarievwe, A. E. Bolotnikov, G. S. Camarda, Y. Cui, A. Hossain, G. Yang, and R. B. James. Point defects : Their influence on electron trapping, resistivity, and electron mobility-lifetime product in cdtexse1- x detectors. *Journal of Applied Physics*, 119(2) :025702, 2016.

[52] I. J Robertson and M. C. Payne. k-point sampling and the kp method in pseudopotential total energy calculations. *Journal of Physics : Condensed Matter*, 2(49) :9837, 1990.

[53] W. L. Jorgensen, J. Chandrasekhar, J. D. Madura, R. W Impey, and M. L. Klein. Comparison of simple potential functions for simulating liquid water. *The Journal of chemical physics*, 79(2) :926–935, 1983.

[54] M. I. Baskes. Application of the embedded-atom method to covalent materials : a semiempirical potential for silicon. *Physical review letters*, 59(23) :2666, 1987.

[55] M. I. Baskes. Modified embedded-atom potentials for cubic materials and impurities. *Physical review B*, 46(5) :2727, 1992.

[56] M. I. Baskes and R. A. Johnson. Modified embedded atom potentials for hcp metals. *Modelling and Simulation in Materials Science and Engineering*, 2(1) :147, 1994.

[57] B.-J. Lee, M. I. Baskes, H. Kim, and Y. K. Cho. Second nearest-neighbor modified embedded atom method potentials for bcc transition metals. *Physical Review B*, 64(18) :184102, 2001.

[58] B.-J. Lee, J.-H. Shim, and M. I. Baskes. Semiempirical atomic potentials for the fcc metals cu, ag, au, ni, pd, pt, al, and pb based on first and second nearest-neighbor modified embedded atom method. *Physical Review B*, 68(14) :144112, 2003.

[59] M. P. Ariza, R. Serrano, J. P. Mendez, and M. Ortiz. Stacking faults and partial dislocations in graphene. *Philosophical Magazine*, 92(16) :2004–2021, 2012.

[60] C. Zou, Y. K. Shin, A. C. T. Van Duin, H. Fang, and Z.-K. Liu. Molecular dynamics simulations of the effects of vacancies on nickel self-diffusion, oxygen diffusion and oxidation initiation in nickel, using the reaxff reactive force field. *Acta Materialia*, 83 :102–112, 2015.

[61] F. El-Mellouhi, N. Mousseau, and L. J. Lewis. Kinetic activation-relaxation technique : An off-lattice self-learning kinetic monte carlo algorithm. *Physical Review B*, 78(15) :153202, 2008.

[62] L. K. Béland and N. Mousseau. Long-time relaxation of ion-bombarded silicon studied with the kinetic activation-relaxation technique : Microscopic description of slow aging in a disordered system. *Physical Review B*, 88(21) :214201, 2013.

[63] P. Brommer, L. K. Béland, J.-F. Joly, and N. Mousseau. Understanding long-time vacancy aggregation in iron : A kinetic activation-relaxation technique study. *Physical Review B*, 90(13) :134109, 2014.

[64] O. A. Restrepo, N. Mousseau, F. El-Mellouhi, O. Bouhali, M. Trochet, and C. S. Becquart. Diffusion properties of fe–c systems studied by using kinetic activation–relaxation technique. *Computational Materials Science*, 112 :96–106, 2016.

[65] A. Jay, M. Raine, N. Richard, N. Mousseau, V. Goiffon, A. Hémeryck, and P. Magnan. Simulation of single particle displacement damage in silicon–part ii : Generation and long-time relaxation of damage structure. *IEEE Transactions on Nuclear Science*, 64(1) :141–148, 2017.

[66] C. Lu, L. Niu, N. Chen, K. Jin, T. Yang, P. Xiu, Y. Zhang, F. Gao, H. Bei, S. Shi, M.-R. He, I. M. Robertson, W. J. Weber, and L. Wang. Enhancing radiation tolerance by controlling defect mobility and migration pathways in multicomponent single-phase alloys. *Nature communications*, 7 :13564, 2016.

[67] S. Plimpton. Fast parallel algorithms for short-range molecular dynamics. *Journal of computational physics*, 117(1) :1–19, 1995.

[68] M. I. Baskes. Determination of modified embedded atom method parameters for nickel. *Materials Chemistry and Physics*, 50(2) :152–158, 1997.

[69] F. J. Cherne, M. I. Baskes, and P. A. Deymier. Properties of liquid nickel : A critical comparison of eam and meam calculations. *Physical Review B*, 65(2) :024209, 2001.

[70] M. Trochet, A. Sauvé-Lacoursière, and N. Mousseau. Algorithmic developments of the kinetic activation-relaxation technique : Accessing long-time kinetics of larger and more complex systems. *The Journal of chemical physics*, 147(15) :152712, 2017.

[71] G. T. Barkema and N. Mousseau. Event-based relaxation of continuous disordered systems. *Physical review letters*, 77(21) :4358, 1996.

[72] R. Malek and N. Mousseau. Dynamics of lennard-jones clusters : A characterization of the activation-relaxation technique. *Physical Review E*, 62(6) :7723, 2000.

[73] A. B. Bortz, M. H. Kalos, and J. L. Lebowitz. A new algorithm for monte carlo simulation of ising spin systems. *Journal of Computational Physics*, 17(1) :10 – 18, 1975.

[74] H. Yildirim, A. Kara, and T. S. Rahman. Origin of quasi-constant pre-exponential factors for adatom diffusion on cu and ag surfaces. *Phys. Rev. B*, 76 :165421, Oct 2007.

[75] H. Chamati, N. I. Papanicolaou, Y. Mishin, and D. A. Papaconstantopoulos. Embedded-atom potential for fe and its application to self-diffusion on fe(100). *Surface Science*, 600(9) :1793 – 1803, 2006.

[76] P. A. Korzhavyi, I. A. Abrikosov, B. Johansson, A. V. Ruban, and H. L. Skriver. First-principles calculations of the vacancy formation energy in transition and noble metals. *Phys. Rev. B*, 59 :11693–11703, May 1999.

[77] E. Asadi, M. A. Zaeem, A. Moitra, and M. A. Tschopp. Effect of vacancy defects on generalized stacking fault energy of fcc metals. *Journal of physics. Condensed matter : an Institute of Physics journal*, 26(11) :115404, 2014.

[78] E. H. Megchiche, C. Mijoule, and M. Amarouche. First principles calculations of vacancy–vacancy interactions in nickel : thermal expansion effects. *Journal of Physics : Condensed Matter*, 22(48) :485502, 2010.

[79] P. K. Nandi, M. C. Valsakumar, S. Chandra, H. K. Sahu, and C. S. Sundar. Efficacy of surface error corrections to density functional theory calculations of vacancy formation energy in transition metals. *Journal of Physics : Condensed Matter*, 22(34) :345501, 2010.

[80] R. W. Siegel. Positron annihilation spectroscopy. *Annual Review of Materials Science*, 10(1) :393–425, 1980.

[81] H. Bakker. A curvature in the in d versus 1/t plot for self-diffusion in nickel at temperatures from 980 to 1400¡c. *physica status solidi (b)*, 28(2) :569–576, 1968.

[82] H. Kronmüller. Vacancies and interstitials in metals. *Eds. Seeger A., Schumacher D., Schilling W., and Diehl J., North-Holland Publ. Co., Amsterdam*, 1970.

[83] J. D. Tucker, T. R. Allen, and D. Morgan. Ab Initio Defect Properties for Modeling Radiation-Induced Segregation in Fe-Ni-Cr Alloys. *13th Environmental Degradation of Materials In Nuclear Power Systems*, (January 2015), 2007.

[84] S. T. Howard. Ab Initio. (10) :6085–6090, 1996.

[85] D. Connétable, É. Andrieu, and D. Monceau. First-principles nickel database : Energetics of impurities and defects. *Computational Materials Science*, 101 :77–87, 2015.

[86] S. Nanaot, K. Kuribayashig, S. Tanigawall, and M. Doyamall. Studies of defects at thermal equilibrium and melting in Cu and Ni by positron annihilation ? 1403.

[87] P. Zhao and Y. Shimomura. Molecular dynamics calculations of properties of the self-interstitials in copper and nickel. *Computational Materials Science*, 14(1-4) :84–90, 1999.

[88] M.-C. Marinica, F. Willaime, and N. Mousseau. Energy landscape of small clusters of self-interstitial dumbbells in iron. *Physical Review B - Condensed Matter and Materials Physics*, 83(9) :1–14, 2011.

[89] Y. Matsukawa and S. J. Zinkle. where N. *Science*, 318(November) :959–962, 2007.

[90] D. S. Aidhy, C. Lu, K. Jin, H. Bei, Y. Zhang, L. Wang, and W. J. Weber. Point defect evolution in ni, nife and nicr alloys from atomistic simulations and irradiation experiments. *Acta Materialia*, 99(Complete) :69–76, 2015.

[91] E. Martínez and B. P. Uberuaga. *Scientific Reports*, 5, 2010.

[92] S. Fukami, H. Sato, M. Yamanouchi, S. Ikeda, and H. Ohno. Coni films with perpendicular magnetic anisotropy prepared by alternate monoatomic layer deposition. *Applied Physics Express*, 6(7) :073010, 2013.

[93] K. Takanashi, M. Mizuguchi, T. Kojima, and T. Tashiro. Fabrication and characterization of l10-ordered feni thin films. *Journal of Physics D : Applied Physics*, 50(48) :483002, 2017.

[94] C. Palmstrøm. Epitaxial heusler alloys : New materials for semiconductor spintronics. *MRS bulletin*, 28(10) :725–728, 2003.

[95] S. Goto, H. Kura, E. Watanabe, Y. Hayashi, H. Yanagihara, Y. Shimada, M. Mizuguchi, K. Takanashi, and E. Kita. Synthesis of single-phase l 1 0-feni magnet powder by nitrogen insertion and topotactic extraction. *Scientific reports*, 7(1) :13216, 2017.

[96] Y. Geng, T. Ablekim, M. A. Koten, M Weber, K. Lynn, and J. E. Shield. Defect generation and analysis in mechanically alloyed stoichiometric fe-ni alloys. *Journal of Alloys and Compounds*, 633 :250 – 255, 2015.

[97] S. Zhao, G. M. Stocks, and Y. Zhang. Defect energetics of concentrated solid-solution alloys from ab initio calculations : Ni 0.5 co 0.5, ni 0.5 fe 0.5, ni 0.8 fe 0.2 and ni 0.8 cr 0.2. *Physical Chemistry Chemical Physics*, 18(34) :24043–24056, 2016.

[98] D. Chakraborty, A. Harms, M. W. Ullah, W. J. Weber, and D. S. Aidhy. Effect of atomic order/disorder on vacancy clustering in concentrated nife alloys. *Computational Materials Science*, 147 :194 – 203, 2018.

[99] F. El-Mellouhi, N. Mousseau, and L. J. Lewis. Kinetic activation-relaxation technique : An off-lattice self-learning kinetic Monte Carlo algorithm. *Physical Review B*, 78(15) :153202, 2008.

[100] L. M. Néel, J. Paulevé, R. Pauthenet, J. Laugier, and D. Dautreppe. Magnetic properties of an iron-nickel single crystal ordered by neutron bombardment. *J. Appl. Phys*, 35 :873–876, 1964.

[101] E. Bitzek, P. Koskinen, F. Gähler, M. Moseler, and P. Gumbsch. Structural relaxation made simple. *Physical review letters*, 97(17) :170201, 2006.

[102] K. J. Laidler and M. C. King. Development of transition-state theory. *The Journal of physical chemistry*, 87(15) :2657–2664, 1983.

[103] Y. Mishin, M. J. Mehl, and D. A. Papaconstantopoulos. Phase stability in the fe–ni system : Investigation by first-principles calculations and atomistic simulations. *Acta materialia*, 53(15) :4029–4041, 2005.

[104] B. Onat and S. Durukanoğlu. An optimized interatomic potential for cu–ni alloys with the embedded-atom method. *Journal of Physics : Condensed Matter*, 26(3) :035404, 2013.

[105] P. Pietrokowsky. Lattice parameter of alpha iron by divergent beam diffraction. *Journal of Applied Physics*, 37(12) :4560–4571, 1966.

[106] E. S. Drexler, N.J Simon, and R. P. Reed. Properties of copper and copper alloys at cryogenic temperatures. Technical report, NIST, 1992.

[107] F. Vincent and M. Figlarz. Quelques pŕecisions sur les param'etres cristallins et l'intensite des raies debye-scherrer du cobalt cubique et du cobalt hexagonal. *C. R. Hebd. Seances Acad. Sci.*, 264C :1270, 1967.

[108] G. Bonny, R. C. Pasianot, and L. Malerba. Fe–ni many-body potential for metallurgical applications. *Modelling and Simulation in Materials Science and Engineering*, 17(2) :025010, 2009.

[109] G. Bonny, D. Terentyev, R. C. Pasianot, S. Poncé, and A. Bakaev. Interatomic potential to study plasticity in stainless steels : the fenicr model alloy. *Modelling and simulation in materials science and engineering*, 19(8) :085008, 2011.

[110] G. Bonny, N. Castin, and D. Terentyev. Interatomic potential for studying ageing under irradiation in stainless steels : the fenicr model alloy. *Modelling and Simulation in Materials Science and Engineering*, 21(8) :085004, 2013.

[111] G. P. P. Pun, V. Yamakov, and Y. Mishin. Interatomic potential for the ternary ni–al–co system and application to atomistic modeling of the b2–l10 martensitic transformation. *Modelling and Simulation in Materials Science and Engineering*, 23(6) :065006, 2015.

[112] G. Bonny, R. C. Pasianot, N. Castin, and L. Malerba. Ternary fe–cu–ni many-body potential to model reactor pressure vessel steels : First validation by simulated thermal annealing. *Philosophical magazine*, 89(34-36) :3531–3546, 2009.

[113] B. Liu, F. Yuan, K. Jin, Y. Zhang, and W. J. Weber. Ab initio molecular dynamics investigations of low-energy recoil events in ni and nico. *Journal of Physics : Condensed Matter*, 27(43) :435006, 2015.

[114] R. R. Bourassa and B. Lengeler. The formation and migration energies of vacancies in quenched copper. *Journal of Physics F : Metal Physics*, 6(8) :1405, 1976.

[115] S. Zhao, Y. Osetsky, and Y. Zhang. Preferential diffusion in concentrated solid solution alloys : Nife, nico and nicocr. *Acta Materialia*, 128 :391–399, 2017.

[116] M. Müller and K. Albe. Kinetic lattice monte-carlo simulations on the ordering kinetics of free and supported fept l10-nanoparticles. *Beilstein journal of nanotechnology*, 2 :40, 2011.

[117] E. Clementi, D. L. Raimondi, and W. P. Reinhardt. Atomic screening constants from scf functions. ii. atoms with 37 to 86 electrons. *The Journal of chemical physics*, 47(4) :1300–1307, 1967.

[118] K. Arakawa, K. Ono, M. Isshiki, K. Mimura, M. Uchikoshi, and H. Mori. Observation of the one-dimensional diffusion of nanometer-sized dislocation loops. *Science*, 318(5852) :956–959, 2007.

[119] R. L. Klueh, P. J. Maziasz, and E. H. Lee. Manganese as an austenite stabilizer in fe cr mn c steels. *Materials Science and Engineering : A*, 102(1) :115–124, 1988.

[120] Z. Wu and Z. Ni. Spectroscopic investigation of defects in two-dimensional materials. *Nanophotonics*, 6(6) :1219–1237, 2017.

[121] J. R. Mihalisin and C. G. Bieber. Progress toward attaining theoretical strength with iron-nickel maraging steels. *JOM*, 18(9) :1033–1036, 1966.

[122] P.-Z. Si and C.-J. Choi. High hardness nanocrystalline invar alloys prepared from fe-ni nanoparticles. *Metals*, 8(1) :28, 2018.

[123] M. Van Schilfgaarde, I. A. Abrikosov, and B. Johansson. Origin of the invar effect in iron–nickel alloys. *Nature*, 400(6739) :46, 1999.

[124] J. Boughaleb, A. Arnaud, S. Monfray, P. J. Cottinet, S. Quenard, F. Boeuf, D. Guyomar, and T. Skotnicki. Design and performance benchmark of various architectures of a piezoelectric bimetallic strip heat engine. *Optical Materials*, 56 :110–115, 2016.

[125] M. Meshii. Effect of point defects on mechanical properties in metals. *Technical Progress Report, 1 Jan.-31 Dec. 1974 Northwestern Univ., Evanston, IL. Dept. of Materials Science.*, 1974.

[126] K. Schroeder. Theory of diffusion controlled reactions of point defects in metals. In *Point Defects in Metals II*, pages 171–262. Springer, 1980.

[127] J.-P. Riviere. Radiation induced point defects and diffusion. In *Application of Particle and Laser Beams in Materials Technology*, pages 53–76. Springer, 1995.

[128] Z. Yongnan, H. Qunying, P. Lei, Z. Yi, F. Ping, Z. Dongmei, Y. Daqing, W. Yichan, and Z. Shengyun. Variation of radiation damage with irradiation temperature and dose in clam steel. *Plasma Science and Technology*, 14(7) :629, 2012.

[129] K. Dawi, C. W. He, M. F. Barthe, P. Desgardin, and A. Volgin. Vacancy defects study in fe based alloys induced by irradiation under various conditions. In *Journal of Physics : Conference Series*, volume 505, page 012007. IOP Publishing, 2014.

[130] H. Huang, J. Gao, B. Radiguet, R. Liu, J. Li, G. Lei, Q. Huang, M. Liu, and R. Xie. Microstructural evolution and hardening of gh3535 alloy under energetic xe ion irradiation at room temperature and 650c. *Journal of Nuclear Materials*, 499 :431–439, 2018.

[131] L. Le Cam. An approximation theorem for the poisson binomial distribution. *Pacific Journal of Mathematics*, 10(4) :1181–1197, 1960.

[132] Y. N. Osetsky, L. K. Béland, A. V Barashev, and Y. Zhang. On the existence and origin of sluggish diffusion in chemically disordered concentrated alloys. *Current Opinion in Solid State and Materials Science*, 2018.

[133] T. Yang, S. Xia, S. Liu, C. Wang, S. Liu, Y. Fang, Y. Zhang, J. Xue, S. Yan, and Y. Wang. Precipitation behavior of al x cocrfeni high entropy alloys under ion irradiation. *Scientific reports*, 6 :32146, 2016.

[134] Q. Li, W. Chen, J. Zhong, L. Zhang, Q. Chen, and Z.-K. Liu. On sluggish diffusion in fcc al–co–cr–fe–ni high-entropy alloys : An experimental and numerical study. *Metals*, 8(1) :16, 2017.

[135] K. Schouteden, B. Amin-Ahmadi, Z. Li, D. Muzychenko, D. Schryvers, and C. Van Haesendonck. Electronically decoupled stacking fault tetrahedra embedded in au (111) films. *Nature communications*, 7 :14001, 2016.

Annexe A

SUPPLEMENTARY MATERIAL FOR THE FIRST ARTICLE

A.1. Proof of difference between states 5SIAa and 5SIAb

States 5SIAa and 5SIAb are shown in FIGA.1. These states are different even that they have the energy and quite similar and we will proof that in this small section. If we label each dumbbell as indicated in FIGA.1, we can calculate all distances between between them. We can remark that the difference between the two states is in the position of the dumbbell1. All the rest stills the same and as consequence all distances not involving dumbbell 1 still the same also. Now let us try to calculate distances between dumbbells that involves dumbbell 1. Distances are indicated in TableA. VI. We can see thru the table that distances are not the same and as consequence the states 5SIAa and 5SIAb are different.

Tableau A. I. Size effect on formation energies in the ground state using EAM potential. One to five self-interstitialatoms (SIA) for cubic boxes varies in number of atoms from 108 to 5324. Values are in eV.

Size \ Defect	1SIA	2SIA	3SIA	4SIA	5SIA
108 atoms	4.7006	7.9813	10.7522	12.5914	15.2834
256 atoms	4.5927	7.8286	10.6413	12.3621	15.1511
500 atoms	4.5591	7.7951	10.5886	12.2136	15.0412
864 atoms	4.5446	7.7790	10.5512	12.1057	14.9621
1372 atoms	4.5373	7.7514	10.5367	12.0910	14.9136
2048 atoms	4.5332	7.7489	10.5236	12.0851	14.8807
2916 atoms	4.5307	7.7420,	10.5182	12.0806	14.8653
4000 atoms	4.5291	7.7391	10.5131	12.0767	14.8582
5324 atoms	4.5288	7.7376	10.5115,	12.0742	14.8531

Tableau A. II. Size effect on formation energies in the ground state using EAM potential. One to five vacancies for cubic boxes varies in number of atoms from 108 to 5324. Values are in eV.

Size \ Defect	1SIA	2SIA	3SIA	4SIA	5SIA
108 atoms	1.6323	3.0382	4.2137	5.1698	6.2491
256 atoms	1.6316	3.0357	4.2130	5.1676	6.2388
500 atoms	1.6315	3.0350	4.2126	5.1655	6.2316
864 atoms	1.6314	3.0347	4.2119	5.1639	6.2255
1372 atoms	1.6316	3.0347	4.2118	5.1637	6.2223
2048 atoms	1.6315	3.0346	4.2116	5.1635	6.2204
2916 atoms	1.6315	3.0346,	4.2115	5.1635	6.2190
4000 atoms	1.6315	3.0345	4.2114	5.1634	6.2187
5324 atoms	1.6315	3.0345	4.2114	5.1634	6.2186

Tableau A. III. Relative configuration energies (E) (top line) and barrier energies for pathways between the six dominant bound states for the divacancy complex using ReaxFF potential. Indexes means the traveled distance in function of nearest neighbor (2 means distance traveled of 2nn for example). Values 1 and 2 in index means displacements with 1nn and 2nn distance respectively. Energies are in eV

To \ From	1^{th}	2^{th}	3^{th}	4^{th}	5^{th}
ΔE	0	0.27	0.29	0.30	0.30
1^{th}	0.97_1	1.29_1	1.11_1	1.08_1	1.36_2
2^{th}	1.55_1	1.28_2	1.32_1	-	1.34_1
3^{th}	1.40_1	1.34_1	-	-	-
4^{th}	1.38_1	-	-	-	-
5^{th}	1.65_2	1.36_1	-	-	-

Tableau A. IV. Relative configuration energies (E) (top line) and barrier energies for pathways between the six dominant bound states for the divacancy complex using MEAM1NN potential. Indexes means the traveled distance in function of nearest neighbor (2 means distance traveled of 2nn for example). Values 1, 2 and 3 in index means displacements with 1nn and 2nn distance respectively. Energies are in eV

To \ From	4^{th}	3^{th}	5^{th}	1^{th}
ΔE	0	0.08	0.18	0.29
4^{th}	-	1.15_1	1.06_1	1.18_1
3^{th}	1.23_1	1.28_2	1.32_1	1.13_1, 1.64_2, 2.36_3
5^{th}	1.24_1	1.42_1	-	-
1^{th}	1.47_1	1.34_1,1.85_2,2.57_3	-	0.58_1

Tableau A. V. Relative configuration energies (E) (top line) and barrier energies for pathways between the six dominant bound states for the divacancy complex using MEAM2NN potential. Indexes means the traveled distance in function of nearest neighbor (2 means distance traveled of 2nn for example). Values 1 and 2 in index means displacements with 1nn and 2nn distance respectively. Energies are in eV

To \ From	4^{th}	3^{th}	5^{th}	1^{th}	2^{th}
ΔE	0	0.10	0.18	0.36	0.36
4^{th}	-	-	-	-	-
3^{th}	-	-	1.59_1	1.60_1	-
5^{th}	-	1.67_1	-	-	-
1^{th}	-	1.86_1, -	-	-	1.51_1
2^{th}	-	-	-	1.51_1	-

Tableau A. VI. Distances between dumbbells in states 5SIAa and 5SIAb.

Distance between dumbbell 1 and	2	3	4	5
For state 5SIAa	1nn	1nn	1nn	3nn
For state 5SIAb	1nn	1nn	2nn	3nn

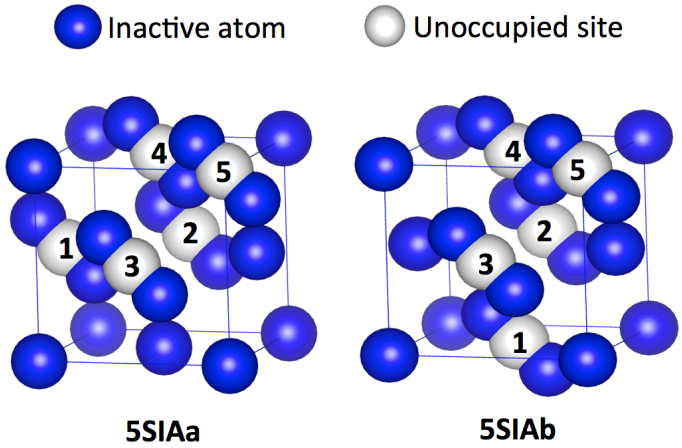

Figure A.1. States 5SIAa and 5SIAb